Steady flow through models of compliant stenoses

ISU
1986
D85
c. 3

by

Patricia Marlene Dubill

A Thesis Submitted to the

Graduate Faculty in Partial Fulfillment of the

Requirements for the Degree of

MASTER OF SCIENCE

Interdepartmental Program: Biomedical Engineering
Major: Biomedical Engineering

Approved:

Signatures have been redacted for privacy

Iowa State University
Ames, Iowa

1986

1561771

TABLE OF CONTENTS

INTRODUCTION

Blood is a vital body fluid used to transport various molecules between organs and specialized tissues. It is pumped by the heart through a highly branched network of distensible tubes called blood vessels. The network is a complex circle which utilizes bulk flow to deliver blood to organs and tissues, and diffusion to exchange molecules between blood and tissue cells. Arteries, which are the bulk flow conduits, carry blood away from the heart, gradually tapering and branching into peripheral beds of arterioles and capillaries, in which molecular exchange takes place. Capillary blood passes into venules, which unite to form larger veins to return blood to the heart. This venous blood circulates through the lungs for gas exchange with inspired air and returns to the heart, thus completing the circle.

All of these components of the circulatory system are important, but arteries are especially significant because they supply oxygen-rich blood necessary to sustain most bodily functions. Sometimes abnormal circumstances materialize that impair flow through an artery, causing energy deprivation (ischemia) to the organ or vascular bed the artery supplies. A major cause of impaired arterial flow is the disease commonly referred to as atherosclerosis. In this disease, a "stenosis," or narrowing, forms by progressive buildup of plaque in an artery's lumen (interior). An important aspect of the study of stenosed arteries is the determination of their effect on flow to peripheral vascular beds. A stenosis influences regional blood flow by limiting the distal vascular bed's normal capability to augment flow when energy requirements increase.

That is, normally, a vascular bed can dramatically alter its resistance (primarily at the arteriolar level) to increase flow, but with a diseased artery a physiologically unattainable decrease in resistance may be required to yield the needed flow rate.

The consequences of this reduced autoregulatory response can be very serious, depending on the location and severity of the stenosis. Blockage of one of the coronary arteries, which supply the heart, may cause severe chest pain (angina) and ultimately a heart attack--the leading cause of death in the United States. Blockage of one of the carotid arteries, which supply the brain, may cause a stroke--the third leading cause of death in the United States. These statistics well-illustrate the importance of studying cardiovascular disease and indicate a need for continued research on blood flow through stenoses.

Many research approaches are used to study the effects of a stenosis, including in vivo experiments related to both naturally occurring and artificially induced stenoses, computer models based on fluid dynamical considerations and anatomical data, and fluid-mechanical experiments utilizing hydraulic models of stenosed arteries. The latter approach is especially useful because it greatly simplifies the complex system that exists in the body, allowing for a better understanding of the significance of specific system parameters and greater accuracy of experimental measurements. Typical hydraulic models are roughly based on the schematic of Figure 1, and are commonly referred to as simple lumped-parameter models. This system models a segment of stenosed artery as a straight rigid tube with some sort of constriction and lumps all resistances downstream of the stenosis into one distal resistance. Mean flow to the

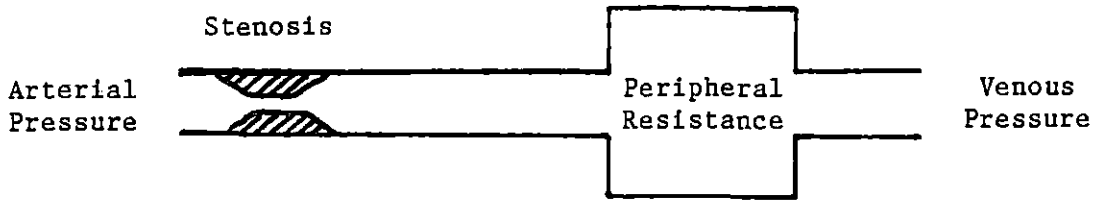

Figure 1. Simple lumped parameter model of a stenosed artery

peripheral beds is then determined by the ratio of the pressure drop across the stenosis to the lumped peripheral resistance.

These simple models that use a rigid stenosis configuration provide considerable insight into the hemodynamic effects of stenoses; however, they are not fully representative of "compliant stenoses" that may also be found in the body. Compliant stenoses are lesions that form eccentrically, so that their residual arterial lumen contains a portion of normal wall segment capable of undergoing a change in geometry, as shown in Figure 2.

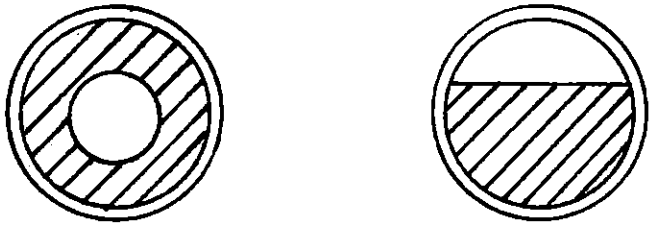

(a) Rigid (b) Compliant

Figure 2. Cross-section of rigid vs. compliant stenosis

Due to the "Bernoulli effect," pressure can be reduced considerably in regions of reduced cross-sectional area, so that the outer tissue pressure exceeds the pressure within the lumen. This may result in a transient

collapse if the residual arterial lumen is sufficiently pliable. Little pressure is recovered distal to a severe stenosis, so it is also conceivable that collapse could occur downstream of a stenosis. Some studies on compliant stenoses (using real arteries) have been done, but the results are difficult to interpret because the fundamental aspects of flow through such stenoses are not yet understood. The intent of the present study is to provide some much needed basic knowledge about the fluid mechanics of compliant stenoses.

The specific objectives of the study were to determine the important system parameters for compliant stenoses, and to develop a pressure-flow equation similar to that available for rigid stenoses. For this initial investigation, only steady flow was considered. Two types of test section were studied: 1) a short collapsible segment with rigid tubing immediately upstream and downstream of an eccentrically placed stenosis, and 2) a long collapsible segment with collapsible tubing downstream of an eccentrically placed stenosis. Static tests were performed on both types of test section to determine the collapse pressure for each stenosis. For different values of "percent stenosis" (percent reduction in cross-sectional area), steady flow tests were run at a constant upstream pressure for various values of external pressure. Flow rate and upstream, downstream, and external pressure were the experimental variables measured and analyzed.

LITERATURE REVIEW

To make the model as physiologically realistic as possible and to be able to ascertain its limitations, certain characteristics of blood, arteries, and arterial stenoses had to be considered. This section reviews these important physiologic characteristics, as well as past studies on rigid stenoses, collapsible tubing, and arterial stenoses.

Physiologic Considerations

The physiologic characteristics most important to consider in designing a hydraulic model are rheological properties of blood, the nature of blood flow in arteries, and geometric and mechanical properties of arteries and stenoses.

Blood rheology

Rheologically, blood is a challenging fluid to study--it is a non-homogeneous suspension of odd-shaped particles which cause it to change viscosity with shear rate and behave as a non-Newtonian fluid at low shear rates. Fortunately, flow in large arteries is at relatively high shear rates, so that constant viscosity and Newtonian flow may reasonably be assumed. Young (1979) specifies the viscosity of human and canine (dog) blood to range from 3-4.5 x 10^{-3} N·s/m^2 (normally) at shear rates above 100 sec^{-1} at 37°C. The density of blood is about 1050 kg/m^3, so it is slightly more dense than, and several times as viscous as water.

Blood flow in arteries

To complicate matters, blood flow in arteries is pulsatile, due to the contraction/relaxation cycle of the heart. Flow and pressure waveforms for a given cycle vary according to location. Typical waveforms are shown in

Figure 3. The significance of unsteady flow effects is generally characterized by the dimensionless alpha parameter

$$\alpha = R\sqrt{\omega/\nu} \quad (1)$$

where: R = lumen radius

ω = fundamental frequency of flow

ν = fluid kinematic viscosity

The value of α decreases progressively from artery to capillary, ranging overall from approximately 0.01 to 20, and in arteries from about 1 to 20 (in humans).

Another important dimensionless parameter to consider is the Reynolds number

$$Re = DU/\nu \quad (2)$$

where: D = lumen diameter

U = characteristic velocity

ν = fluid kinematic viscosity

The Reynolds number also varies greatly throughout the circulation, typically from 10^{-3} to 10^{4} in humans, the higher values being at the arterial level (from about one hundred up). The Reynolds number is a measure of the ratio of viscous to inertial effects and is used to determine whether flow is laminar or turbulent. For the most part, arterial flow is laminar, although branching and pathologic circumstances such as stenoses may cause localized disturbed flow and turbulence.

Arterial geometry and mechanics

Even more complicating than blood's rheological properties and pulsatility of flow is the complex geometry of the circulation, as described previously. In addition to being tapered, highly branched, and

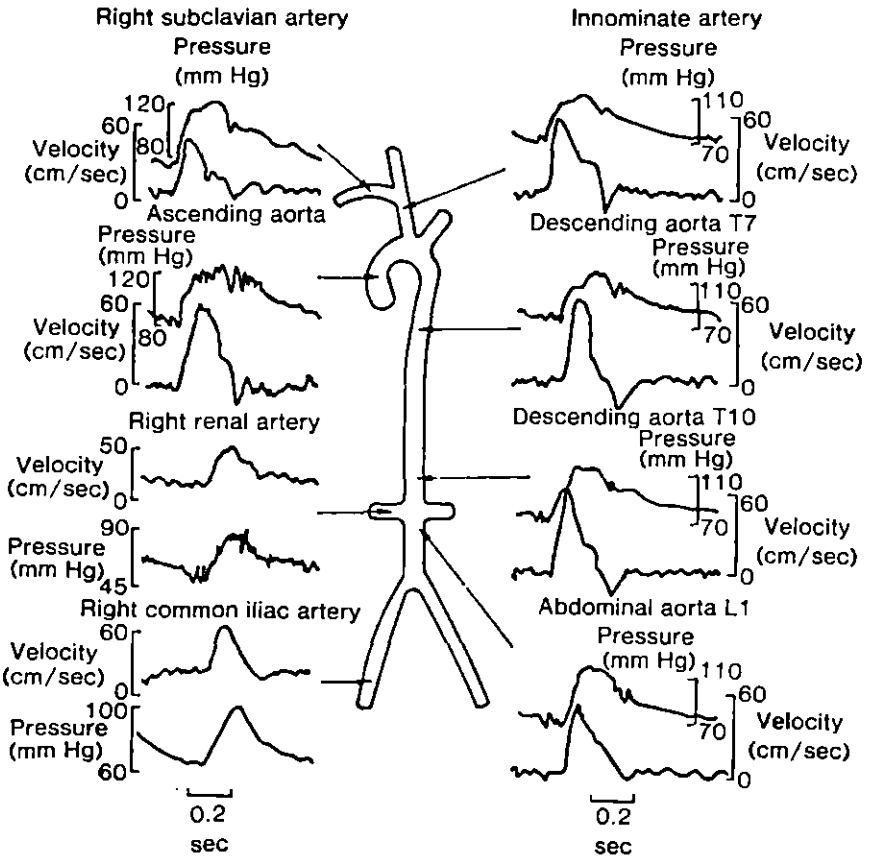

Figure 3. Flow and pressure waveforms in various arteries (Milnor 1982)

curved, arteries are of non-circular cross-section and change diameter as blood pulsates through them. Further vessel diameter changes may occur when physiologic stimuli elicit vasodilation or vasoconstriction, although most of this sort of response occurs at the arteriolar level. Typical values of lumen diameter, wall thickness, and length for various arteries are given by Caro et al. (1978).

The elastic properties of the vascular wall are as difficult to characterize as the geometric properties. Most notably, arteries are anisotropic, elastically non-linear, and viscoelastic. Anisotropic means that arteries have direction-dependent properties--that is, for example, they have a different value of radial, circumferential, and longitudinal elastic modulus. In addition to having different elastic moduli in different directions, arteries have different elastic moduli at different stresses. Thus, a single elastic modulus, as is valid for linear elastic materials, does not exist--an incremental modulus must be determined for a specific radius. Arterial mechanics also depends on the viscous properties of the arterial wall, which make the arterial stess-strain relationship dependent on time and frequency; i.e., the vessel wall exhibits viscoelastic characteristics.

A further consideration in arterial mechanics is tethering. Connective tissue attached to arteries tethers them to surrounding structures and serves to stretch them longitudinally. According to Milnor (1982), when arteries are surgically released from surrounding structures they retract 20 to 40 percent of their initial length. Tethering also serves to limit longitudinal wall motion caused by the pulsatility of flow.

Stenosis geometry

The final physiologic topic to consider is geometric characteristics of arterial stenoses. One significant fact is that stenoses are often located near the origin of branches, making the geometry preceding them complex. Entrance effects have not been studied extensively, but it is believed that the converging geometry of the upstream end of a stenosis smooths out entrance effects. Some stenoses exist as a single localized obstruction and others are more diffuse. Most models use a single localized stenosis. The most important parameter used to characterize a localized stenosis is the percent stenosis

$$\text{Percent stenosis} = (1 - A_1/A_o) \times 100 \tag{3}$$

where: A_1 = minimum cross-sectional area

A_o = unobstructed lumen area

Other important characteristics are the length of the stenosis and the way it is situated in an artery--approximately concentric or eccentric.

The significance of the latter characteristic has not been considered in detail by researchers of stenosis models. As previously noted, concentric stenoses are effectively rigid, whereas eccentric stenoses may be compliant, depending on the characteristics of the residual arterial wall. Freudenberg and Lichtlen (1981) made post-mortem studies of 384 stenotic coronary artery segments and found that 74% of them contained a portion of normal wall segment. The criteria they used to define "normal" were based on thickness of the residual arterial wall. It should be noted that other investigators using different criteria found a lower percentage of stenoses containing a normal wall segment; however, the percentage of

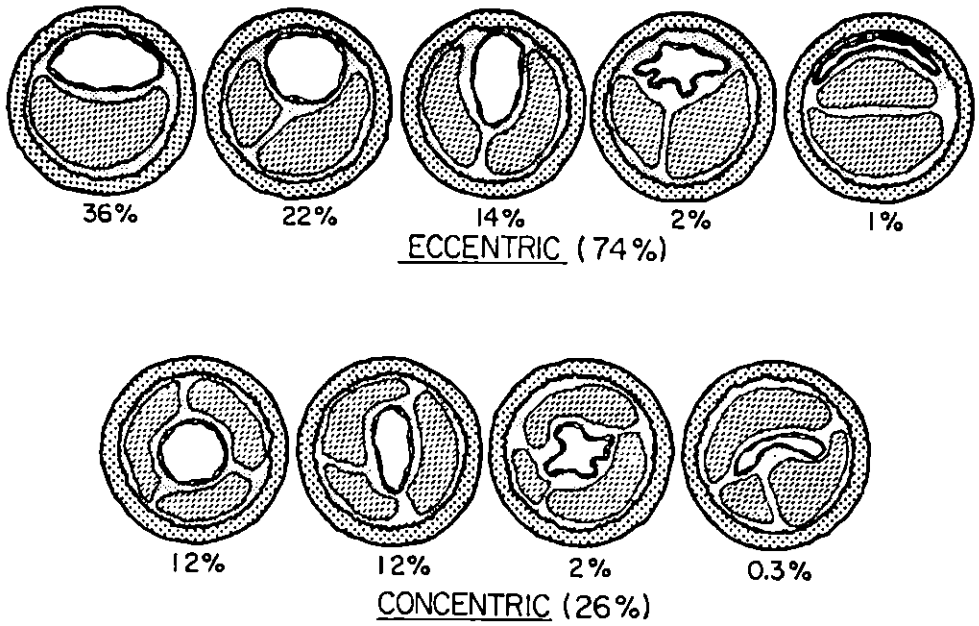

Figure 4. Prevalence of various shapes of stenosis cross-section (Brown et al., 1984)

compliant stenoses was still substantial. Figure 4 shows a breakdown of percentages of various shapes of stenoses found by Freudenberg and Lichtlen. Knowledge of the shapes of physiologically occurring stenoses is necessary to design similar shapes of model stenoses.

Rigid Stenosis Studies

Even though past researchers did not consider the potential dynamic behavior of stenoses, much useful information has been gained from their rigid stenosis models. One important finding is that there exists a "critical stenosis" for which a further increase in severity will cause a significant reduction in flow. Clinically, the existence of a critical stenosis is a very important concept. Unfortunately, there is no one value

of critical stenosis in the circulation, as it depends not only on percent stenosis, but, at least indirectly, on peripheral resistance and collateral flow. Values of critical stenosis from 69 to 95 percent have been found to exist, with typical values being about 80 percent. These values apply to resting flow rates--the value for the critical stenosis is reduced at elevated flow rates, where the critical stenosis can be as low as 50 percent.

Dimensional analysis

A very important hemodynamic effect of stenoses is the pressure drop which develops across the stenosis. Therefore, it is important to understand how various factors influence the pressure drop. Because of the many complicating factors that would be involved in an analytical solution to the problem, the pressure-flow relationship must, in general, be determined experimentally. To make the experiments as fluid dynamically similar to physiologic situations as possible, dimensional analysis is generally used. Young (1979) formulated the following dimensionless groups for the pressure drop based on the parameters in Figure 5:

$$\frac{\Delta P}{\rho U^2} = f\left(\underbrace{\frac{L}{D}, \frac{A_1}{A_o}, \frac{\lambda_i}{D}}_{\text{geometric parameters}}, \underbrace{\frac{DU_p}{\nu}}_{\text{Re}}, \underbrace{\frac{U_s}{U_p}, \frac{\tau_1}{\tau}}_{\text{flow waveform parameters}}, \underbrace{\frac{t}{\tau}}_{\text{time scaling parameter}}, \underbrace{\frac{D}{2}\sqrt{\frac{2\pi}{\tau\nu}}}_{\text{frequency parameter}}\right) \quad (4)$$

where: λ_i/D represent a series of geometric terms to include all significant lengths λ_i required to adequately describe the stenosis

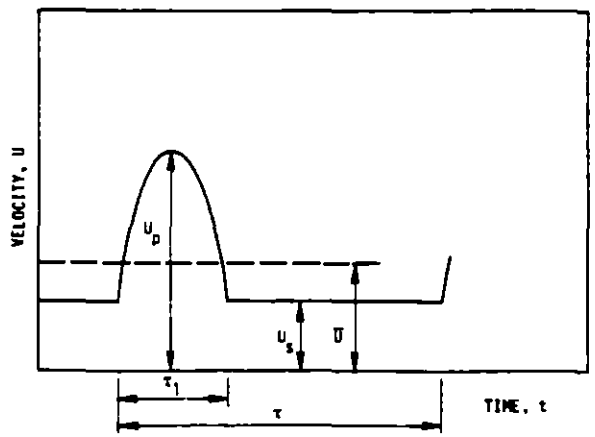

(a) Waveform parameters

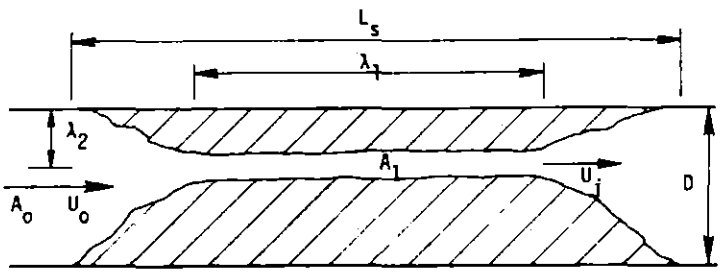

(b) Geometric parameters

Figure 5. Parameters used in dimensional analysis of a rigid stenosis model (Young, 1979)

Pressure-flow relationship

After running numerous experiments on various stenosis models, Young found the following equation to describe the flow

$$\Delta P = K_v \frac{\mu}{D} U + \frac{K_t}{2} \left[\frac{A_o}{A_1} - 1 \right]^2 \rho |U| U + K_u \rho L \frac{dU}{dt} \qquad (5)$$

where: K_v, K_t, and K_u = empirically determined constants

The first term, involving velocity to the first power, accounts for viscous losses, and is only dominant at very low Reynolds numbers. The second term, involving velocity to the second power, accounts for turbulent losses, and is dominant at higher Reynolds numbers. The last term, which is dropped for steady flow models, accounts for the pressure drop caused by the fluid acceleration.

Some important conclusions about stenoses can be drawn from an evaluation of Equation (5).

1) Pressure drop is strongly influenced by the area ratio A_o/A_1 and the velocity, as well as other geometric properties of the stenosis and artery, properties of blood, and the flow waveform.

2) The pressure-flow relationship is non-linear, so that stenosis resistance depends on velocity. Thus, the value of critical stenosis depends on velocity, and decreases as the velocity increases.

3) Percent stenosis is extremely important when a certain value is reached--once the critical range is entered, flow is greatly affected by very small increases in stenosis severity. This critical range is initiated at lower values of percent stenosis when the flow rate is

elevated.

4) Stenosis length and entrance and exit angle were studied extensively by Lipscomb and Hooten (1978) and found to have little effect on flow, except for very long stenoses. This is due to the minimal effects of the viscous term in the equation at physiologic Reynolds numbers.

5) The dynamic nature of the flow is fairly insignificant for moderate to severe stenoses.

Other interesting characteristics of rigid stenosis flow include localized velocity, wall shearing stress and pressure distribution, separation phenomena, and turbulence. These topics are reviewed by Young (1979).

Collapsible Tube Studies

Another topic that provides useful background information pertinent to compliant stenosis studies is flow through (non-stenosed) collapsible tubing subjected to external pressure. Important aspects of this problem include the study of hydrostatic tube properties, as well as the study of both experimental and theoretical flow through collapsible vessels.

Hydrostatic tube properties

Of particular interest in the area of hydrostatic tube properties are the pressure-volume and pressure-area relationships of collapsible tubing. Moreno et al. (1970) determined these relationships for thin-walled latex tubing (Penrose® surgical drain tubing). The researchers discovered that the tubing showed a distinct two-regime behavior of large and small compliance when distended from an oval to a circular cross-section, and concluded that the modulus of flexural rigidity, rather than simply the modulus of elasticity, is the significant quantity relating pressure and

volume of a collapsed tube.

Further support for this conclusion about flexural rigidity is provided by Fung (1984). Fung derived an equation for critical buckling pressure of a thin-walled circular tube in the form

$$(P_e - P)_{cr} = \frac{3E'I}{R^3} = \frac{Et^3}{4(1-\upsilon^2)R^3} \quad \left(= \frac{Et^3}{3R^3} \text{ for Penrose}^{®} \right) \qquad (6)$$

where: $E'I$ = flexural rigidity of tube
t = tube thickness
υ = Poisson's ratio for tube
E = elastic modulus of tube
R = inside radius of tube

At the above critical value, the buckled cross-section is elliptical in shape. When the transmural pressure exceeds the critical value, the "post-buckling mode" is entered. In this mode, progressive increase in transmural pressure causes pinching of the tube into a dumbbell shape. It is necessary to understand such hydrostatic mechanical tube properties to determine how they are coupled to the fluid dynamic behavior of collapsible tubes.

Experimental apparatus for flow studies

Many experimental investigations have been conducted on flow through thin-walled elastic tubing. The apparatus most commonly used, often called a "Starling resistor device," consists of a segment of flexible tubing mounted on rigid tubing and enclosed in an airtight chamber. The variables generally of interest are the flow rate, Q, controlled by varying upstream and/or downstream resistances R_1 and R_2, and the inlet, outlet and external pressures P_1, P_2 and P_e. Figure 6 shows a schematic of a Starling resistor

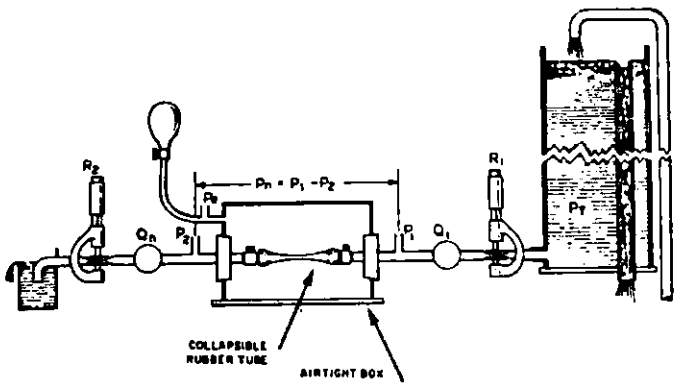

Figure 6. Schematic of a Starling resistor device (Conrad, 1969)

device.

Experimental results of flow studies

Some very basic early studies on collapsible tubing by Rodbard and Saiki (1953), Rodbard (1955), and Holt (1959) revealed that increasing the pressure gradient (P_1-P_2) by increasing P_1 causes an increase in flow, but increasing the gradient by decreasing P_2 causes the flow to either increase, stay the same, or decrease, depending on whether the resultant change in transmural pressure causes the tube to remain open or collapse. Thus, the elastic tube behaves essentially as a rigid tube when it is open, but unlike a rigid tube when it is collapsed, where flow becomes independent of changes in P_2. Permutt and Riley (1963) likened this phenomenon to flow over a waterfall, which depends only on conditions at the top of the fall, not on the height--hence, the term "vascular waterfall" was coined to describe the behavior of a collapsed tube. Other terms used to describe the vascular waterfall include flow limitation, sluice effect, Starling resistor phenomenon, and mechanical autoregulation

of flow.

Another phenomenon collapsible tubing exhibited under certain conditions was oscillation, or "flutter," a repetitive cycle of opening and closing of the tube. Investigators reasoned that when the internal pressure fell sufficiently to initiate collapse, the velocity increased by the Bernoulli effect and a further fall in lateral pressure occurred, causing progressive closure of the tube and cessation of flow. The stagnation pressure thus became totally available as lateral pressure, which forced the tube to reopen, flow to resume, and the cycle to repeat. The characteristics of the oscillations were found to depend primarily on wall elasticity, flow rate, and outlet pressure.

Conrad (1969) performed more systematic tests on collapsible tubing, studying pressure-flow relations for conditions of constant external pressure and downstream resistance for various values of inlet and outlet pressure. He found that three flow states exist, designated by their respective values of transmural pressure relative to a critical transmural pressure. Table 1 describes these three flow states and Figure 7 shows a typical pressure-flow relationship and photographs of the tube for various points on the curve. In states I and III, the relationship is linear, like Poiseuille flow, with a higher value of resistance in the collapsed state of III than in the open state of I because of the lower effective cross-sectional area in III. In region II, the relationship is non-linear, however, because of the large changes in geometry the tube undergoes there. Region II represents the highly compliant portion of the pressure-volume curve found by Moreno et al. Conrad referred to the negative slope in region II as a negative dynamic resistance, and found that oscillations

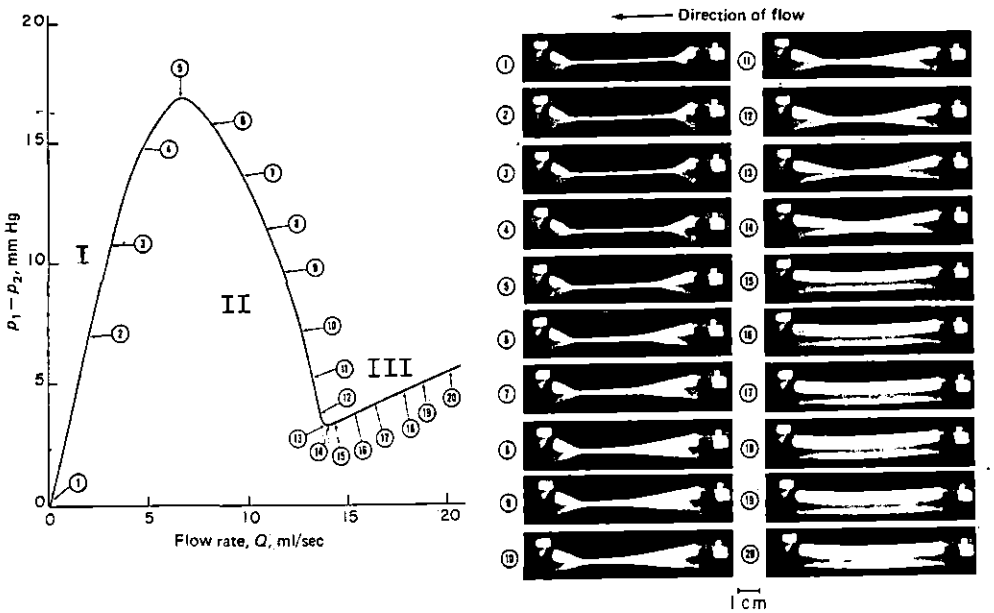

(a) Pressure-flow relations (b) Side views of the collapsible tubing at various stages of the experiment

Figure 7. Behavior of a Starling resistor at constant external pressure and downstream pressure (Conrad, 1969)

Table 1. Three flow states for a Starling resistor device

Region	State		Geometry
I	P_c [a] > P_{crit} [b]	Collapsed	A pair of relatively rigid tunnels
II	$P_c \cong P_{crit}$	Partially Collapsed	An easily distorted asymmetric pinch
III	$P_c < P_{crit}$	Open	A relatively rigid cylinder

[a] P_c = transmural pressure at the least supported point.

[b] P_{crit} = critical transmural pressure.

occurred only in that region.

Mathematical models of experimental results

Conrad developed an electrical analog for his data (a "flow-controlled non-linear resistance") and Katz et al. (1969) derived an intuitively based mathematical model from similar data. These models gave fairly reasonable descriptions of the experimental results using the gradient of (P_1-P_2) as the significant variable. Brower and Noordergraaf (1973) later developed a better quantitative curve-fitting model for Conrad's and Katz's data by recognizing that the pressure differentials (P_1-P_2) and (P_e-P_2) were the significant variables. The latter model was not of a form that allowed its extension to other data, however. A more analytical model was developed by Holmberg and Wilson (1970). It was also only qualitatively accurate, although by studying tubes of different sizes and elasticities, the researchers were able to define two significant values of transmural pressure in terms of tube properties. They found that up to a transmural pressure of $2.3[(1/3)E(t/R)^3]$ little tube deformation occurred, and that transmural pressures exceeding the value $8E(t/R)^3$ caused oscillatory behavior to cease.

Theoretical analyses on the mechanism of flow limitation

Empirically based mathematical models of collapsible tube behavior are very useful, but models of a more theoretical nature are also needed to accurately explain the physics of the flow. Two different theories on the mechanism of flow limitation have been advanced. One involves the relation of wave speed to fluid velocity and the other involves pressure-related compensatory adjustments of tube resistance.

Wave speed (inertial) mode of flow limitation Griffiths (1971a, 1971b) was the first investigator to recognize the potential significance of wave speed in collapsible tube flow. From his elementary one-dimensional theory of steady flow through an elastic tube, he determined that a maximum flow (i.e. flow limitation) does exist, and occurs when the flow speed, u, equals the wave speed, c. This value of maximum flow is given by the relationship

$$Q_{max} \cong \frac{A^3}{\rho}\left[\frac{d(P-P_e)}{dA}\right]^{\frac{1}{2}} \qquad (7)$$

where: $P-P_e$ = negative transmural pressure

$\frac{d(P-P_e)}{dA}$ = reciprocal of slope in A vs. $(P-P_e)$ curve at the value of A under consideration

For tubes with a circular cross-section, this "sonic speed" represents the speed of pressure waves in the tube. Griffiths theorized that flow is subsonic ($u<c$) in the uncollapsed portion of an elastic tube and supersonic ($u>c$) in the collapsed portion. He found the flow rate to depend on the characteristics of the flow upstream of the transition to supersonic flow, since disturbances cannot be propagated upstream against a supersonic flow.

Griffiths pointed out that subsonic flow is always stable and supersonic flow may be stable or unstable. Brower and Scholten (1972) provided experimental evidence supporting the theory that fluid velocity approaching phase velocity may be the mechanism of instability in collapsible tube flow, although the experimental phase velocities they found were generally greater than the theoretical phase velocities.

Shapiro (1977) derived a much more complicated equation for one-dimensional steady flow in a collapsible tube. He defined the speed

index, $S \equiv u/c$, which is analogous to the Mach number of gas dynamic flows. Shapiro found that certain changes in factors that effect flow have the opposite effect in subcritical (subsonic) flow than in supercritical (supersonic) flow. For example, in subcritical flow, friction causes a pressure drop, but in supercritical flow, friction causes a pressure rise. This paradox is evident from the presence of the term $(1-S^2)$ in the denominator of each term of the expression Shapiro developed.

Shapiro investigated various flow patterns through an extensive analysis of the variation of the speed index with distance along the tube. He proposed that for a Starling resistor device, either the flow reaches critical speed and then becomes subcritical again, or it becomes supercritical, followed by a return to subcritical flow (where the flexible tubing attaches to the rigid tube downstream). In either case, the tube will act like a "choked-flow device," similar to a Laval nozzle. Elliott and Dawson (1978) provided experimental support for the existence of an "elastic jump" (analogous to the hydraulic jump of open channel flow) as the mechanism of energy dissipation causing the flow-limiting transition back to subcritical flow.

Frictional mode of flow limitation Another theory on the mechanism of flow limitation is the "frictional mode," as described by Fry et al. (1980). In this mode, flow is limited by compensatory changes in flow resistance of the elastic tube in response to changes in outlet pressure. Based on this mechanism, Rubinow and Keller (1972) analytically derived a pressure-flow relation for the human iliac artery, which did predict flow limitation for large negative values of transumural pressure.

Fry et al. also derived a mathematical model analytically (for a Starling resistor device) and found that the pressure differential (P_1-P_e) is a quadratic function of flow, independent of downstream pressure despite changes in tube geometry resulting from variations in P_2. Frictional pressure losses control the length of the collapsed portion in such a way as to keep the pressure upstream of it (P_3) constant. Fry described the constricted portion as a "pressure-regulating segment," rather than a flow-limiting segment. For a given external pressure, flow depends solely on the pressure drop (P_1-P_3) and characteristics of the upstream conduit configuration.

Even though the physics of collapsible tube flow is still a current research topic, the above information is useful in attempting to understand collapsible tube flow in the body. Much of the work reviewed was applied to collapsible tubes other than arteries, but the work still may be relevant to the compliant stenosis problem.

Arterial Stenosis Studies

The information gained from collapsible tube studies combined with knowledge of model rigid stenosis behavior may in fact aid in interpreting the controversial results from arterial stenosis studies. Most of the atherosclerotic research relevant to the compliant stenosis problem has focused on coronary arteries, although several studies have considered carotid arteries. Coronary arteries are of particular interest because of the large external pressures they are subjected to by the heart. Both in vivo and in vitro studies on artificially induced and naturally occurring stenoses have been conducted to study the contributions of various factors to the dynamic behavior of arterial stenoses. The parameters receiving

attention include intraluminal pressure (pressure inside the vessel) and vasomotor tone.

Influence of intraluminal pressure

Logan (1975) compared the in vitro effects of intraluminal pressure on stenosis resistance for concentric and eccentric stenoses in post-mortem segments of human coronary arteries. He determined that the elasticity of eccentric stenoses resulted in increases in resistance (and thus greater flow loss) at lowered perfusion pressures, and found that the rigidity of concentric lesions resulted in minimal, if any, changes in resistance with perfusion pressure. Schwartz et al. (1980) studied the effects of pressure on non-circumferential, artificially induced coronary stenoses in vivo and concluded that changes in coronary pressure result in passive narrowing and distention of the stenotic segment, causing changes in resistance. Thus, the severity of eccentric lesions with a portion of normal wall segment is dependent on intraluminal pressure.

Influence of vasomotor tone

Also of interest in the study of compliant stenoses are the effects of vasomotor tone on resistance and flow. These effects are subdivided into two categories: vasodilation and vasoconstriction.

Vasodilation The effect of vasodilation on coronary blood flow has been studied extensively in vivo over the last few years. Maximal vasodilatory response has been evoked by reactive hyperemia (temporary complete occlusion of an artery) and by vasoactive drugs that dilate either the distal coronary vasculature or the proximal coronary arteries. Studies by Gould et al. (1975) and Gould (1978) revealed that worsening of ΔP (P_1-P_2) occurs with vasodilation of an artificially stenosed artery, which

progressively limits the reactive hyperemic response as stenosis severity increases. (This phenomenon occurs for both rigid and compliant stenoses.) Walinsky et al. (1979) and Schwartz et al. (1979) found that reactive hyperemia induced vasodilation actually caused a decrease in flow through in vivo canine coronary arteries (partially occluded by an external circumferential snare). These researchers proposed that passive collapse of the artery by or distal to the stenosis (due to the fall in distal pressure associated with dilation) was the cause of the reduction in flow. They voiced concern that certain pharmacologic interventions intended to increase flow to ischemic myocardium might have the same effect as reactive hyperemia induced vasodilation--that is, to reduce the flow instead of increase it.

Since vasodilators are frequently used to preclude the need for high-risk bypass surgery, the potential for such adverse consequences with vasodilator therapy provided an impetus for gaining greater quantitative understanding of how various vasoactive drugs affect flow through a stenosed artery. Santamore and Walinsky (1980) studied the effects of intracoronary administration of isoproterenol and nitroglycerin (coronary vasodilators) in dogs, and found a 22% reduction in flow with isoproterenol and only a 1% increase in flow with nitroglycerin. In contrast, coronary arteriography studies in humans by Doerner et al. (1979) revealed a significant decrease in stenosis severity following administration of nitroglycerin and nitroprusside.

These conflicting results were discussed by Gould (1980), who proposed several possible mechanisms of changing stenosis severity. He suggested intraluminal pressure changes as one possible mechanism and indicated that

the effects of vasodilation depend on the location of the dilation relative to the stenosis. Vasodilation of the distal vasculature seems to reduce the flow, whereas proximal arterial vasodilation appears to enhance the flow. Interestingly, this is similar to the behavior of a collapsed tube, for which flow can only be augmented by altering the upstream conditions.

Vasoconstriction Further evidence for the significance of vasomotor tone to compliant stenoses was provided by Santamore et al. (1980, 1981) by studying the effects of vasoconstriction on in vitro coronary arterial segments. Vasoconstriction alone and vasoconstriction with an external snare occluder that did not permit active constriction of the stenosed region produced little effect on flow, whereas vasoconstriction combined with an internal balloon catheter type of stenosis, which did allow for constriction in the partially occluded region, caused significant changes in flow. Thus, the vasoconstriction and non-circumferential stenosis acted synergistically.

Considering the evidence for dynamic severity of eccentric stenoses (and the fact that even flow through normal coronary arteries may be modulated by a waterfall mechanism, as discussed by Downey and Kirk (1975), Eng and Kirk (1984), and Uhlig et al. (1984)), there is a definite need for further study of the problem. Brown et al. (1984) suggested that changes in vasomotor tone probably interact with changes in flow and pressure, but it is not known how much of the effect is due to each factor individually. Conrad et al. (1980) studied the behavior of a collapsed femoral artery and found it to be similar to Penrose tubing (including a negative dynamic resistance and oscillations), but his studies did not include a stenosis.

Basic information on how compliant stenosis flow differs from flow in rigid stenoses and collapsible tubing is thus needed.

MATERIALS AND PROCEDURES

To investigate the fundamental aspects of flow through compliant stenoses, the present study used a hydraulic model similar to the simple lumped-parameter model of Figure 1, except that the stenosed segment was part of a Starling resistor device. Since some controversy remains as to whether collapse in the stenosed area or distal to it is significant, short and long segments of thin-walled tubing containing an eccentric stenosis were studied. With the addition of several parameters not included in the rigid stenosis model, a new dimensional analysis was performed. A collapse pressure was determined hydrostatically for each configuration, and pressure-flow relationships were determined for conditions of steady flow.

Dimensional Analysis

To minimize the number of flow parameters and put them in the correct context, dimensional analysis was applied to the problem. The analysis was divided into two parts, designated as before and after "collapse."

Based on the parameters illustrated in Figure 8, the following variables were considered to be important for the non-collapsed state:

$$U = f\ (\ P_1-P_2,\ P_1-P_e,\ D,\ A_1,\ t,\ L,\ L_c,\ L_s,\ \ell_c,\ \rho,\ \mu,\ \upsilon,\ E\ )$$

These parameters were assembled into the following dimensionless groups:

$$\frac{P_1-P_2}{\rho U^2} = \phi\left(\frac{\lambda_i}{D},\ \upsilon,\ Re,\ \frac{E\rho D^2}{\mu},\ \frac{P_1-P_e}{E},\ \frac{A_1}{A_o}\right) \qquad (8)$$

where: λ_i/D represents all length terms used (L, L_c, L_s, t and ℓ), and $A_o = \pi D^2/4$.

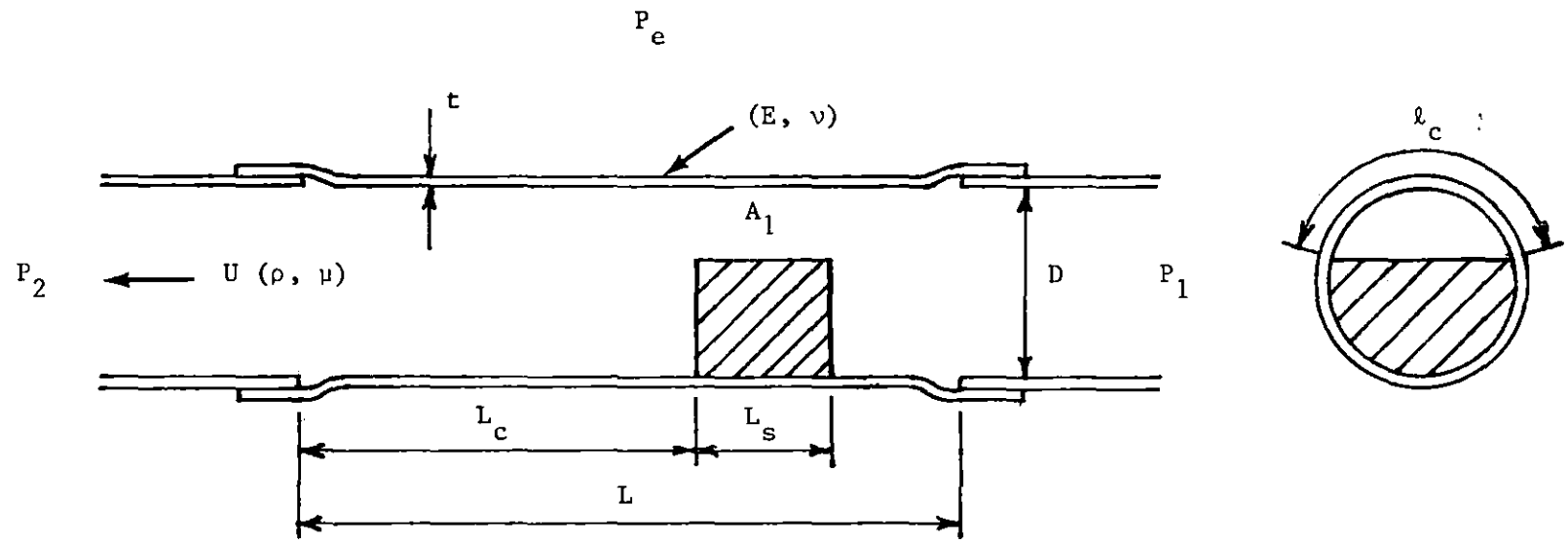

Figure 8. System parameters used in dimensional analysis of the compliant stenosis models (all dimensions measured at atmospheric pressure)

Since all of the dimensionless groups except for the Reynolds number were kept constant for a given test, the above relationship implies that velocity (flow rate) would be a function of P_1-P_2 for the non-collapsed state, as it is for rigid stenosis models.

Based on previous work on collapsible tubing, the variables considered to be important for the collapsed state were:

$$U = f\ (\ P_1-P_e,\ D,\ A_1,\ t,\ L,\ L_c,\ L_s,\ \ell_c,\ \rho,\ \mu,\ \upsilon,\ E\ )$$

These variables were assembled into the following dimensionless groups:

$$\frac{P_1-P_e}{\rho U^2} = \phi\left(\frac{\lambda_i}{D},\ \upsilon,\ Re,\ \frac{E\rho D^2}{\mu},\ \frac{A_1}{A_o}\right) \qquad (9)$$

This relationship implies that the velocity (flow rate) in the collapsed state would be a function of P_1-P_e, as it is in collapsible tubing without a stenosis. Since the flow was steady, no time or frequency parameters were included in the analysis.

Materials

The use of two types of stenosed segments was intended to allow for collapse in the stenosed area and/or downstream of it. The segments are shown photographically in Figures 9 and 10, and schematically in Figures 11 and 12. In the short segment, the stenosis was centered longitudinally in the test section, and in the long segment, the stenosis was located upstream of the center of the test section, so that most of the collapsible tubing was downstream of the stenosis, where the internal pressure was lowest and collapse occurred. The collapsible tubing was mounted on rigid tubing of 1/4 inch internal diameter and 1/64 inch thickness.

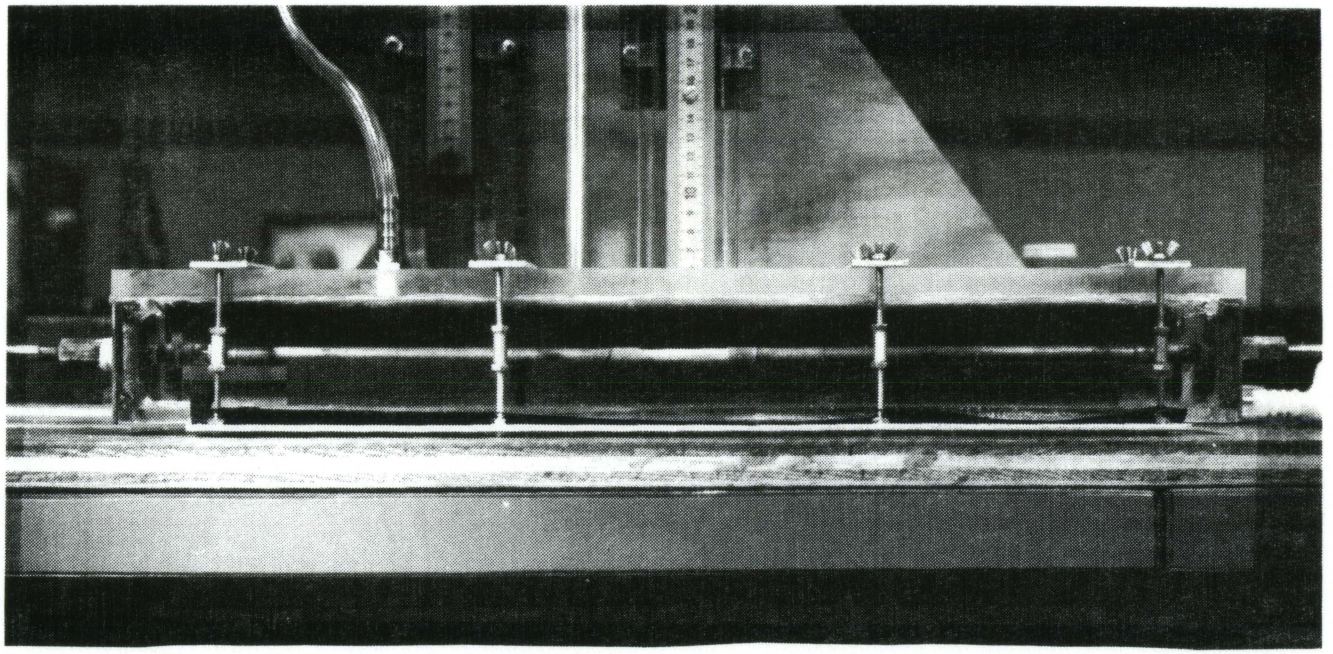

Figure 9. Photograph of the test section for the short compliant configuration

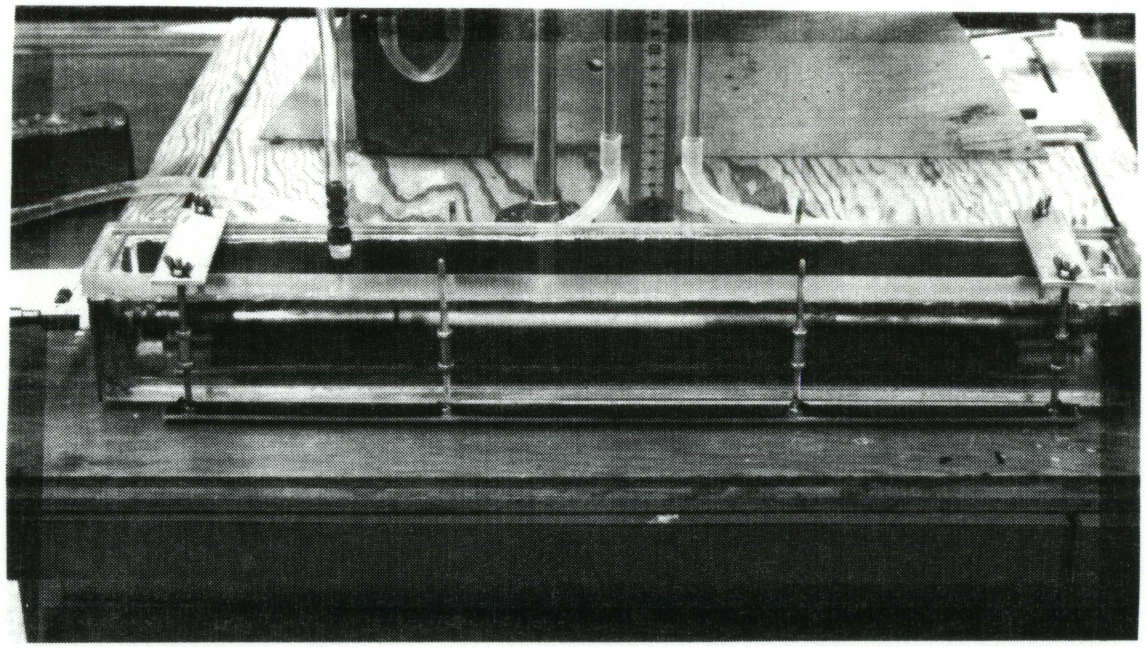

Figure 10. Photograph of the test section for the long compliant configuration

Figure 11. Schematic drawing of the short compliant test section

Figure 12. Schematic drawing of the long compliant test section

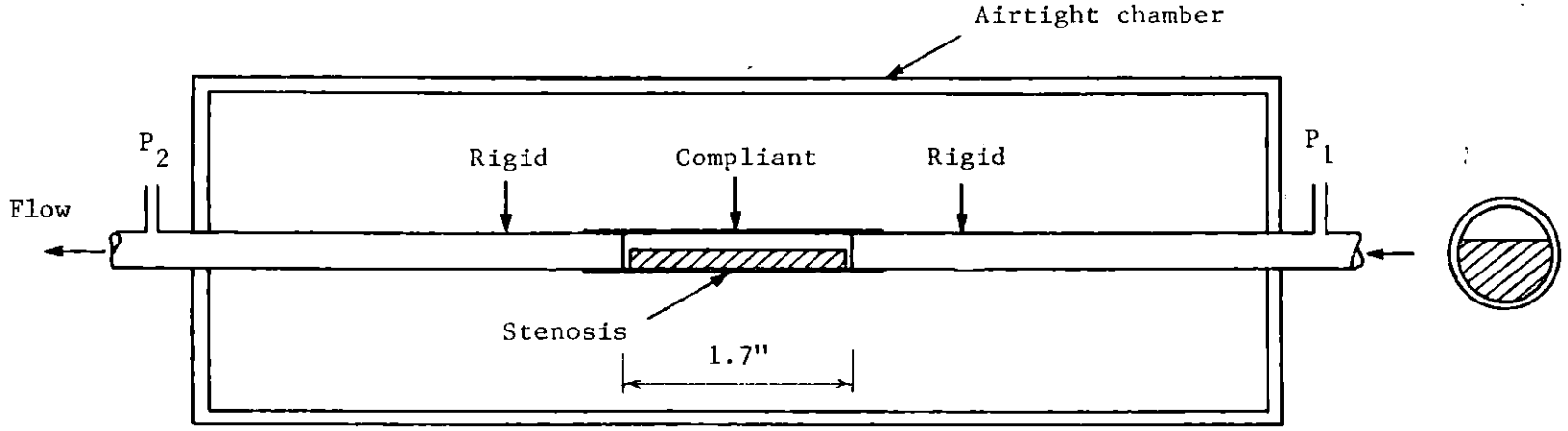
Airtight chamber
P2
P1
Flow
Rigid
Compliant
Rigid
Stenosis
1.7"

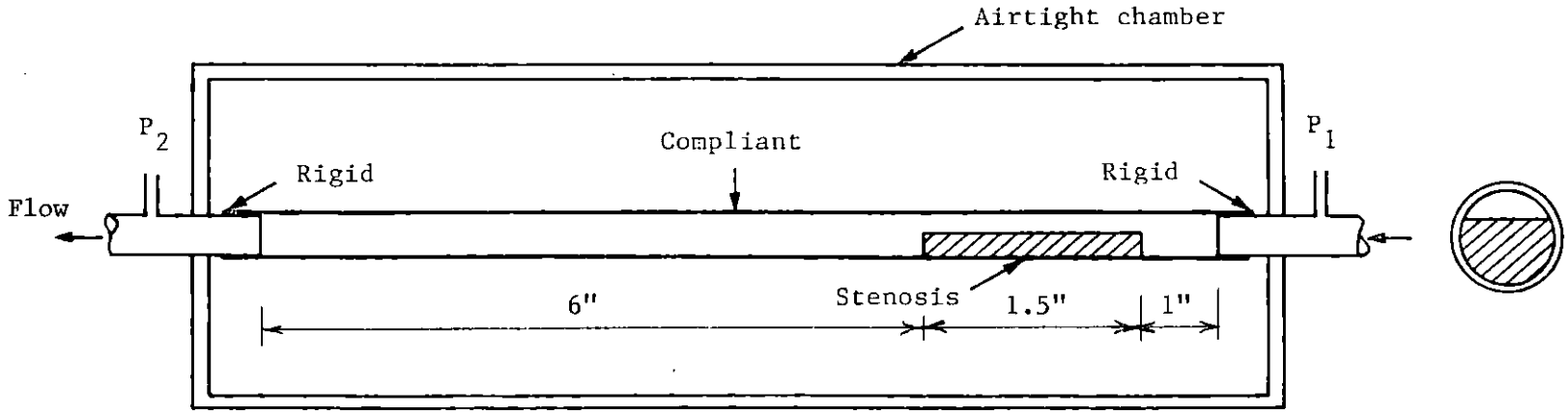
Airtight chamber
P2
P1
Flow
Rigid
Compliant
Rigid
6"
Stenosis
1.5"
1"

Collapsible tube properties

The collapsible tubing used was x-ray opaque Penrose®[1] drain tubing. It had an internal diameter of approximately 0.23 inches and a thickness of approximately 0.012 inches. This gave a t/D ratio of about 0.052, which is one half the value typically found for arteries. The longitudinal dimensions are shown in Figures 11 and 12. The value of L_c/D was approximately 26, and is important in considering end effects, which were reduced in significance by using a large ratio. The elastic modulus and Poisson's ratio for Penrose® tubing were measured by Holmberg and Wilson (1970) and found to be about 178 psi and 0.5, respectively. The value of E is comparable to that of human pulmonary artery and the value of Poisson's ratio is typical of all arteries. Since mechanical properties of the tube change gradually with time after exposure to air and light, all tests were performed within 3 days of the time of initial exposure of a given tube.

Stenosis characteristics

The stenoses were machined from a brass rod of the same internal diameter as the elastic tubing and were of the shape shown in Figure 13. That cross-section seemed to be a reasonable idealization of the most common of the eccentric stenosis configurations in Figure 4, and was one which could be readily fabricated. The stenoses were cemented into the flexible tubing with a very thin layer of super strength adhesive. Three values of percent stenosis were used in an attempt to include both critical and subcritical (yet severe) stenoses--values of 75%, 85%, and 89.4% were

[1] No. 91801, Davol Inc., Providence, Rhode Island.

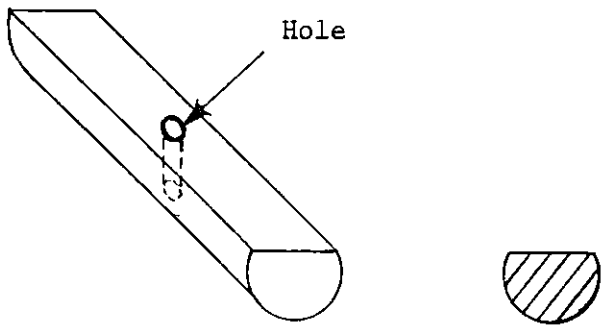

Figure 13. Shape and cross-section of eccentric stenosis used

studied. Percent stenosis was based on the cross-sectional area of the rigid tubing to which the collapsible tube was attached. The length of each stenosis was 1.5 inches, giving an L_s/D ratio of about 6. A small hole (1/16 inch diameter) was drilled in the center of the 75% stenosis (as shown in Figure 13) for the purpose of measuring the pressure in the stenosed region.

Fluid properties

The fluid used for all tests was water, which was kept at a constant temperature of 25°C. At this temperature, Weast (1976, pp. F-5 and F-51) specifies that water has a density of 997.0479 kg/m^3 and a viscosity of 8.904×10^{-4} $N \cdot s/m^2$.

Procedures

Static tests and steady flow tests were performed on both lengths of stenosed segment.

Static tests

For each value of percent stenosis, static tests were executed by closing off one end of the test section and leaving the other end open to a water manometer. At various values of internal pressure, external pressure was applied until "collapse" occurred. Collapse was determined "by eye," and was defined differently for the two configurations. Collapse of the short segment occurred in the stenosed region and was relatively large, so that the critical pressure measured corresponded to a large reduction in cross-sectional area in the stenosed region. Collapse of the long segment occurred in the area downstream of the stenosis, and the measured value of critical pressure represented collapse of the tube into an elliptical cross-section.

For the short configuration, the pieces of flexible tubing used to study the three values of percent stenosis were all cut from the same longer tube, so that any differences in measured pressures between stenoses would be due primarily to the percent stenosis, not to variations in mechanical properties for different tubes (tubes from different packages). Differences due to possible variation in tube properties were studied by performing similar tests on segments cut from another tube. Variation in tube properties was also studied for the long configuration, by testing three segments from different tubes. For both configurations, to eliminate variations due to possible lack of precision in mounting the compliant segments on the rigid tubing, each segment was tested, removed, and retested. Three values of external pressure were recorded for each value of internal pressure.

Steady flow tests

Steady flow in the system was maintained by means of the constant head tank with overflow mechanism shown in Figures 14 and 15. This system maintained a constant value of upstream pressure to within about 1 mm of water. Flow entered the test section through a long (∿100D), circular rigid pipe, (to minimize entrance effects), and was controlled by the adjustable clamp resistances R_1 and R_2, which were applied to the flexible plastic tubing upstream and downstream of the test section, as shown in Figure 16. All of the tubing downstream of the connection to the constant head tank (except for the test segment) had a 1/4 inch internal diameter.

The steady flow tests were run at a constant value of upstream pressure, so that flow was controlled predominantly by the downstream resistance, as is typical of the circulation. Two values of upstream pressure (54.5 and 69.5 cm water) were studied for the short segment and one value (54.5 cm water) was studied for the long segment. The additional value of P_1 for the short segment was used in an attempt to determine if P_1-P_e is the driving pressure for that type of configuration, as it was found to be for collapsible tubing alone. Since collapse of the long segment was similar to that of collapsible tubing alone, the long segment was only studied for one value of P_1. The values of P_1 selected allowed for a wide range of Reynolds numbers in the physiologic range of interest.

Tests were run for constant values of P_1-P_e, which was varied for a given P_1 by varying P_e. Thus, for a given test, P_1-P_2 was varied with flow rate. The external pressure was always less than upstream pressure, and was applied in increments of 10 cm of water, beginning with the highest value that did not significantly alter the pressure-flow relation from that

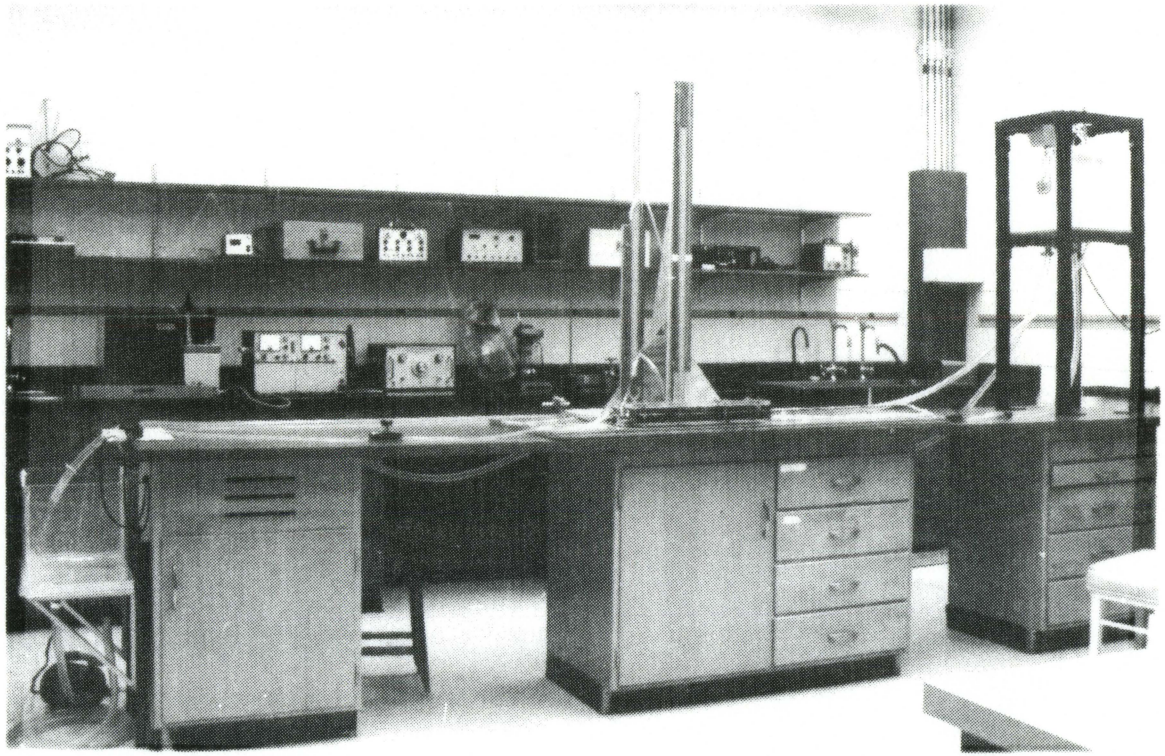

Figure 14. Photograph of the steady flow apparatus

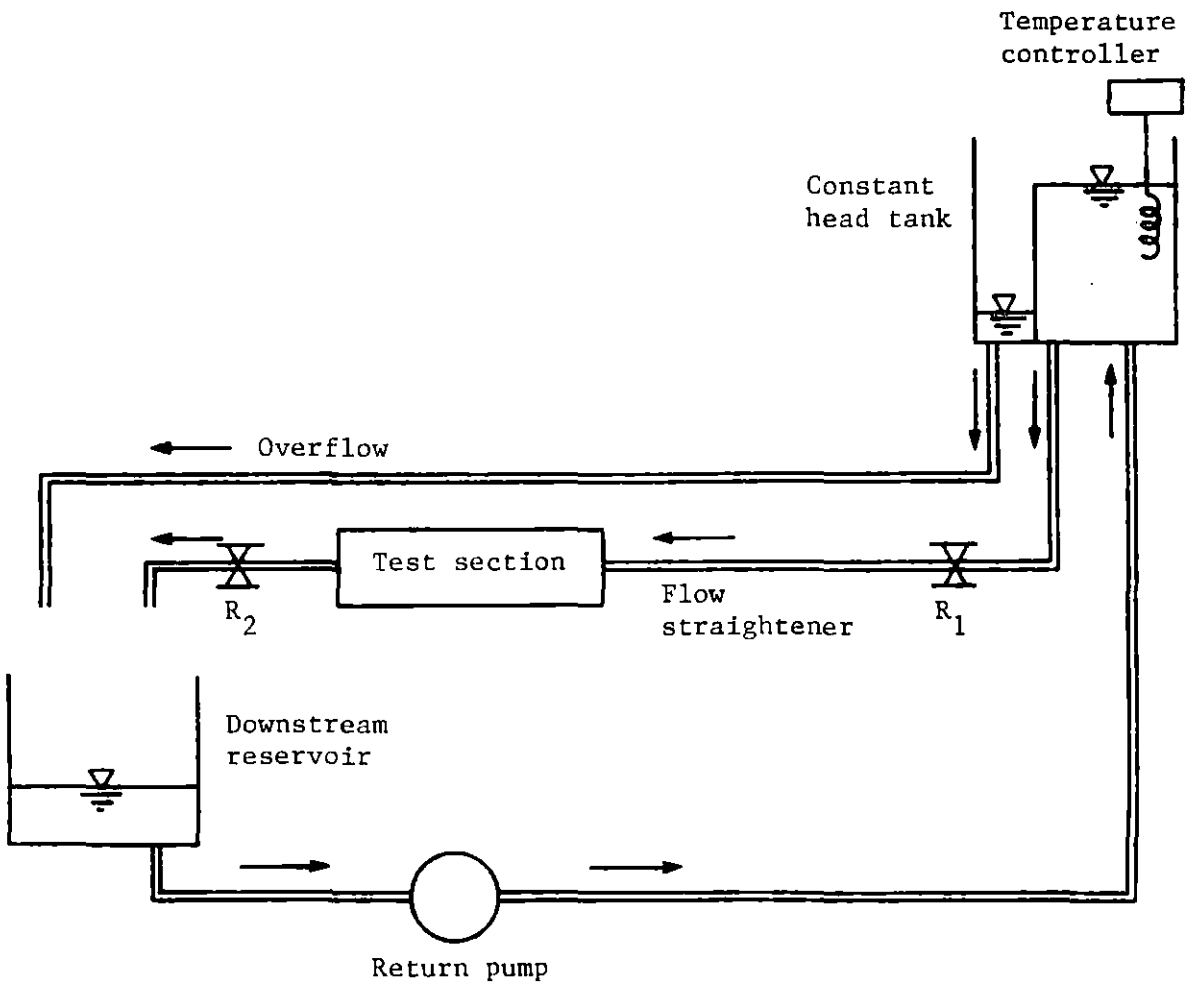

Figure 15. Schematic diagram of steady flow system

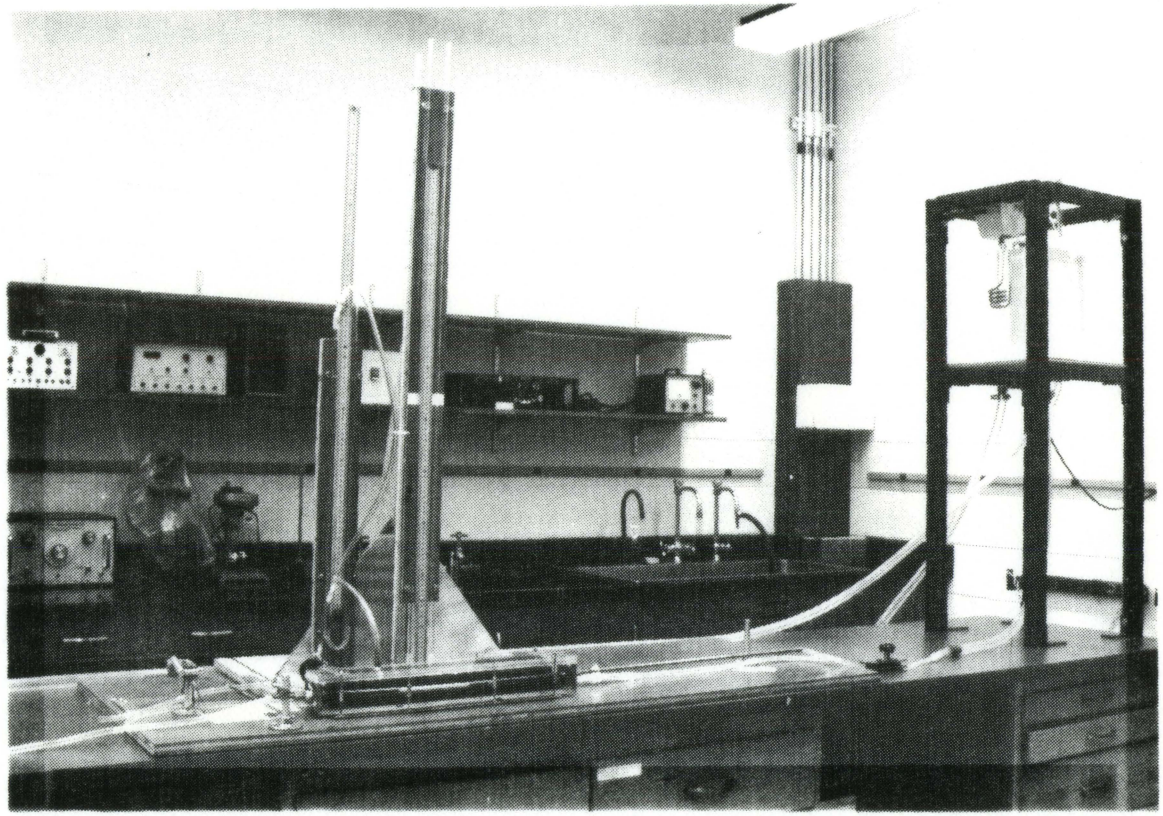

Figure 16. Close-up of the steady flow system parameters

of zero external pressure. Tests on rigid stenoses (for the short configuration) were done for comparison with the tests on compliant stenoses at zero external pressure. Rigidity was achieved by encompassing the stenosed segment with Permatex®[1] RTV Blue gasket maker, which was subsequently removed to perform the compliant tests.

Upstream and downstream pressures were measured with water manometers and external pressure was measured with a U-tube manometer. Pressure drop due to the stenosis was estimated by subtracting the Poiseuille losses between the two pressure taps from the calculated values of P_1-P_2. The pressure drop for Poiseuille flow is given by

$$\Delta P_p = \frac{128\mu LQ}{\pi D^4} \tag{10}$$

Flow rate was measured by timed collection in a graduated cylinder, over a period of 30 seconds.

The pressure-flow data were collected for Reynolds numbers ranging from approximately 700 to 3500 for the 75% stenosis, 400 to 2800 for the 85% stenosis, and 300 to 1900 for the 89.4% stenosis. Poiseuille losses were most significant at the lower Reynolds numbers for the 75% stenosis (being as high as 20 percent of the total pressure drop) and were much less significant at higher Reynolds numbers and percent stenoses. Estimation of the pressure just upstream of the stenosis by subtracting the Poiseuille loss between the upstream pressure tap and the stenosis indicated that the upstream pressure was within 2% of the fixed proximal pressures (69.5 and

---

[1]No. 80627, Loctite Corporation, Kansas City, Kansas.

54.5 cm water).

To observe the amplitude and frequency characteristics of the tube oscillations that sometimes occurred, P_2 and the pressure in the center of the stenosis, P_s, were recorded using a strain gauge pressure transducer and a dynograph recorder. These recordings were only made for the 75% stenosis. Further details regarding apparatus specifications and accuracy of measurements are given in the Appendix.

RESULTS AND DISCUSSION

The steady flow behavior of compliant stenoses subjected to external pressure deviated greatly from rigid stenosis behavior. For both the long and short configurations, the pressure-flow relations more closely resembled those found in past studies on collapsible tubing, for which flow behaved essentially as it would in a rigid tube up to a critical transmural pressure, and became independent of downstream pressure beyond the critical pressure. Thus, to adequately describe compliant stenosis flow, a two-regime model of some sort is needed. The present study used a very simple kind of two-regime model: a rigid-type relation similar to Equation (5), valid up to the critical transmural pressure, and a constant flow equation, valid for the region of flow limitation.

Static Tests

Static tests were performed on each configuration to empirically estimate the critical collapse pressures (P_{cr}) which would cause significant deviation from rigid stenosis flow.

Short configuration

The collapse pressures for the short segments were found to be a function of percent stenosis, increasing as percent stenosis increased. The higher collapse pressures for the more severe stenoses may be attributed to the lower $\ell_c/(\pi D)$ ratios for those stenoses. That is, the more severe stenoses provided greater structural support to the tubing than did the 75% stenosis. The average values of collapse pressure (external pressure minus internal pressure) for the 75%, 85% and 89.4% stenoses were 20.3, 31.9, and 33.0 cm water, respectively. No appreciable differences in

collapse pressures were found between the first and second mounting of a given segment, or between one tube and another for a given percent stenosis.

Long configuration

Percent stenosis was not a consideration in collapse of the long segment, since collapse was not in the stenosis, but downstream of it. Thus, the major potential source of variability for the long segment was variance of tube thickness and elasticity. For the three tubes tested, the following average collapse pressures were measured: 4.5, 4.7, and 4.2 cm water. The average of these three values is 4.5 cm water. The values for the long segments were considerably lower than those for the short segments because the collapsible portion of the long segment was not structurally supported by the stenosis (except for end effects), as was the collapsible portion of the short segment. Also, the percent reduction in cross-sectional area for "collapse" was smaller for the long segment than for the short segment. As with the short configuration, all values for a given tube at various internal pressures were within several mm water of each other. Since the long section collapsed into an approximately elliptical cross-section, a comparison between the experimentally determined critical pressure and the theoretically derived critical pressure of Equation (4) should be made. Using the approximate value of elastic modulus given in the previous section, Equation (4) predicts a critical pressure of 4.7 cm water. This theoretical value compares well with the average experimental value of 4.5 cm water.

The results of the static tests are summarized in Table 2. The tests were only intended to provide estimates of the transmural pressures that

Table 2. Summary of statically determined critical collapse pressures

Stenosis[a]		Average measured P_{cr} (cm water)	Standard deviation σ (cm water)	Number of internal pressures studied
75%	S	20.3	0.29	5
85%	S	31.9	0.47	4
89.4%	S	33.0	0.28	4
75%	L	4.5	0.30	6
85%	L	4.7	0.27	6
89.4%	L	4.2	0.31	6

[a] S = short configuration, L = long configuration.

would cause flow limitation in the steady flow experiments. Since the tests were static, thus excluding fluid dynamic considerations, the collapse pressures measured may not accurately predict the critical values for steady flow conditions.

Steady Flow Studies

The results of the steady flow tests are presented in a variety of ways. First, comparisons between the rigid and compliant (zero external pressure) configurations for the short segment are made. Second, the (pressurized) pressure drop and flow data for each configuration at a given upstream pressure and percent stenosis are presented, including data on oscillations for the 75% stenosis. Then, to get an idea of the effective severity of the segments in the collapsed state, zero external pressure data for the higher values of percent stenosis are plotted with the data for lower values of percent stenosis. Next, comparisons between the short and long configurations are made. Then, to determine if (P_1-P_e) is the driving pressure for the short configuration, as it was found to be for unstenosed collapsible tubes, the basic data for the two values of P_1 for a given percent stenosis are considered together. Following that is an examination of the applicability of the statically determined collapse pressures and the importance of (P_e-P_2), presented by partitioning the basic curves into regions for which (P_e-P_2) is less than zero, greater than zero but less than P_{cr}, and greater than P_{cr}. Finally, the experimental pressure-flow data are plotted against the values predicted by the segmented model.

Results of the (short) rigid vs. compliant configuration

Some differences between rigid and compliant stenosis flow at zero external pressure were expected, since compliancy allows for passive expansion and contraction of the tube with changes in internal pressure. The differences found between rigid and compliant stenosis flow are shown in Figures 17 and 18. For a given percent stenosis, the pressure-flow relations for the rigid stenoses at both values of P_1 were essentially the same, as expected, but the relations for the compliant stenoses differed from each other at different values of P_1, and deviated more from the rigid configuration at the higher value of P_1. For a given pressure drop, flow through the rigid stenosis was less than flow through the compliant stenosis, except for the 89.4% stenosis at low values of P_2 (corresponding to high flow rates). This implies that a small passive contraction occurred when the pressure in the stenosis fell sufficiently, as a result of the Bernoulli effect. It also implies that percent stenosis was not constant for the compliant configuration.

Results for the pressurized compliant configurations

Each of the plots of the compliant pressure-flow data is for a single value of percent stenosis and upstream pressure. Data for different values of external pressure are distinguished by different symbols, and regions in which the tube exhibited oscillations are identified by dotted lines.

Short configuration Pressure-flow relations for the short configuration are shown in Figures 19-24, and the data are listed in the Appendix. For a given percent stenosis, the behavior of the short segments was qualitatively the same for both values of upstream pressure; however, the behavior for different values of percent stenosis was not the

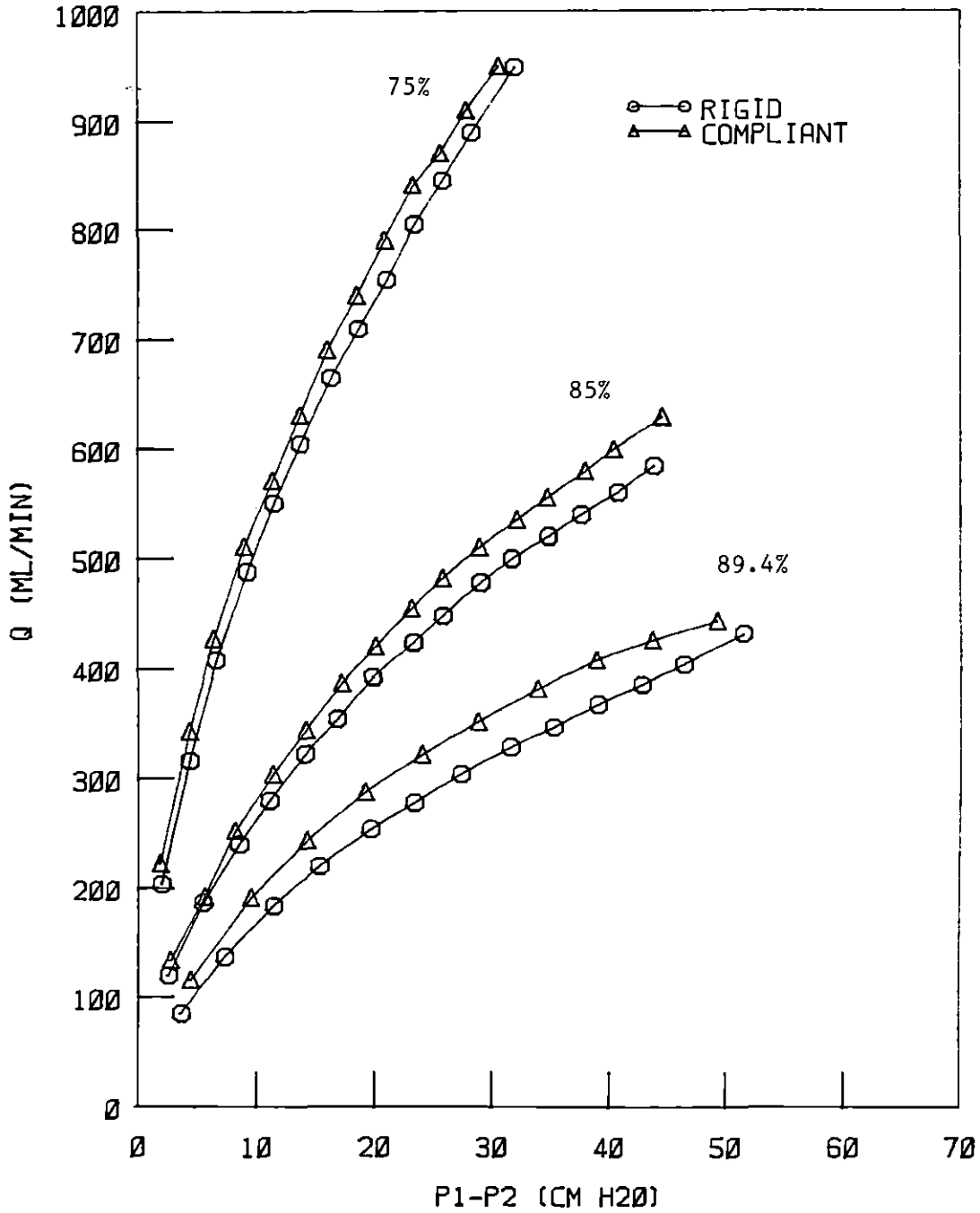

Figure 17. Pressure-flow data for the short rigid vs. compliant (PE=0) configurations at an upstream pressure of 54.5 cm water

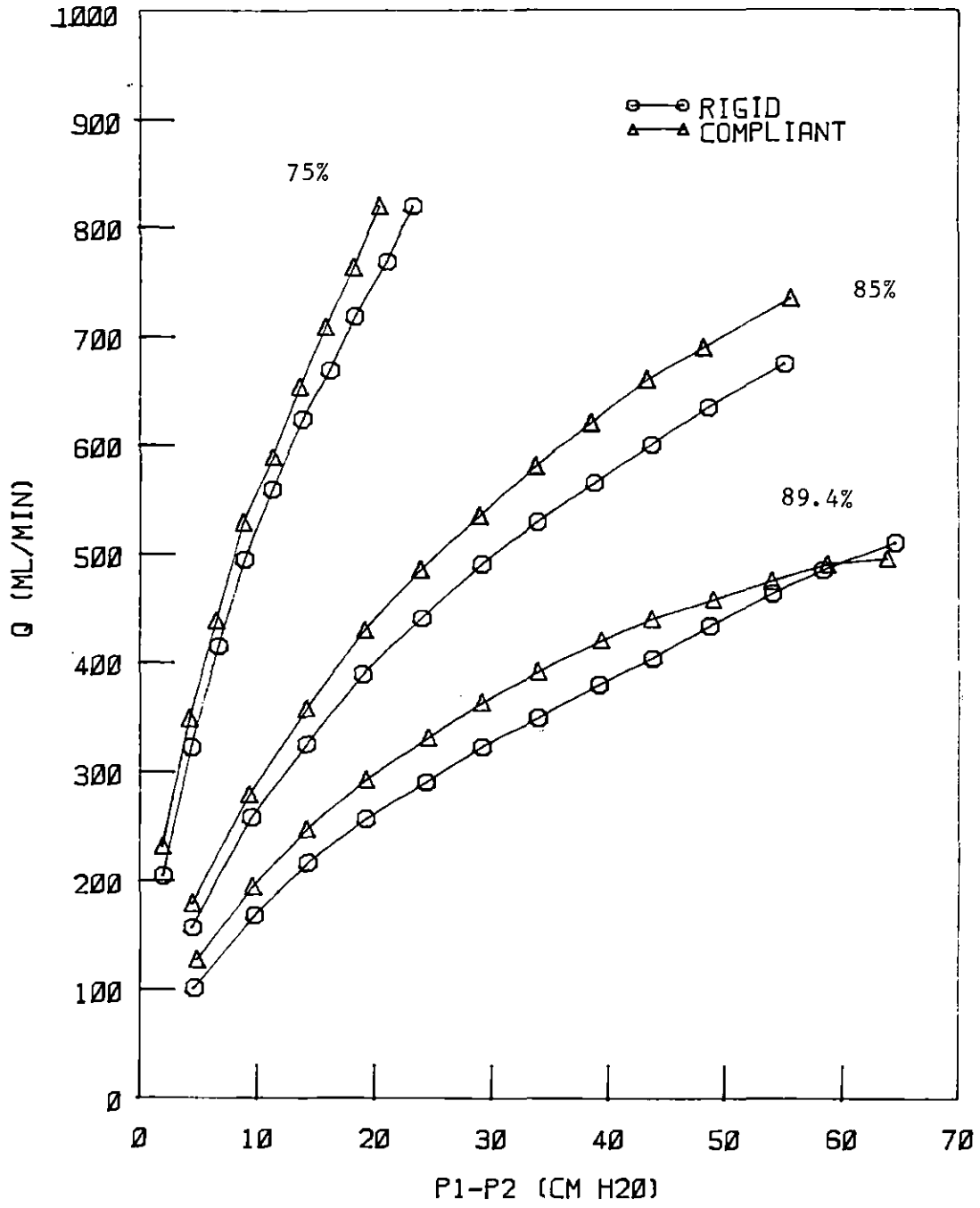

Figure 18. Pressure-flow data for the short rigid vs. compliant (PE=0) configurations at an upstream pressure of 69.5 cm water

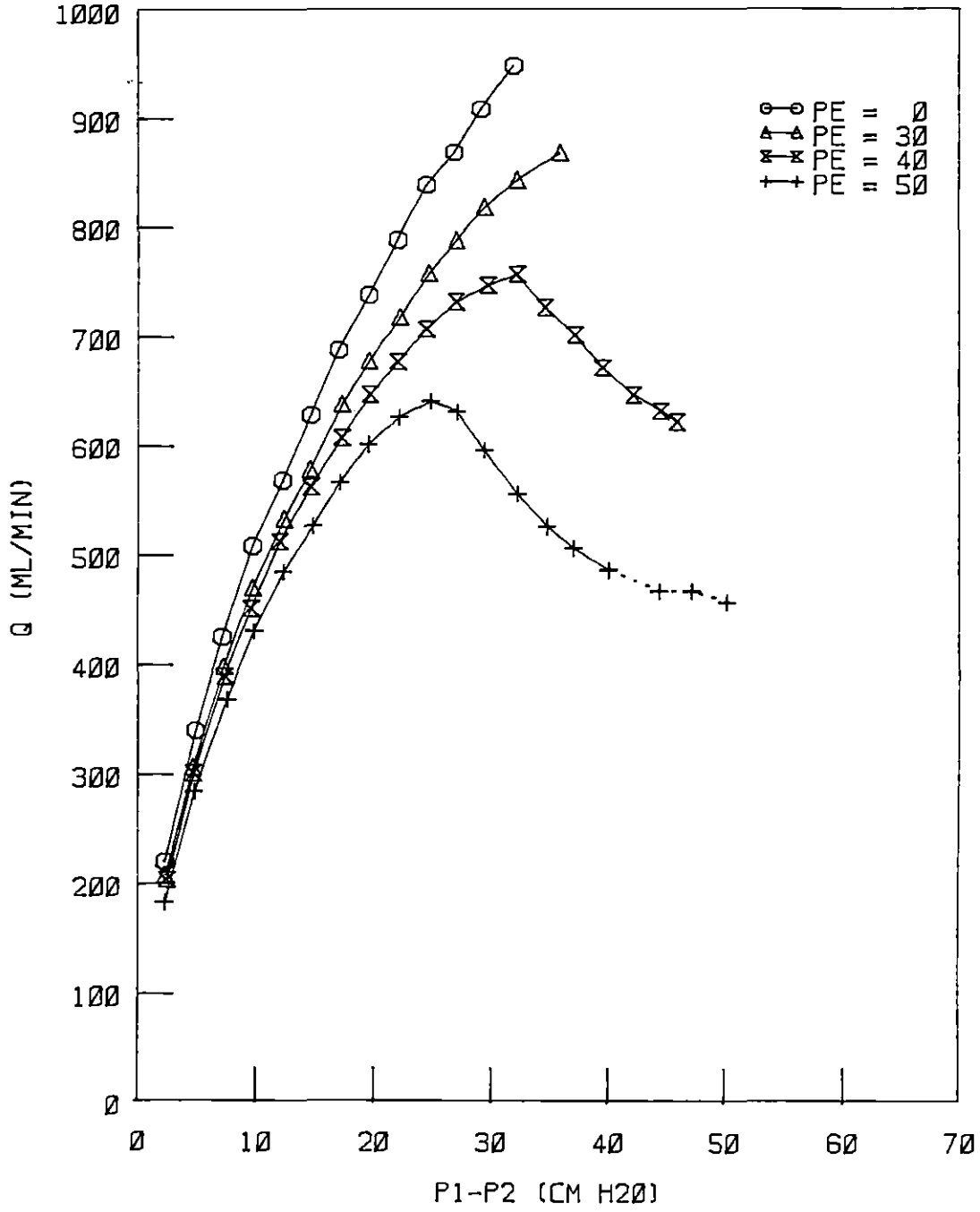

Figure 19. Pressure-flow data for the short compliant 75% stenosis at an upstream pressure of 54.5 cm water (all pressures in cm water, dotten lines denote oscillations)

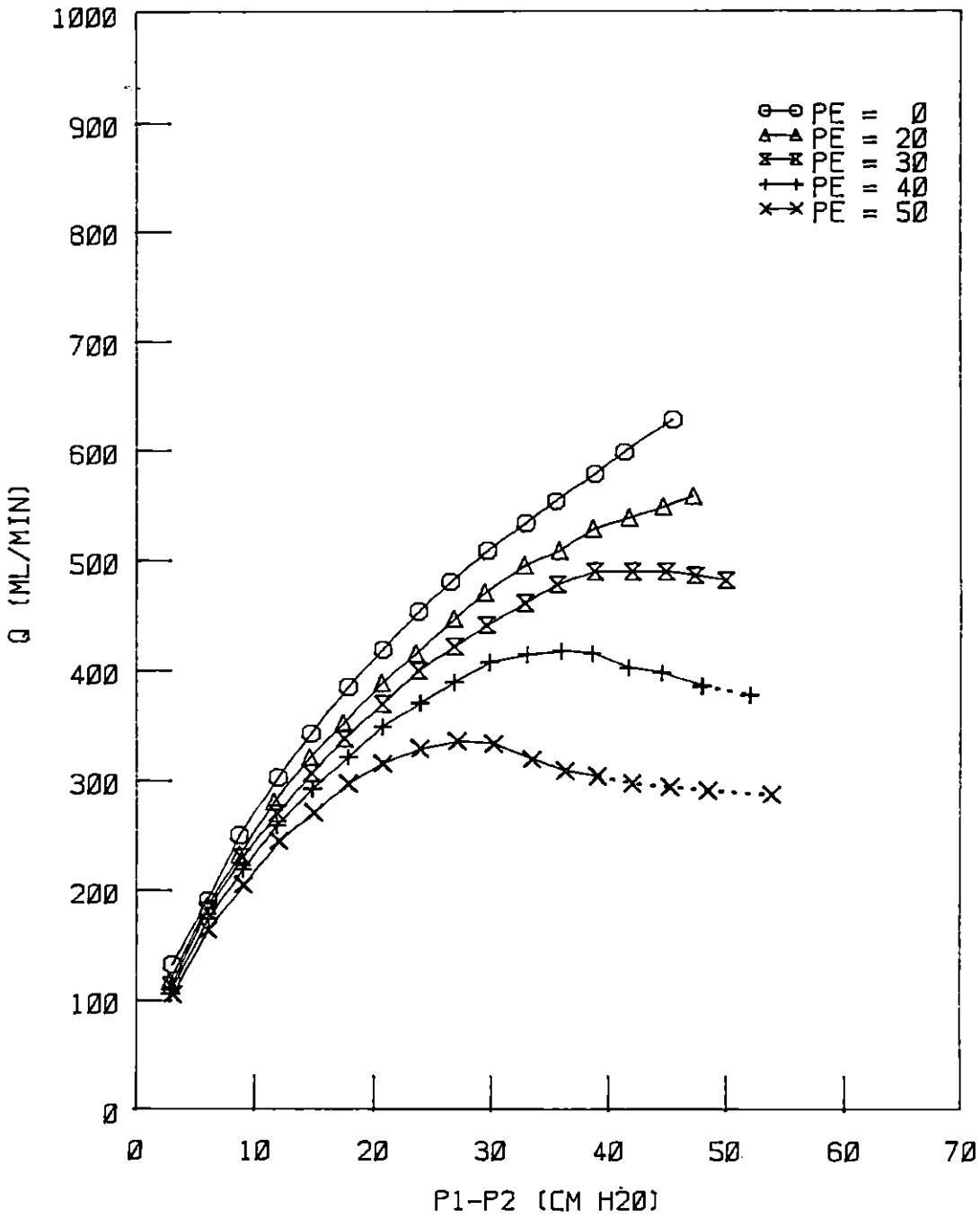

Figure 20. Pressure-flow data for the short compliant 85% stenosis at an upstream pressure of 54.5 cm water (all pressures in cm water, dotted lines denote oscillations)

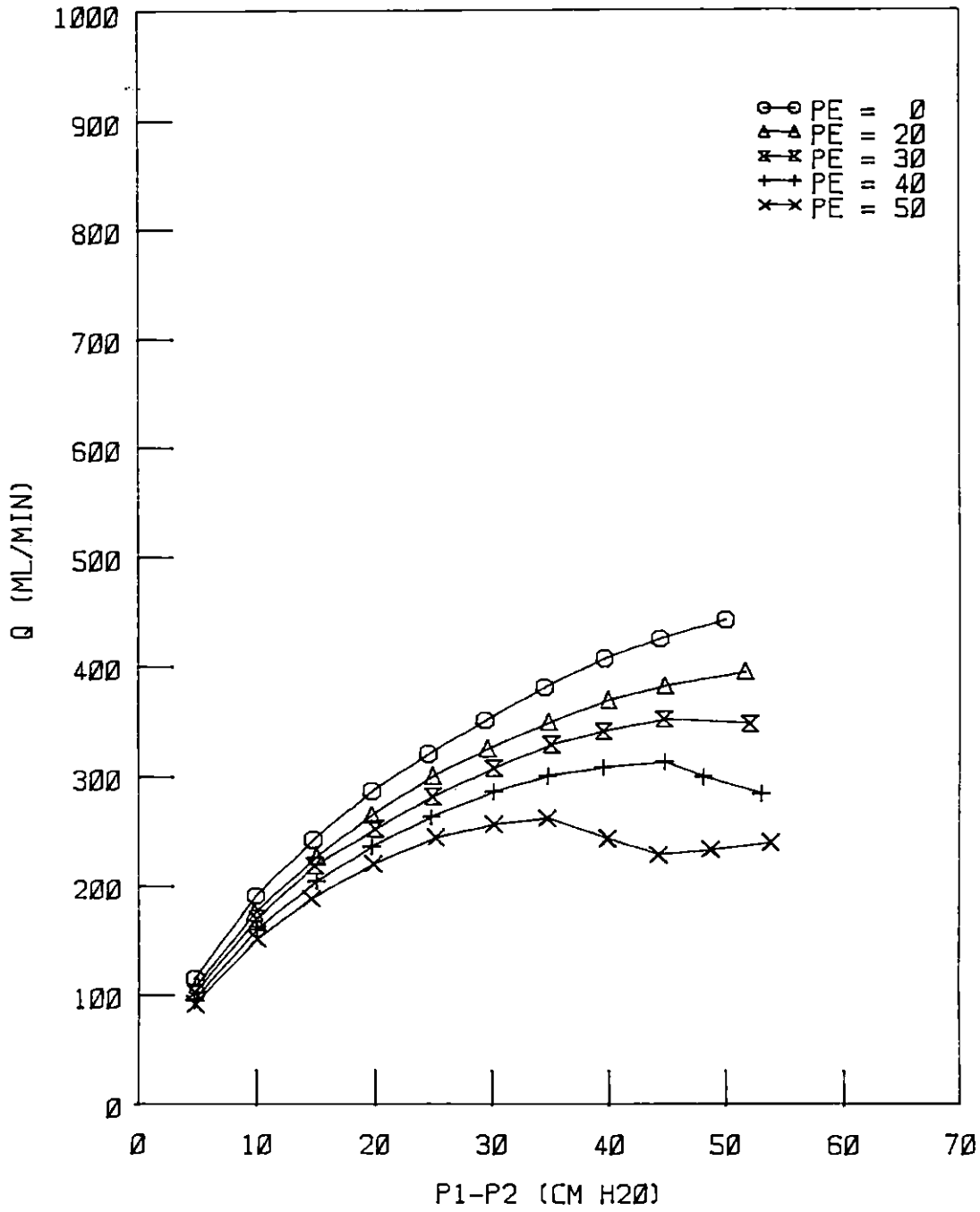

Figure 21. Pressure-flow data for the short compliant 89.4% stenosis at an upstream pressure of 54.5 cm water (all pressures in cm water, dotted lines denote oscillations)

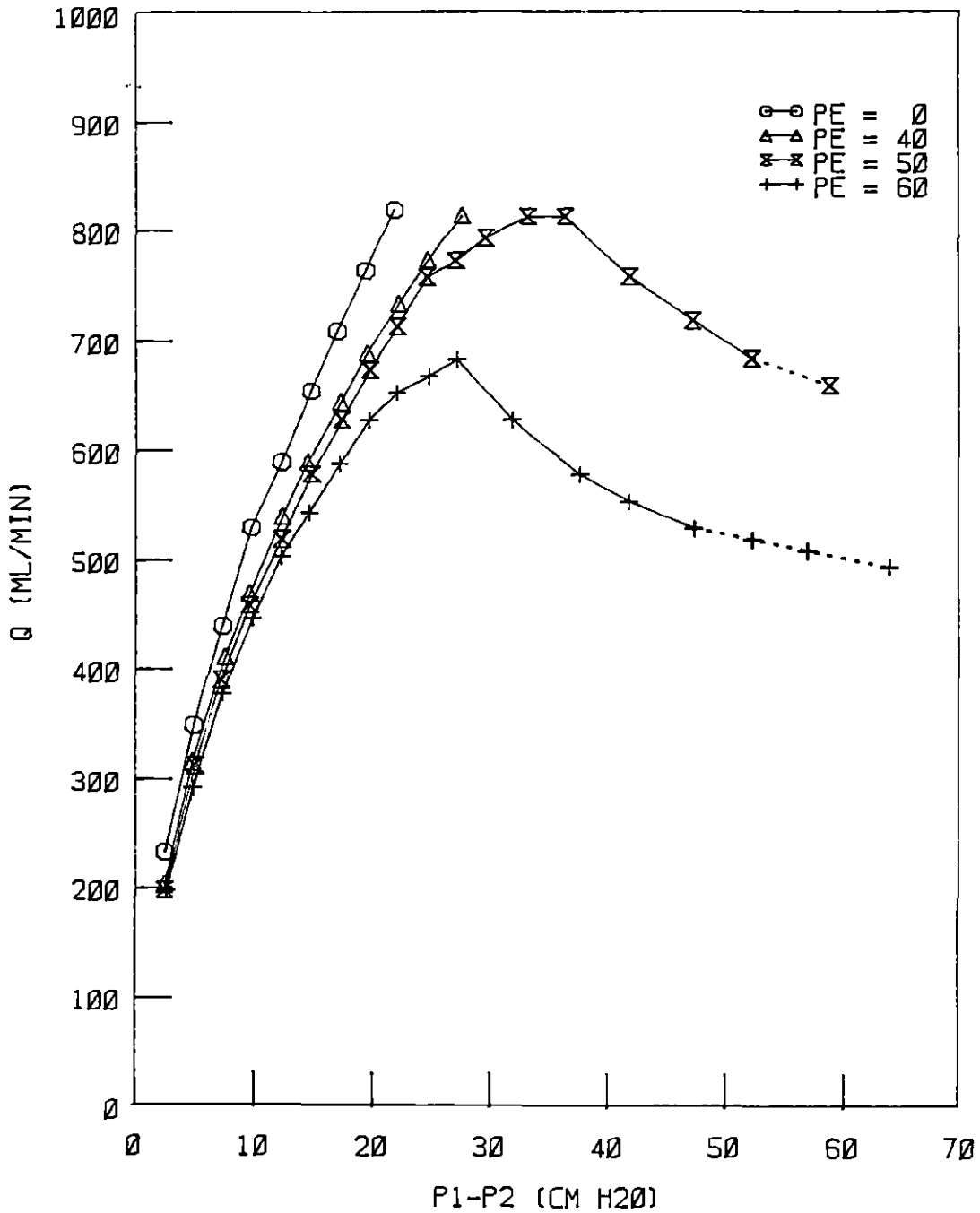

Figure 22. Pressure-flow data for the short compliant 75% stenosis at an upstream pressure of 69.5 cm water (all pressures in cm water, dotted lines denote oscillations)

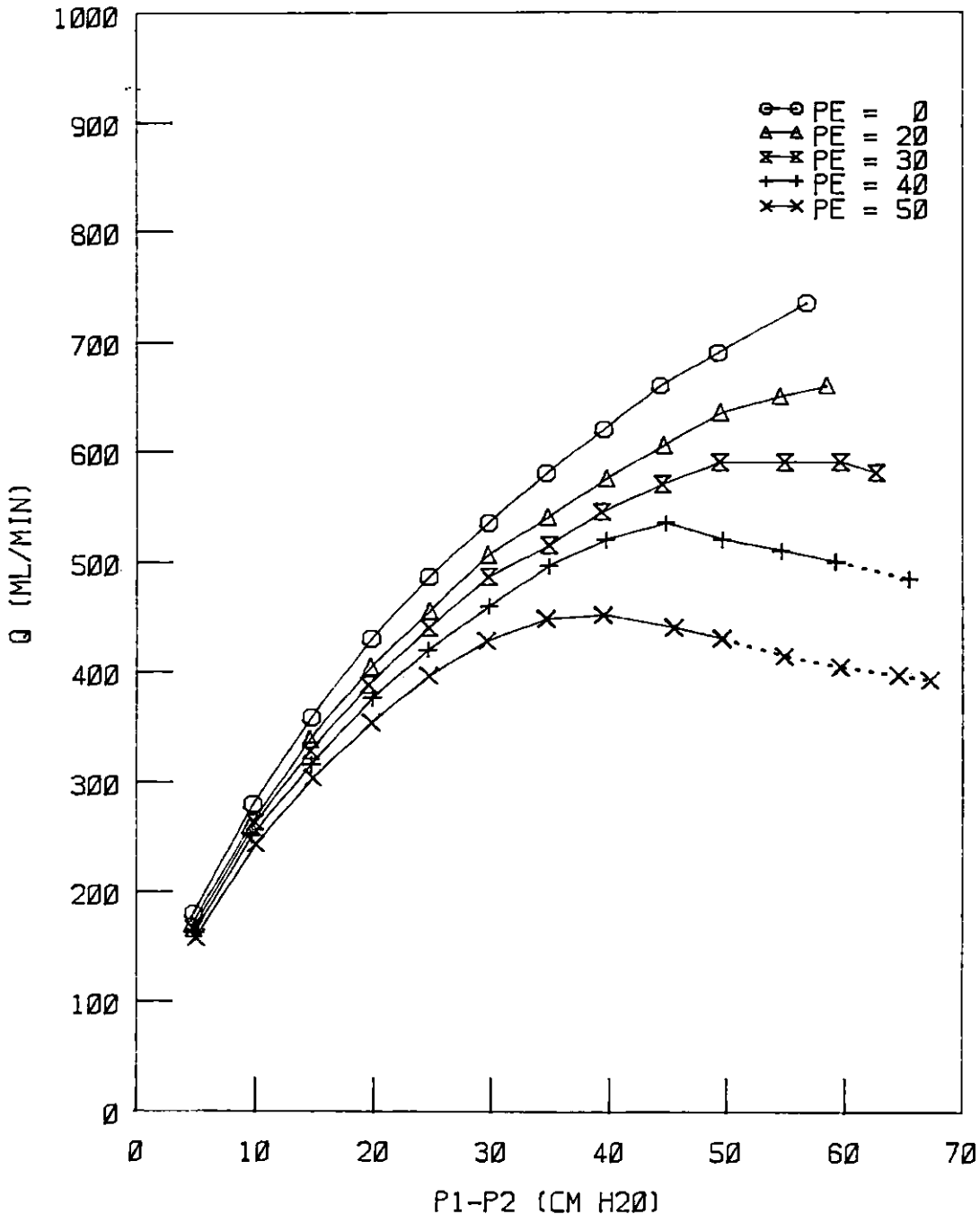

Figure 23. Pressure-flow data for the short compliant 85% stenosis at an upstream pressure of 69.5 cm water (all pressures in cm water, dotted lines denote oscillations)

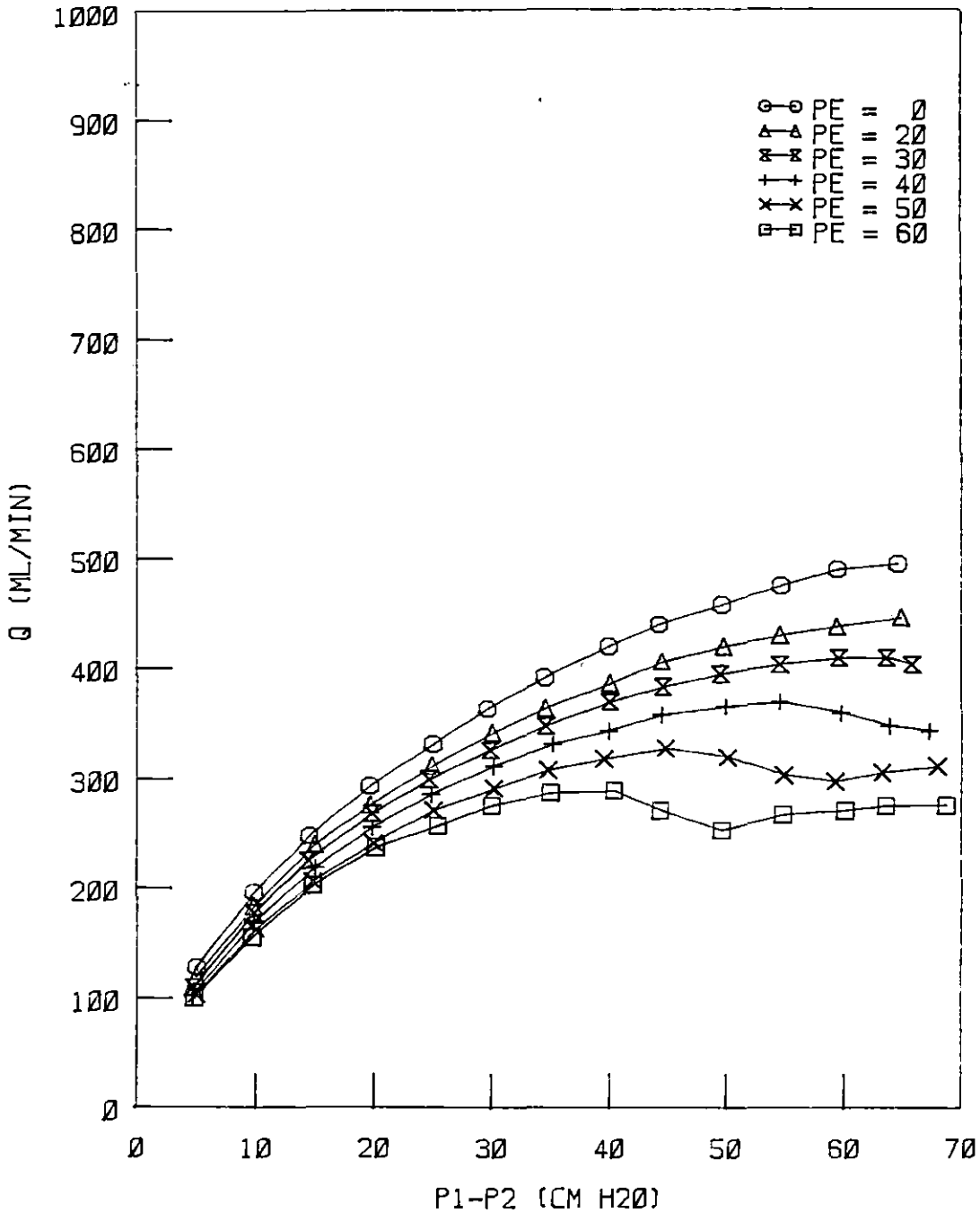

Figure 24. Pressure-flow data for the short compliant 89.4% stenosis at an upstream pressure of 69.5 cm water (all pressures in cm water, dotted lines denote oscillations)

same. For values of external pressure sufficiently high to cause collapse, flow in the 75% stenosis reached a maximum and dropped off abruptly after a critical point was reached, and when the tube started to oscillate (beyond the critical point) flow tended to level off. Flow in the 85% and 89.4% stenoses decreased much more gradually after reaching a maximum, and oscillations occurred for the 85% stenosis but not for the 89.4% stenosis. For all cases, the maximum flow reached prior to collapse decreased with increasing external pressure for a given P_1.

Collapse of the tube in the stenosed region occurred at the downstream end of the stenosis, and was large, especially for the 75% stenosis. Figure 25 shows side views of the 75% stenosis in the open and collapsed states.

Oscillations for the 75% and 85% stenoses occurred in the negative dynamic resistance regions, and were at high frequencies, as high as 35 cycles/second for the 75% stenosis. Recordings of the downstream pressure for the 75% stenosis at two values of P_2 are shown in Figure 26. The amplitude was larger for the lower value of P_2 and the frequencies were about the same for both values of P_2. These oscillation characteristics are summarized in Table 3.

The oscillation measurements taken in the stenosed area (at the center, upstream of the collapsed portion) were of the same shape as those measured at the downstream pressure tap, but were of much larger amplitude. They are shown in Figures 27 and 28 for various values of downstream and external pressure. The amplitude was larger at lower values of P_2 and was smaller for larger values of P_e. Frequencies were higher at the higher

Figure 25. Close-ups of the short configuration in the open and collapsed states (75% stenosis)--dashed lines outline the stenosis

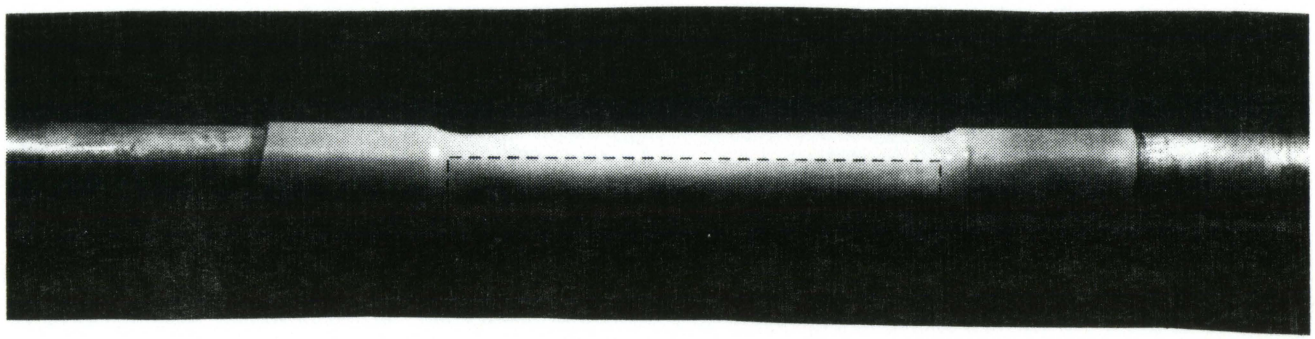

(a) OPEN: $P_1 = 54.5$, $P_e = 0$ cm water

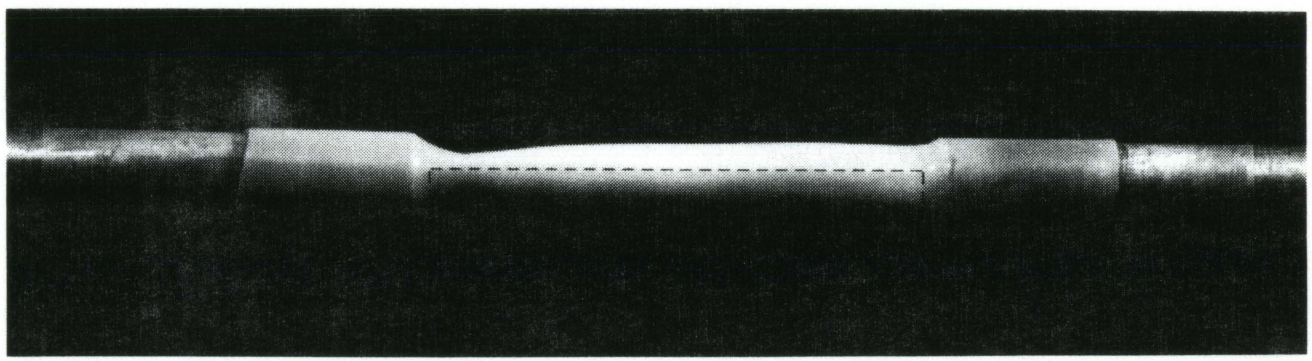

(b) COLLAPSED: $P_1 = 54.5$, $P_e = 50$, $P_e - P_2 = 40$ cm water

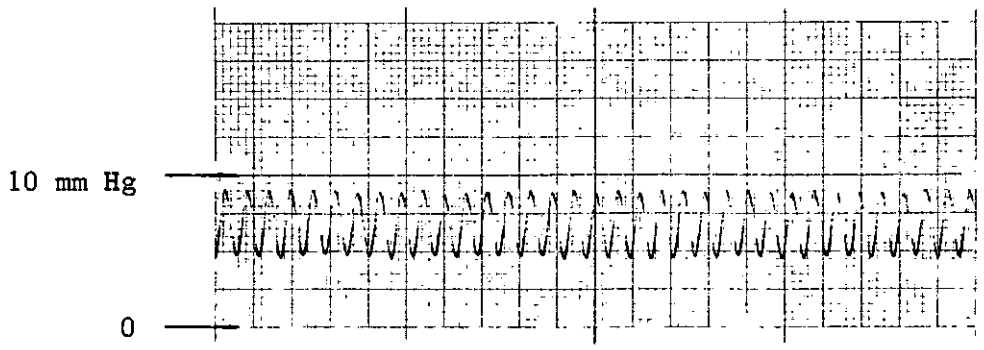

(a) $P_2 \cong 12.7$ cm water

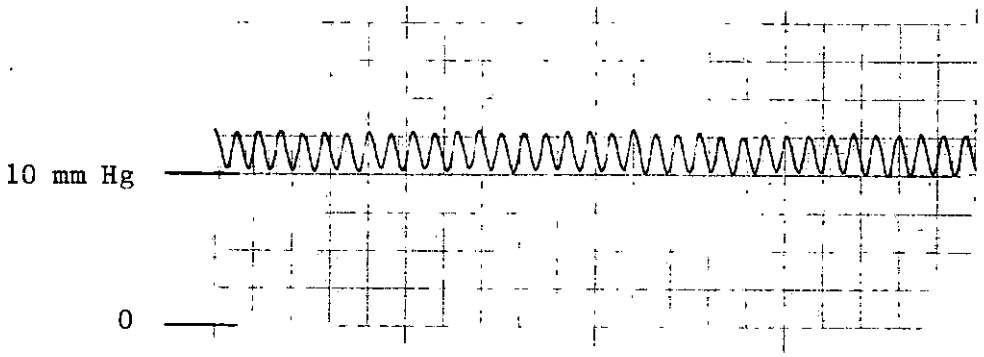

(b) $P_2 \cong 17.4$ cm water

Figure 26. Oscillation recordings of downstream pressure for the short configuration 75% stenosis at P_l = 69.5 cm water and P_e = 60 cm water (chart speed = 100 mm/sec)

Table 3. Frequency and amplitude characteristics of tube oscillations

Stenosis	P_2 (cm water)	P_e (cm water)	Frequency (Hz)	Amplitude (cm water)
75% Short[a]	17.4	60	34.5	3.4
	12.7	60	35.0	5.8
75% Long	17.8	30	1.5	32.2
	16.3	30	1.6	35.6
	27.9	40	1.4	6.8
	25.2	40	1.8	17.0
	22.7	40	2.0	15.3
	20.1	40	3.2	11.9
	17.8	40	3.4	7.8
	37.6	50	1.5	5.1
	35.2	50	?[b]	?[b]

[a]Upstream pressure = 69.5 cm water.

[b]The amplitude was too small to determine the frequency.

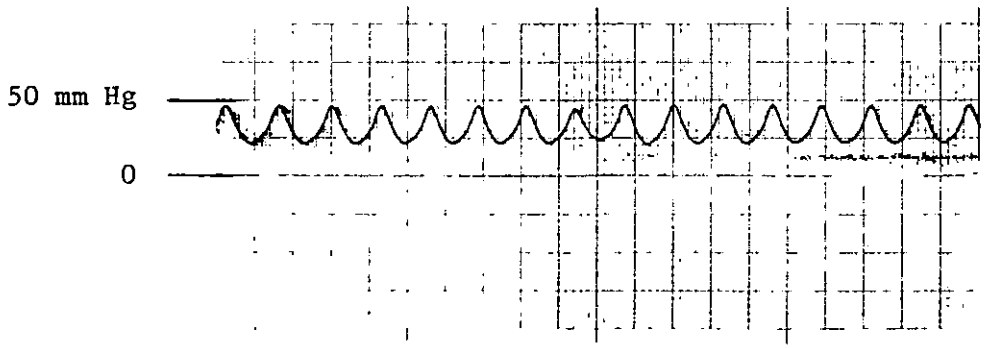

(a) $P_2 \cong 11$ cm water

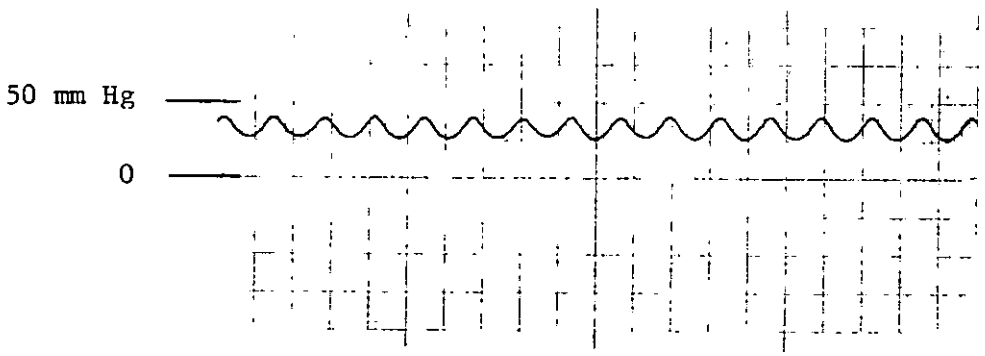

(b) $P_2 \cong 13$ cm water

Figure 27. Oscillation recordings of stenosis pressure for the short configuration 75% stenosis at P_1 = 69.5 cm water and P_e = 50 cm water (chart speed = 100 mm/sec)

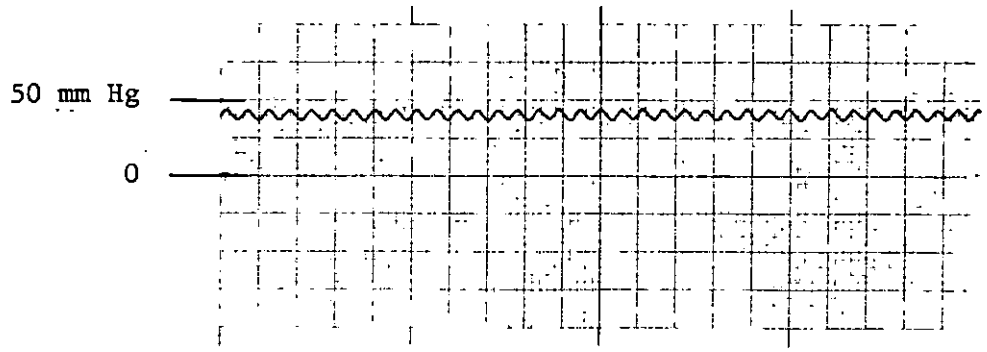

(a) $P_2 \cong 6$ cm water

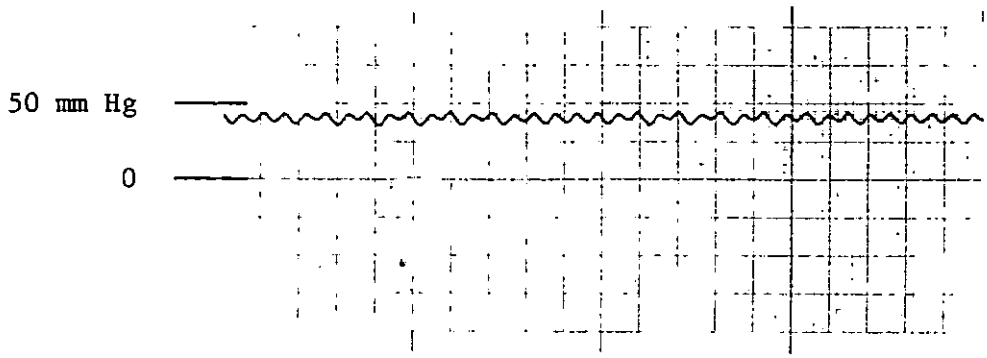

(b) $P_2 \cong 8$ cm water

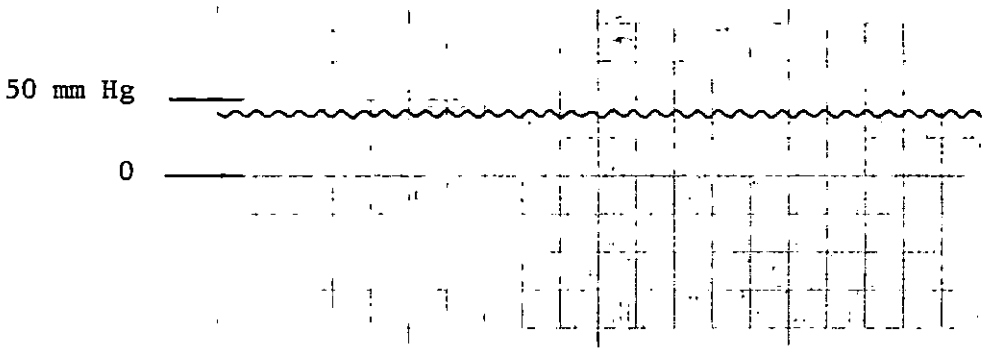

(c) $P_2 \cong 10$ cm water

Figure 28. Oscillation recordings of stenosis pressure for the short configuration 75% stenosis at P_1 = 69.5 cm water and P_e = 60 cm water (chart speed = 100 mm/sec)

value of P_e. These characteristics are summarized in Table 4.

Long configuration Results for the long segments are shown in Figures 29-31 and the data are listed in the Appendix. The behavior was qualitatively similar for all three values of percent stenosis. After a critical transmural pressure was reached, flow essentially leveled off, showing independence of further decreases in P_2. A relatively small decrease in flow (less than 5 percent) before leveling off was seen for the 75% stenosis. The flow rate at which flow leveled off decreased as external pressure increased. Oscillations occurred for all three values of percent stenosis.

Collapse initiated at the downstream end of the tube and progressed upstream to the location of the stenosis, with progressive decrease of P_2 beyond the critical value. Visible collapse did not occur in the stenosed region or upstream of it. Photographs of the tube in the open and collapsed states are shown in Figure 32. As can be seen from these photos, the tube was well into the post-buckling mode at high values of transmural pressure.

Oscillations of the segment at the downstream end occurred for all three values of percent stenosis, but not at all values of external pressure. For the 75% and 85% stenoses, oscillations appeared to initiate after the maximum flow rate was reached, and for the 89.4% stenosis, oscillations appeared to initiate when the maximum flow rate was reached. Recordings of the oscillations for the 75% stenosis are shown in Figures 33-36. The amplitudes were large and of a much different shape than those of the short segments. As shown in Table 3, for a given external pressure,

Table 4. Frequency and amplitude characteristics of P_s

P_2 (cm water)	P_e (cm water)	Frequency (Hz)	Amplitude (cm water)
11	50	16	33.9
13	50	15	20.3
6	60	37	13.6
8	60	37	10.0
10	60	37	6.8

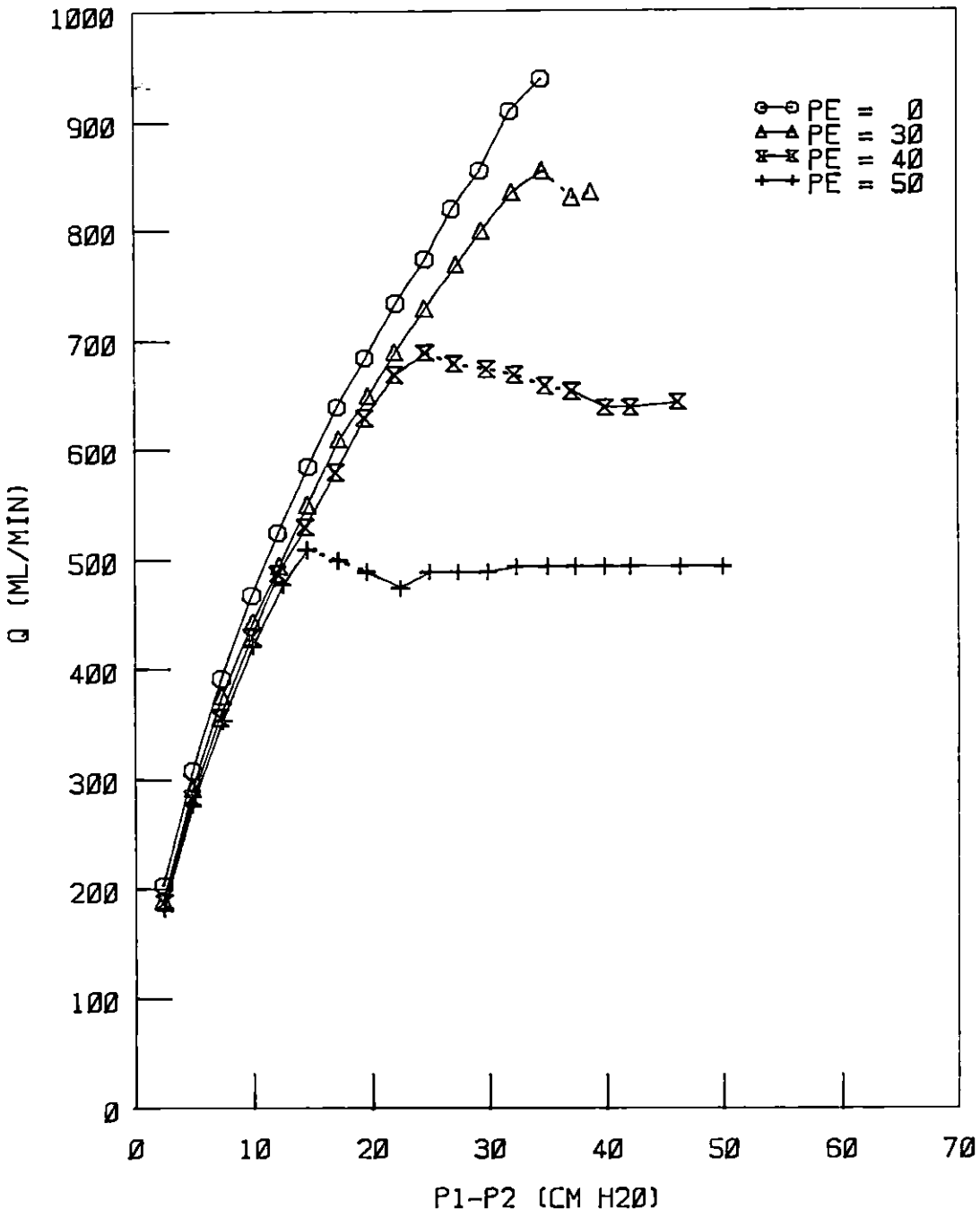

Figure 29. Pressure-flow data for the long compliant 75% stenosis at an upstream pressure of 54.5 cm water (all pressures in cm water, dotted lines denote oscillations)

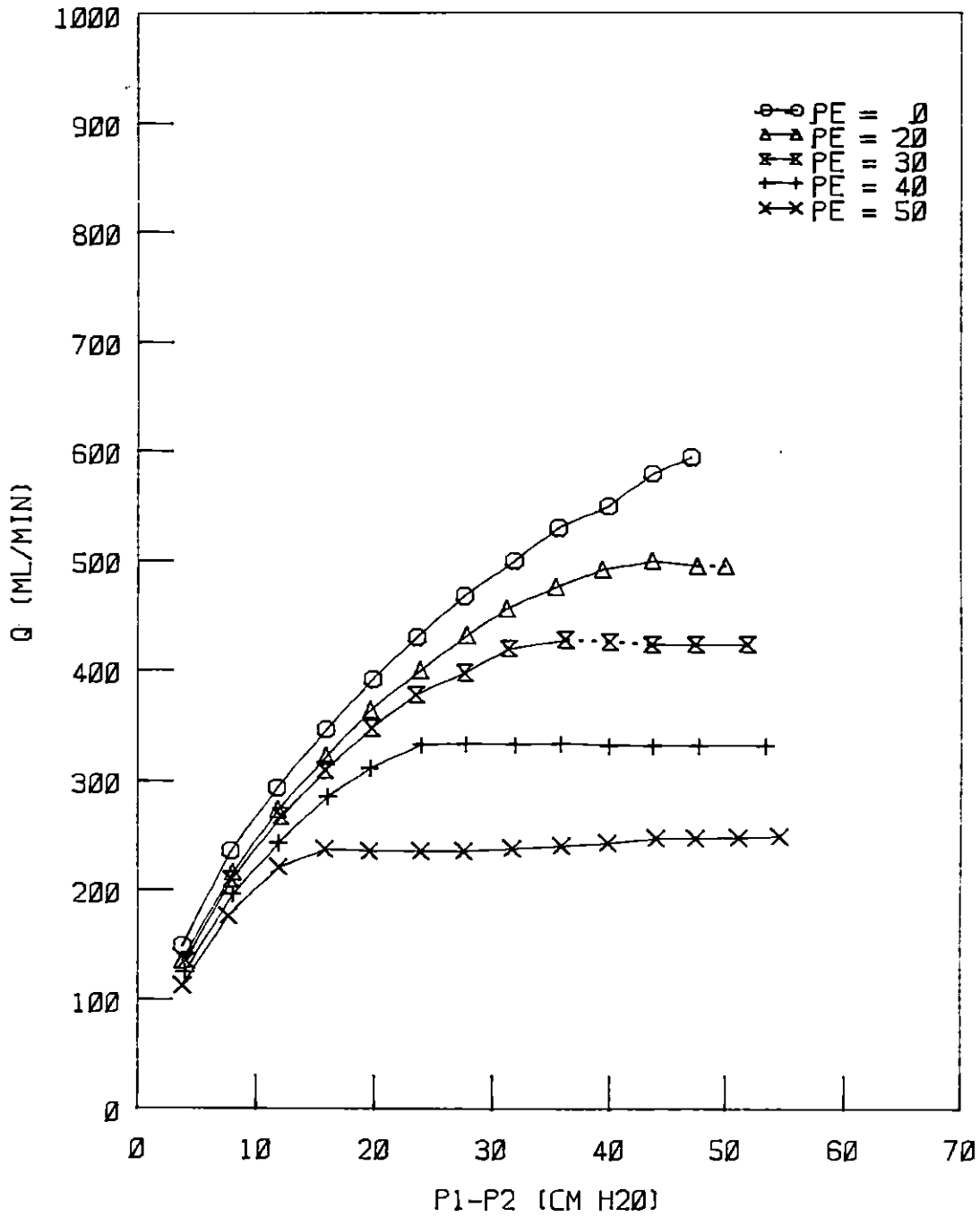

Figure 30. Pressure-flow data for the long compliant 85% stenosis at an upstream pressure of 54.5 cm water (all pressures in cm water, dotted lines denote oscillations)

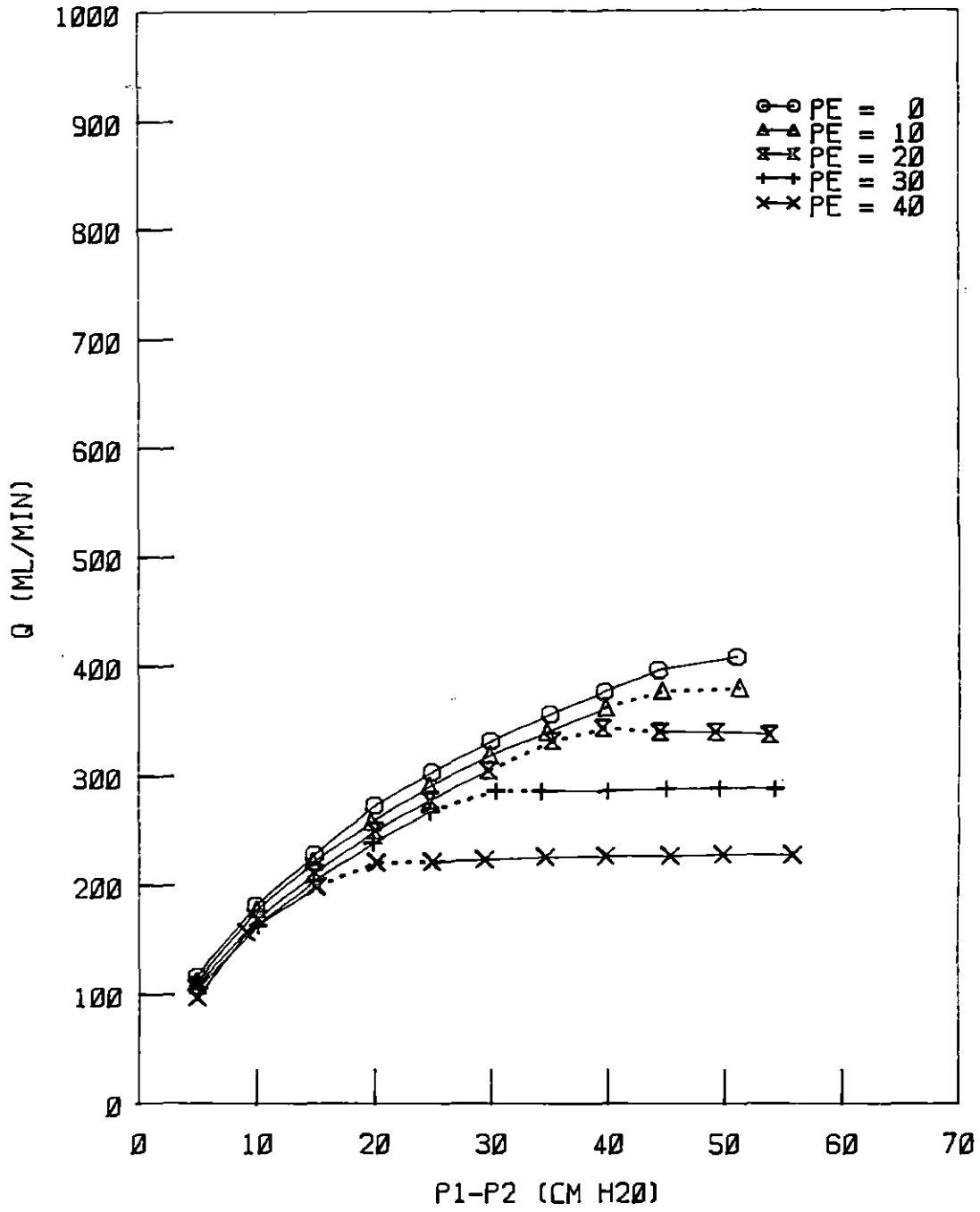

Figure 31. Pressure-flow data for the long compliant configuration at an upstream pressure of 54.5 cm water (all pressures in cm water, dotted lines denote oscillations)

Figure 32. Close-ups of the long configuration in various stages of collapse (75% stenosis)--arrows indicate the location of the stenosis

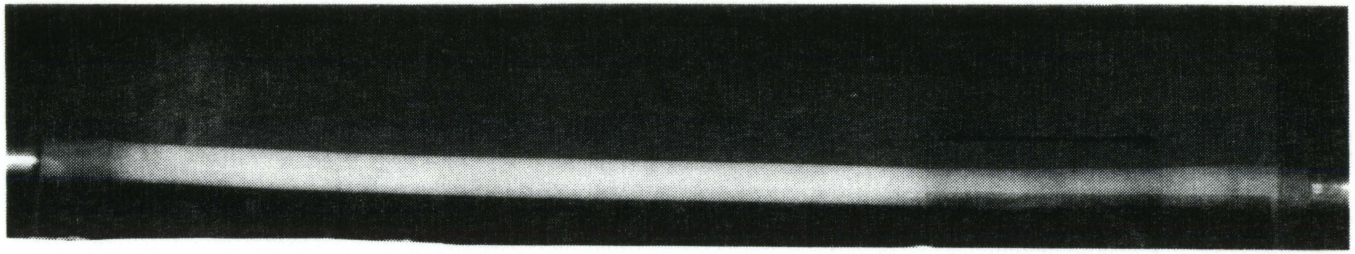

(a) OPEN: $P_e = 0$

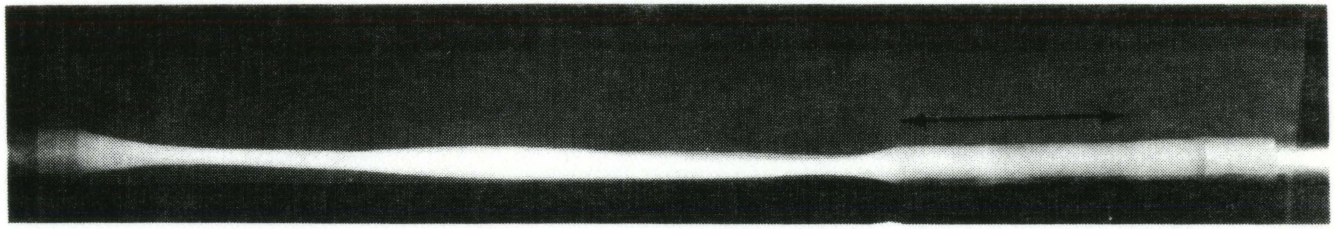

(b) COLLAPSED: $P_e = 30$, $P_e - P_2 = 10$ cm water

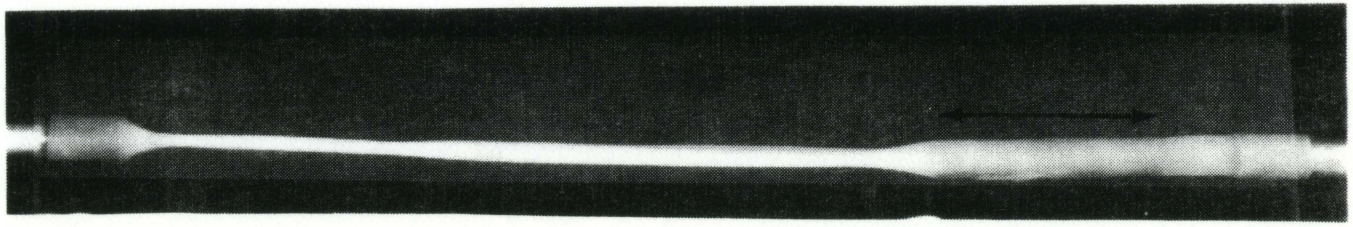

(c) COLLAPSED: $P_e = 50$, $P_e - P_2 = 40$ cm water

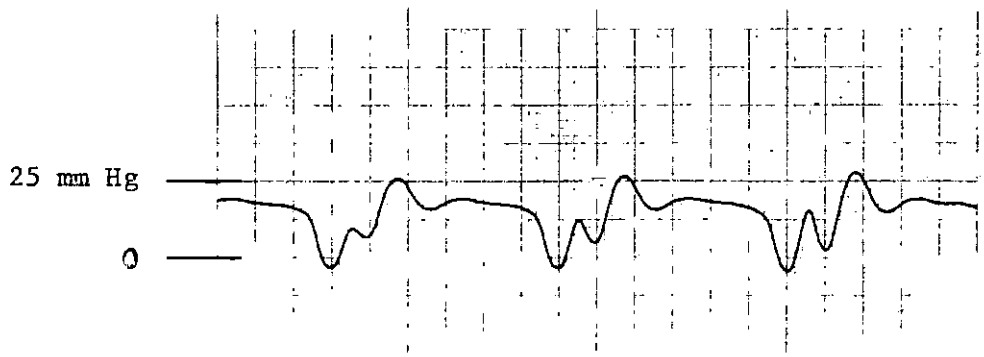

(a) $P_2 \cong 16.3$ cm water

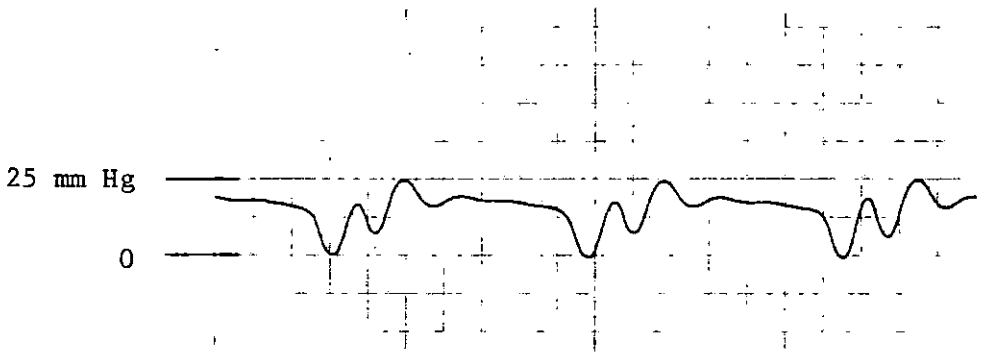

(b) $P_2 \cong 17.8$ cm water

Figure 33. Oscillation recordings of downstream pressure for the long configuration 75% stenosis at P_1 = 54.5 cm water and P_e = 30 cm water (chart speed = 50 mm/sec)

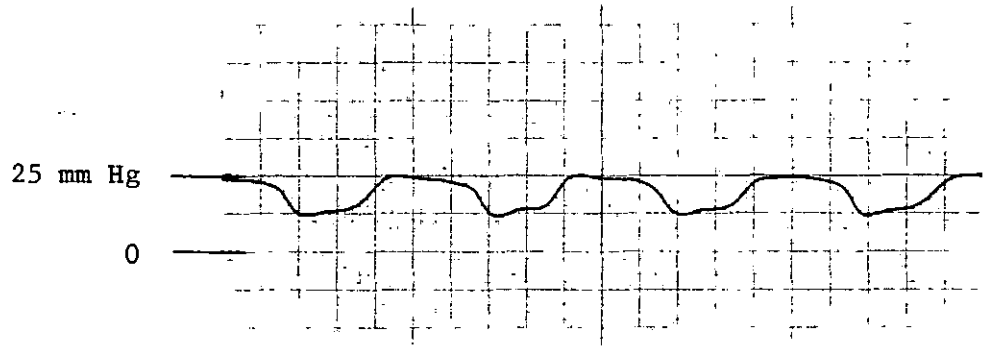

(a) $P_2 \cong 17.8$ cm water

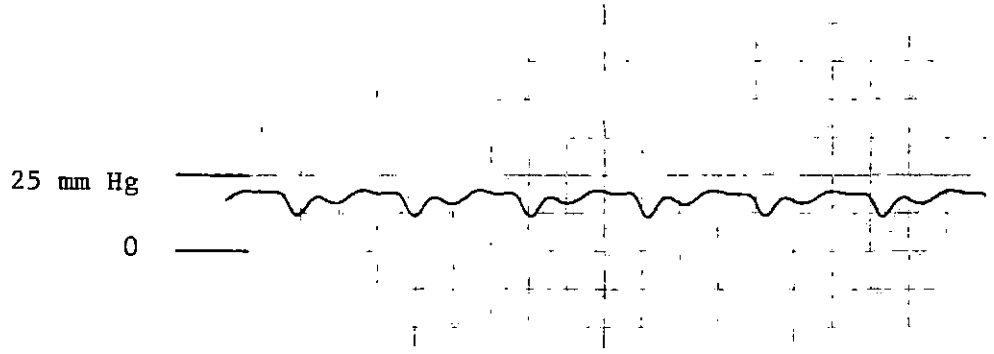

(b) $P_2 \cong 20.1$ cm water

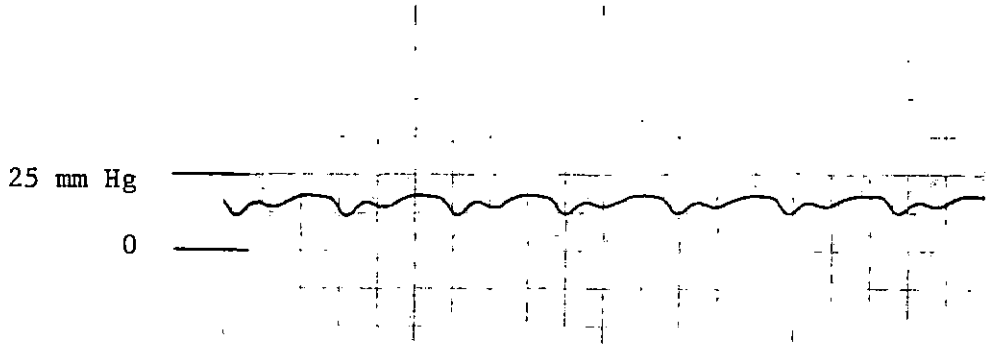

(c) $P_2 \cong 22.7$ cm water

Figure 34. Oscillation recordings of downstream pressure for the long configuration 75% stenosis at P_1 = 54.5 cm water and P_e = 40 cm water (chart speed = 50 mm/sec)[1]

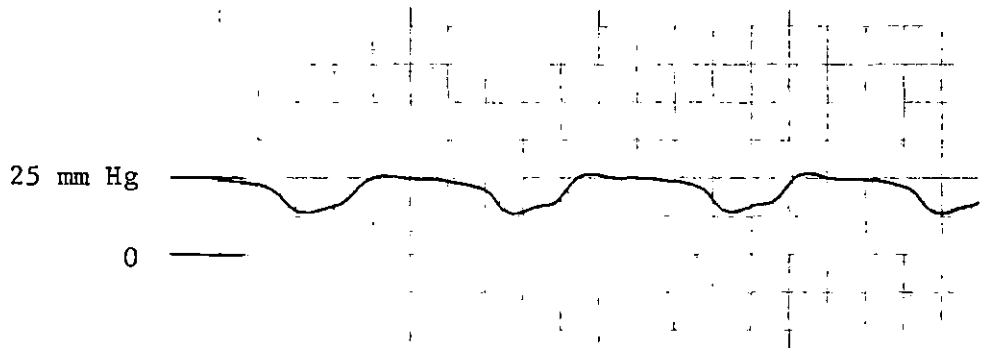

(a) $P_2 \cong 25.2$ cm water

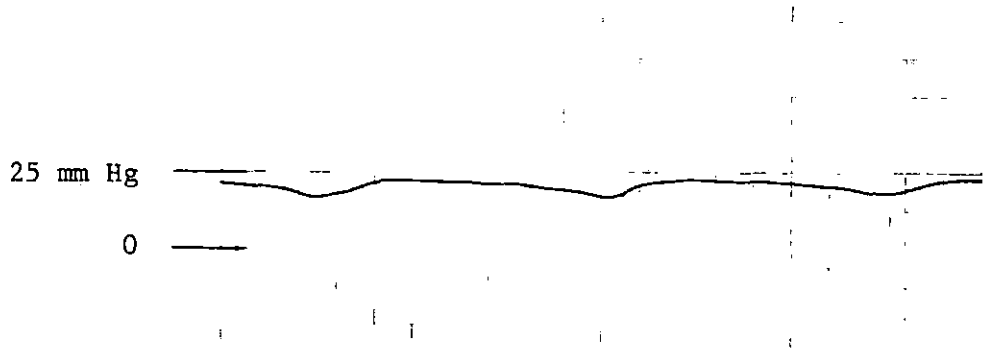

(b) $P_2 \cong 27.9$ cm water

Figure 35. Oscillation recordings of downstream pressure for the long configuration 75% stenosis at P_1 = 54.5 cm water and P_e = 40 cm water (chart speed = 50 mm/sec)

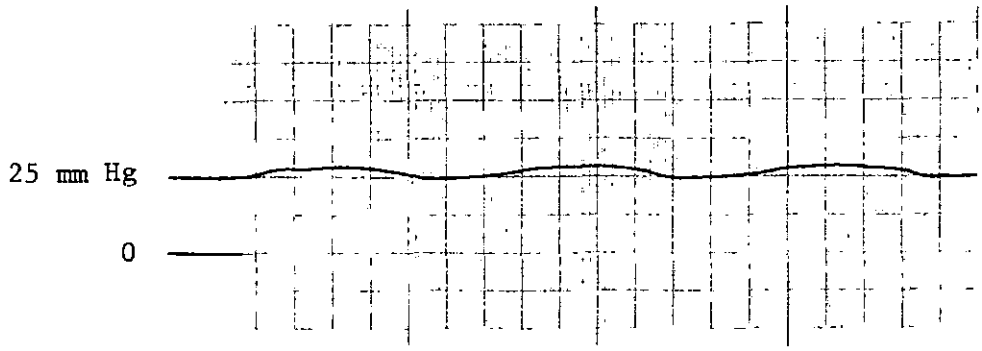

(a) $P_2 \cong 35.2$ cm water

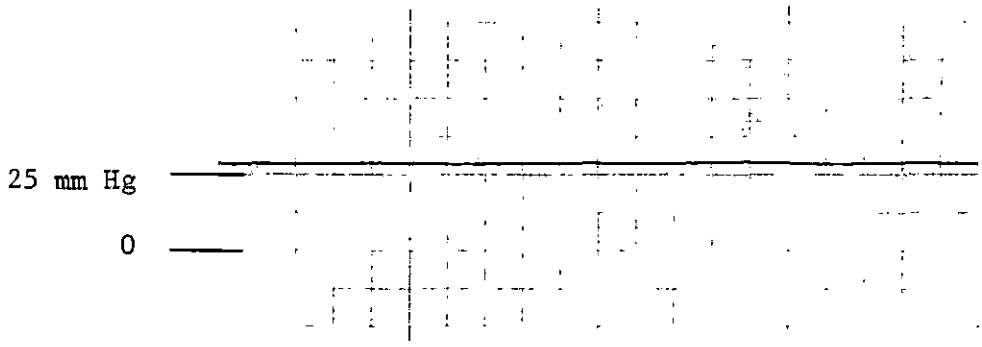

(b) $P_2 \cong 37.6$ cm water

Figure 36. Oscillation recordings of downstream pressure for the long configuration 75% stenosis at P_1 = 54.5 cm water and P_e = 50 cm water (chart speed = 50 mm/sec)

amplitude increased as P_2 decreased, except for cases in which oscillations eventually ceased as P_2 was progressively lowered, as at external pressures of 40 and 50 cm water. In those cases, amplitude increased to a maximum as P_2 decreased, and then decreased with further reduction in P_2. Frequencies were much lower in the long segment than in the short segment, and increased as P_2 decreased for a given P_e. For a given value of P_2, frequency increased as external pressure increased, and for a given value of P_e-P_2, the frequencies were approximately the same. This relationship with P_e-P_2 did not exist for amplitude, however. For a given value of P_e-P_2, amplitude decreased as P_e increased.

Analysis of the effective severity of collapsed segments

To understand the qualitative differences between the pressure-flow relations for different values of percent stenosis, some idea of the effective severity of the tubes in the collapsed state is needed.

Short configuration For the short configuration, Figures 37-40 show the zero external pressure curves for the 85% and 89.4% stenoses plotted with the 75% stenosis data, and the zero external pressure curves for the 89.4% stenosis plotted with the 85% stenosis data.

75% stenosis These plots reveal that in the collapsed state, after the maximum flow was reached, and P_2 was progressively decreased, the effective severity of the 75% stenosis became as high as 85% and 89.4%, depending on the value of external pressure. Thus, as P_2 was progressively lowered, the 75% stenosis configuration underwent a transition from sub-critical to (effectively) critical stenosis. After an effective severity of approximately 85% was exceeded, the slope of the $Q-\Delta P$ curves

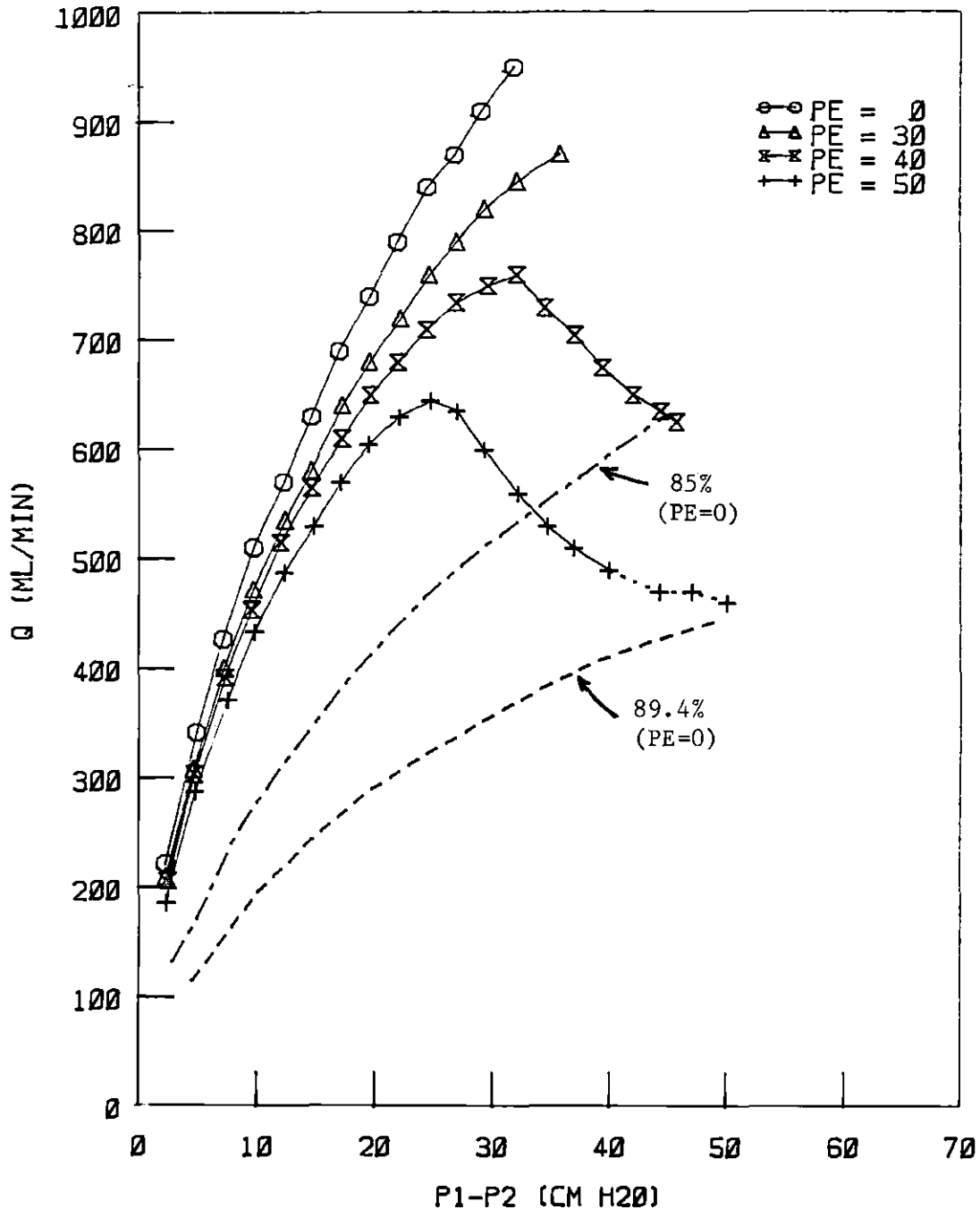

Figure 37. Analysis of effective severity: zero external pressure data for the 85% and 89.4% stenoses with the data for the 75% stenosis (short configuration, upstream pressure = 54.5 cm water, all pressures in cm water)

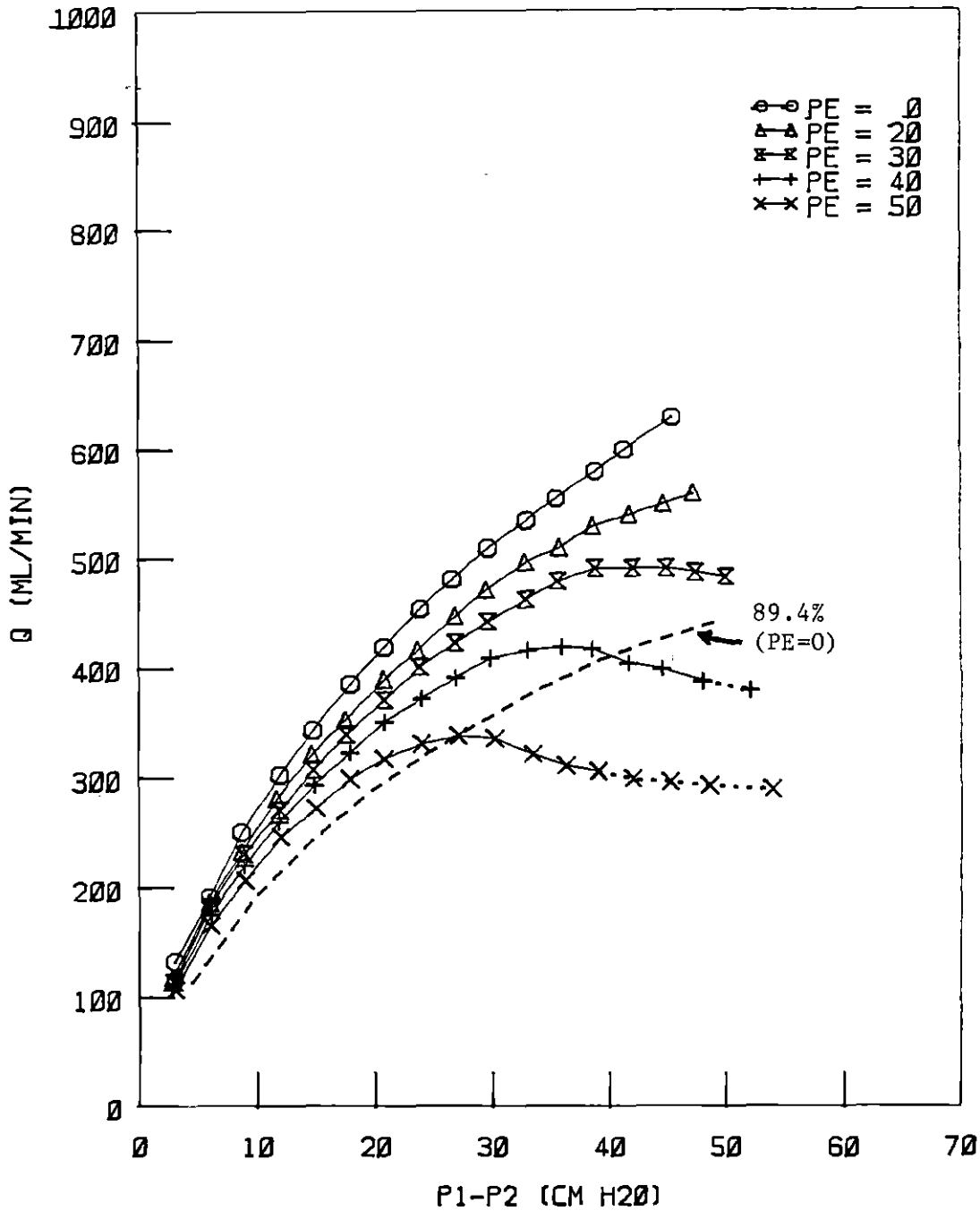

Figure 38. Analysis of effective severity: zero external pressure data for the 89.4% stenosis with the data for the 85% stenosis (short configuration, upstream pressure = 54.5 cm water, all pressures in cm water)

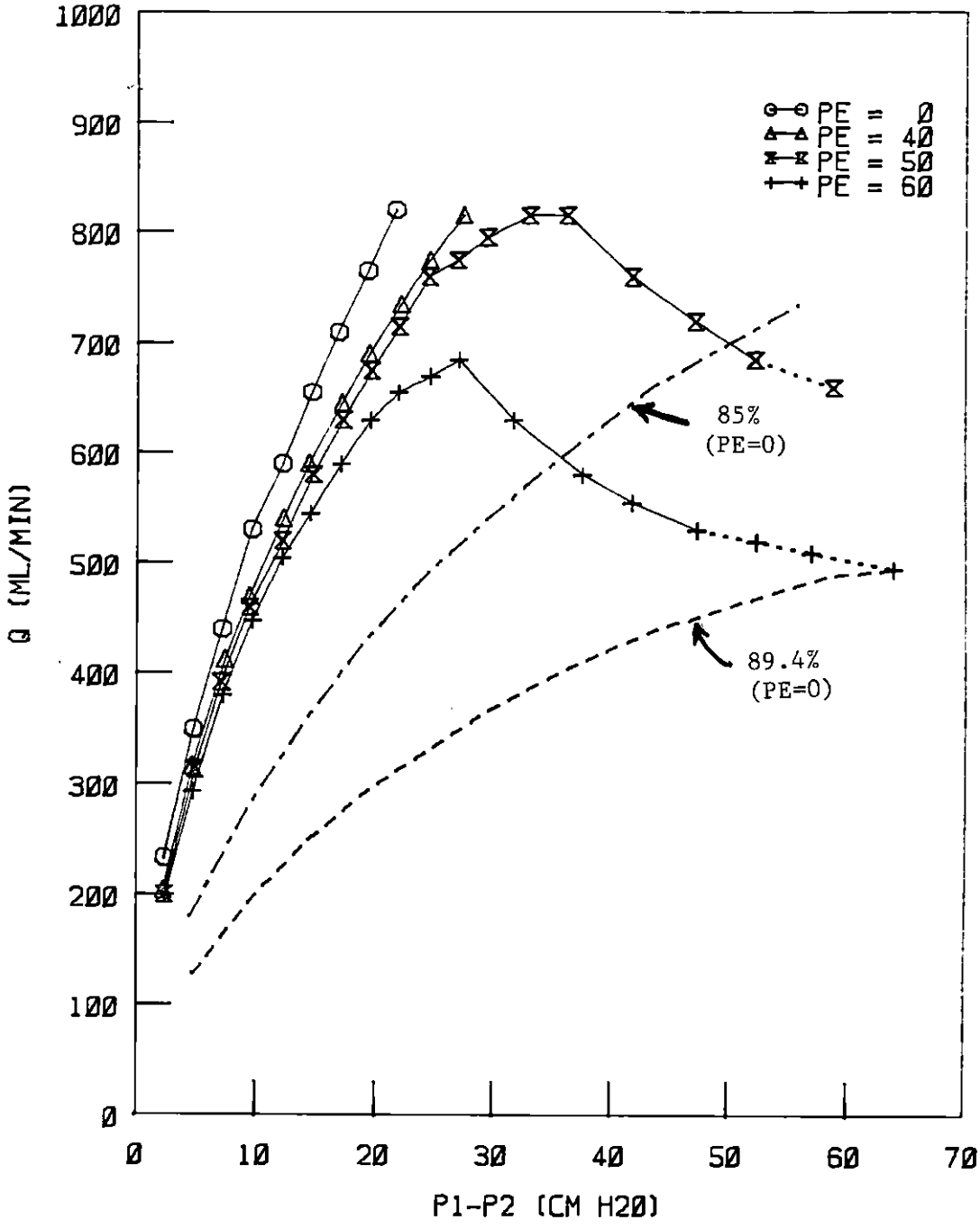

Figure 39. Analysis of effective severity: zero external pressure data for the 85% and 89.4% stenoses with the data for the 75% stenosis (short configuration, upstream pressure = 69.5 cm water, all pressures in cm water)

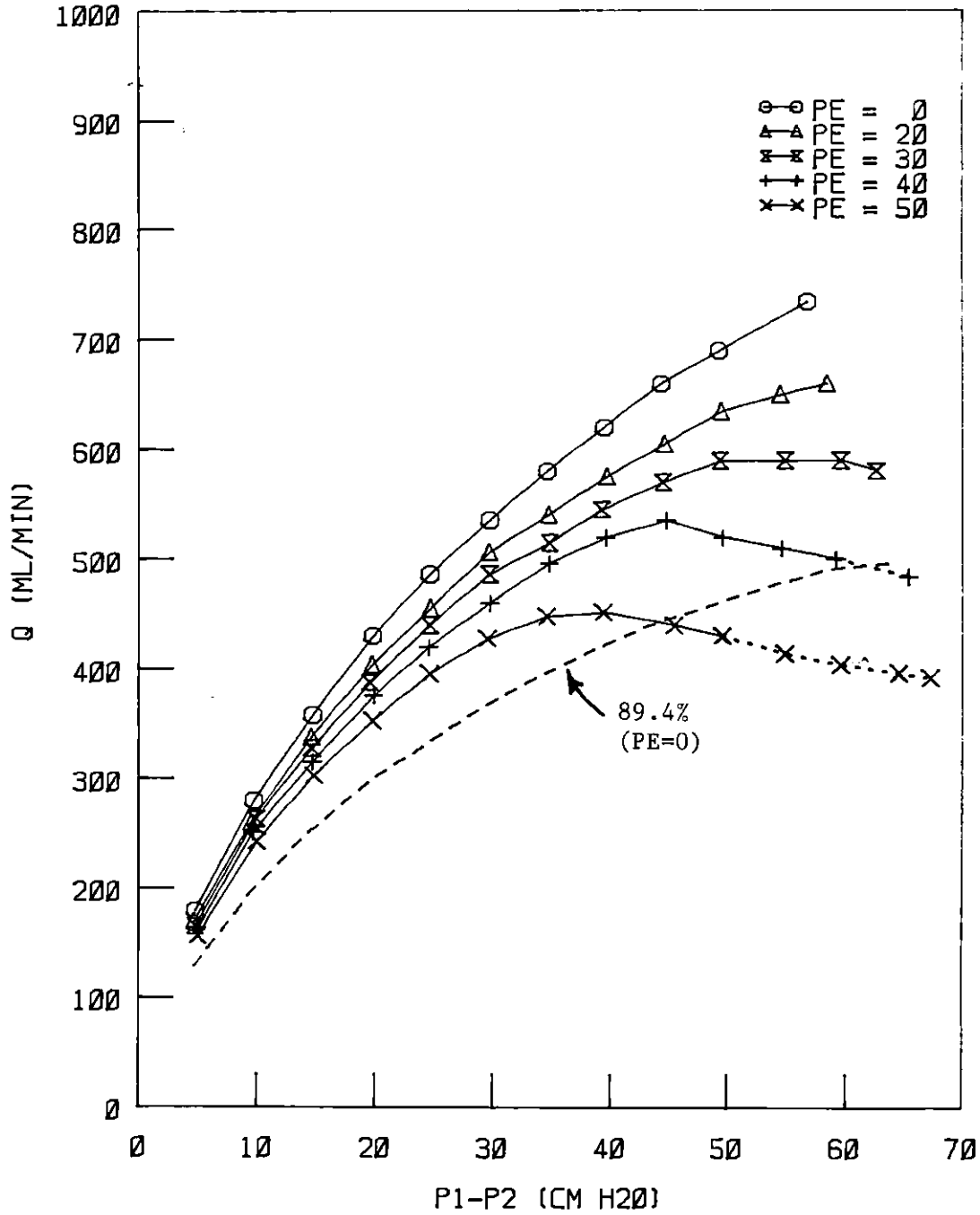

Figure 40. Analysis of effective severity: zero external pressure data for the 89.4% stenosis with the data for the 85% stenosis (short configuration, upstream pressure = 69.5 cm water, all pressures in cm water)

decreased as P_2 was reduced. Thus, it appears that the short segment exhibited a region of high compliance at collapse, followed by a region of lesser compliance after collapse (as does collapsible tubing alone in the post-buckling mode).

85% stenosis The situation for the 85% stenosis was different, since an 85% stenosis is critical even for a rigid configuration (i.e., it is critical even in the absence of either passive contraction or collapse). For some values of external pressure, when the flow reached a maximum (which occurs just before collapse), the effective severity had already reached 89.4%, indicating that passive contraction is significant for values of percent stenosis that are considered critical in the rigid configuration. As did the 75% stenosis, the 85% stenosis appeared to exhibit a region of higher compliance at collapse, and lower compliance in the post-buckling mode. The slopes of the Q- ΔP curves at collapse were lower for the 85% stenosis than for the 75% stenosis, probably because of the greater stiffness of the 85% stenosis (evidenced by its higher static collapse pressure). As the 75% and 85% stenoses entered their respective regions of lesser compliance after collapse, their Q- ΔP slopes became approximately the same. This is illustrated in Figure 41, which shows the data for the 75% stenosis at P_e = 60 cm water, and for the 85% stenosis at P_e = 40 cm water (both at P_1 = 69.5 cm water). The two curves almost exactly overlap as the effective severity approaches 89.4%.

Long configuration Similar comparisons for the long segments, shown in Figures 42 and 43, reveal that the segment with a 75% stenosis did not reach an effective severity of 89.4%, but did exceed a value of 85%. The segment with an 85% stenosis exhibited an effective severity greater

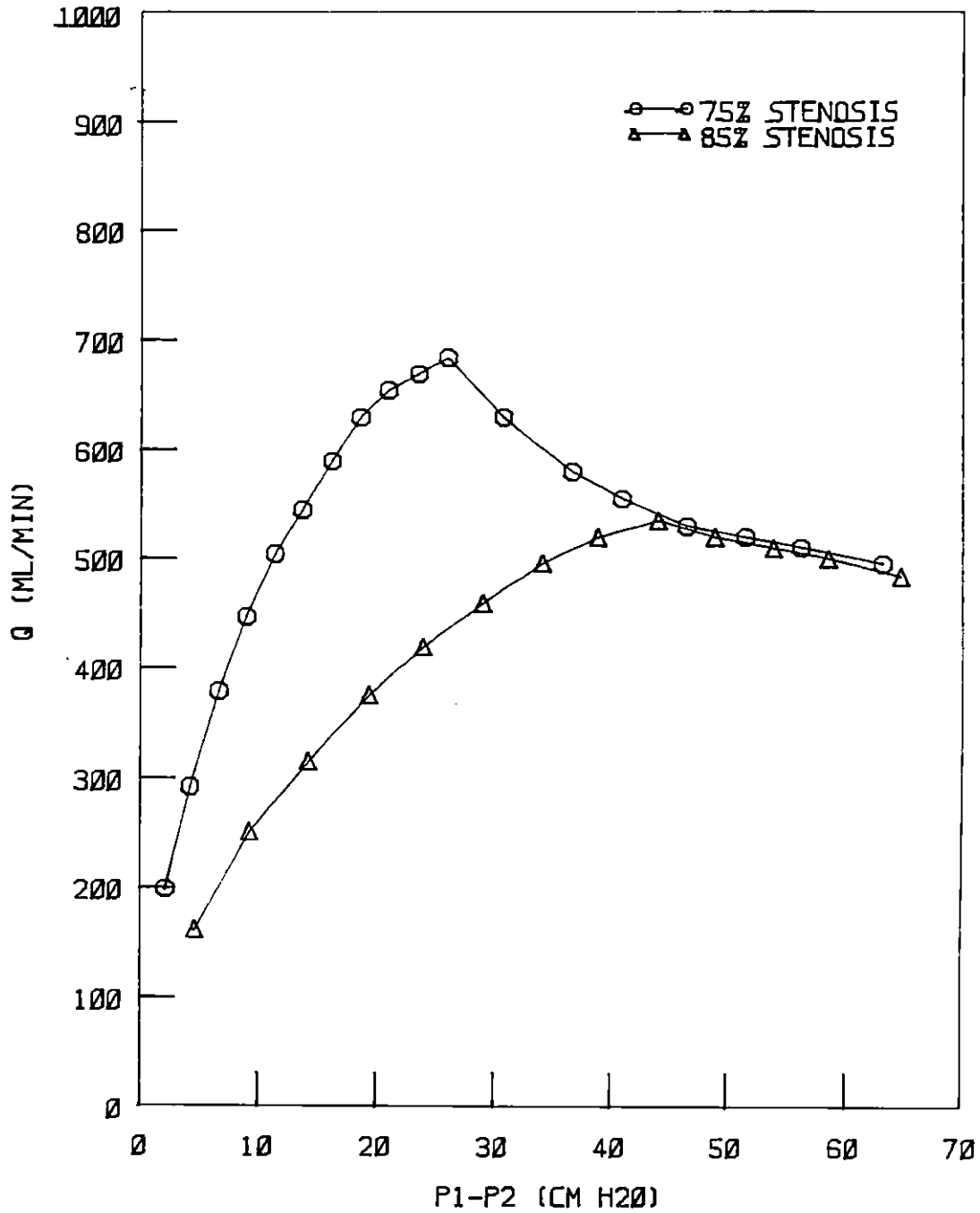

Figure 41. Pressure-flow data for the short 75% stenosis at an external pressure of 60 cm water and for the short 85% stenosis at an external pressure of 40 cm water (upstream pressure = 69.5 cm water)

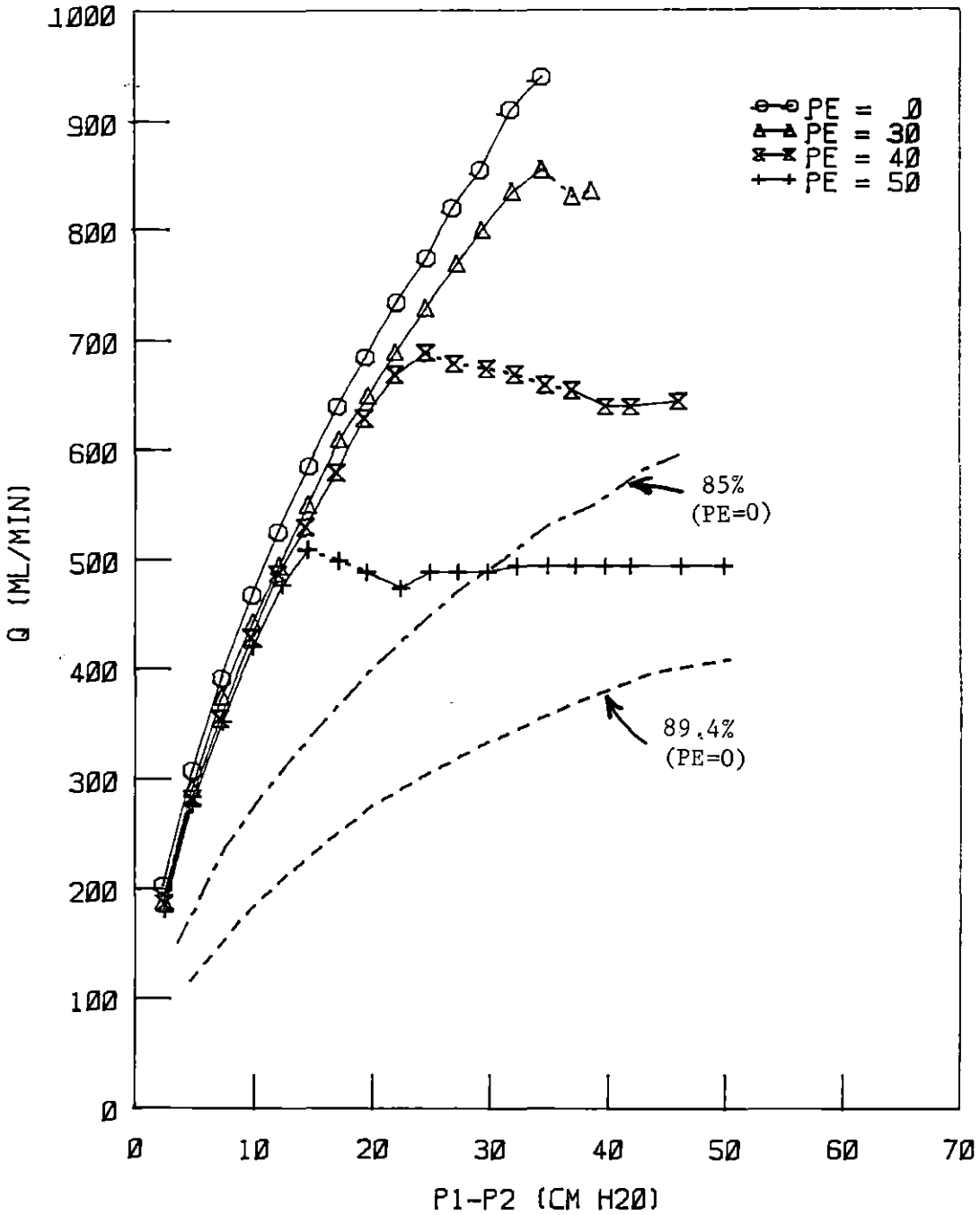

Figure 42. Analysis of effective severity: zero external pressure data for the 85% and 89.4% stenoses with the data for the 75% stenosis (long configuration, upstream pressure = 54.5 cm water, all pressures in cm water)

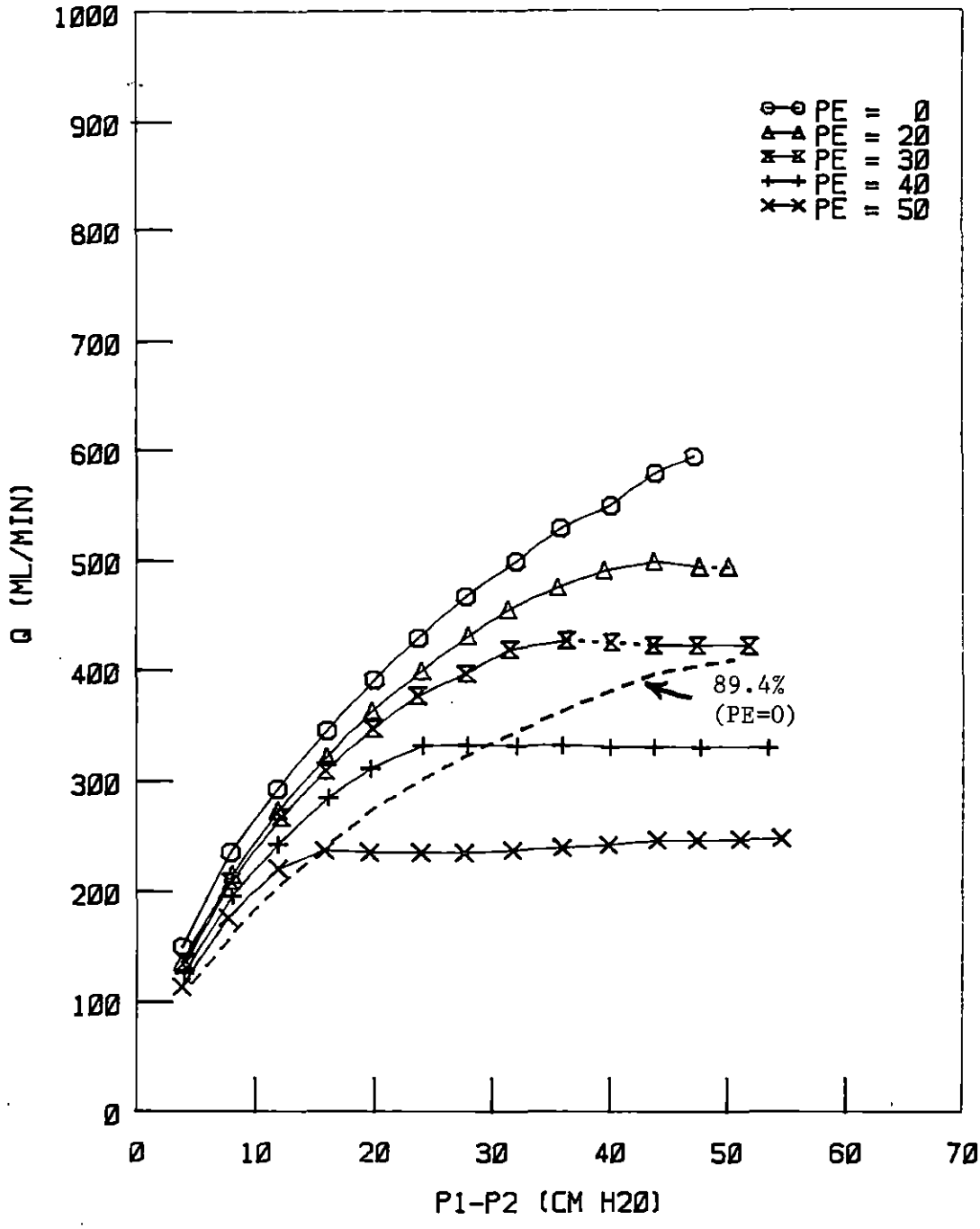

Figure 43. Analysis of effective severity: zero external pressure data for the 89.4% stenosis with the data for the 85% stenosis (long configuration, upstream pressure = 54.5 cm water, all pressures in cm water)

than 89.4% for some values of external pressure.

Results of the short vs. long compliant configurations

The differences between the pressure-flow relationships for the short and long configurations were not very great for the smaller values of external pressure, but were large for the larger external pressures. Whereas flow in the short segments reached a maximum and then decreased for further reductions in P_2, flow in the long segments tended to simply level off. Figures 44-46 show representative pressure-flow differences between the long and short configurations for a given percent stenosis at an external pressure of 40 cm water. For the 85% and 89.4% stenoses, the flow rates at which the long configurations leveled off were always lower than those reached by the short configurations at equivalent external pressures. Data for the long and short configurations with a 75% stenosis overlapped at low values of P_2. Thus, it would seem that collapse of the downstream section creates a more severe situation than does collapse in the stenosed region, except for very low values of P_2.

The differences in qualitative behavior between the short and long configurations may be related to the fact that collapse occurs in different locations for the two configurations, and thus may have different effects on upstream conditions. For the collapsed long segment, changes in downstream conditions did not affect upstream conditions, probably in the same manner as for collapsible tubing alone, as discussed previously. For the short segment, with collapse in the stenosed area, upstream conditions did appear to be affected by collapse. Decreasing the downstream pressure such that collapse occurred seemed essentially equivalent to inserting a more severe stenosis, which would cause a reduction in flow if the increase

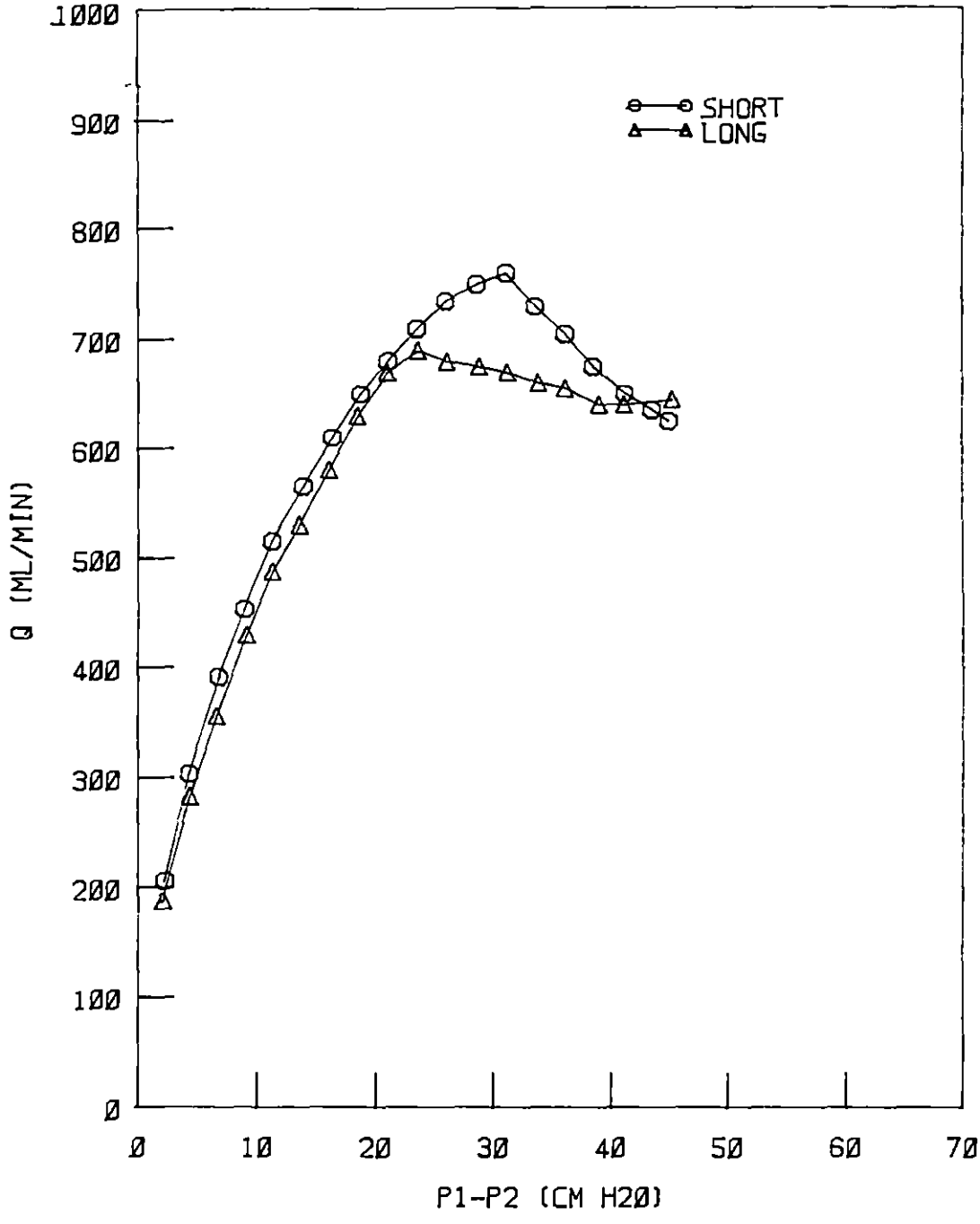

Figure 44. Comparison between short and long configurations: data for the 75% stenoses at an upstream pressure of 54.5 cm water and an external pressure of 40 cm water

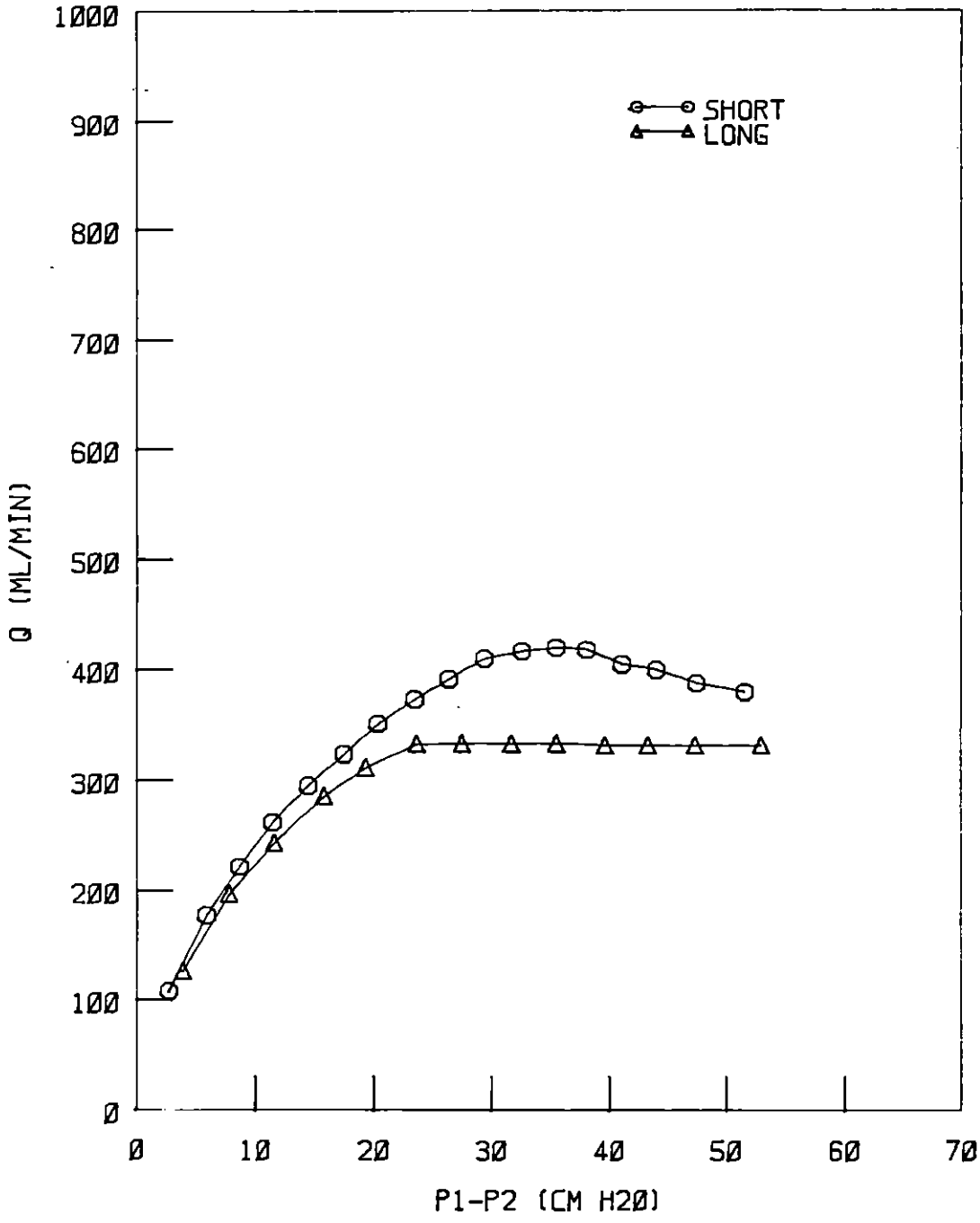

Figure 45. Comparison between short and long configurations: data for the 85% stenoses at an upstream pressure of 54.5 cm water and an external pressure of 40 cm water

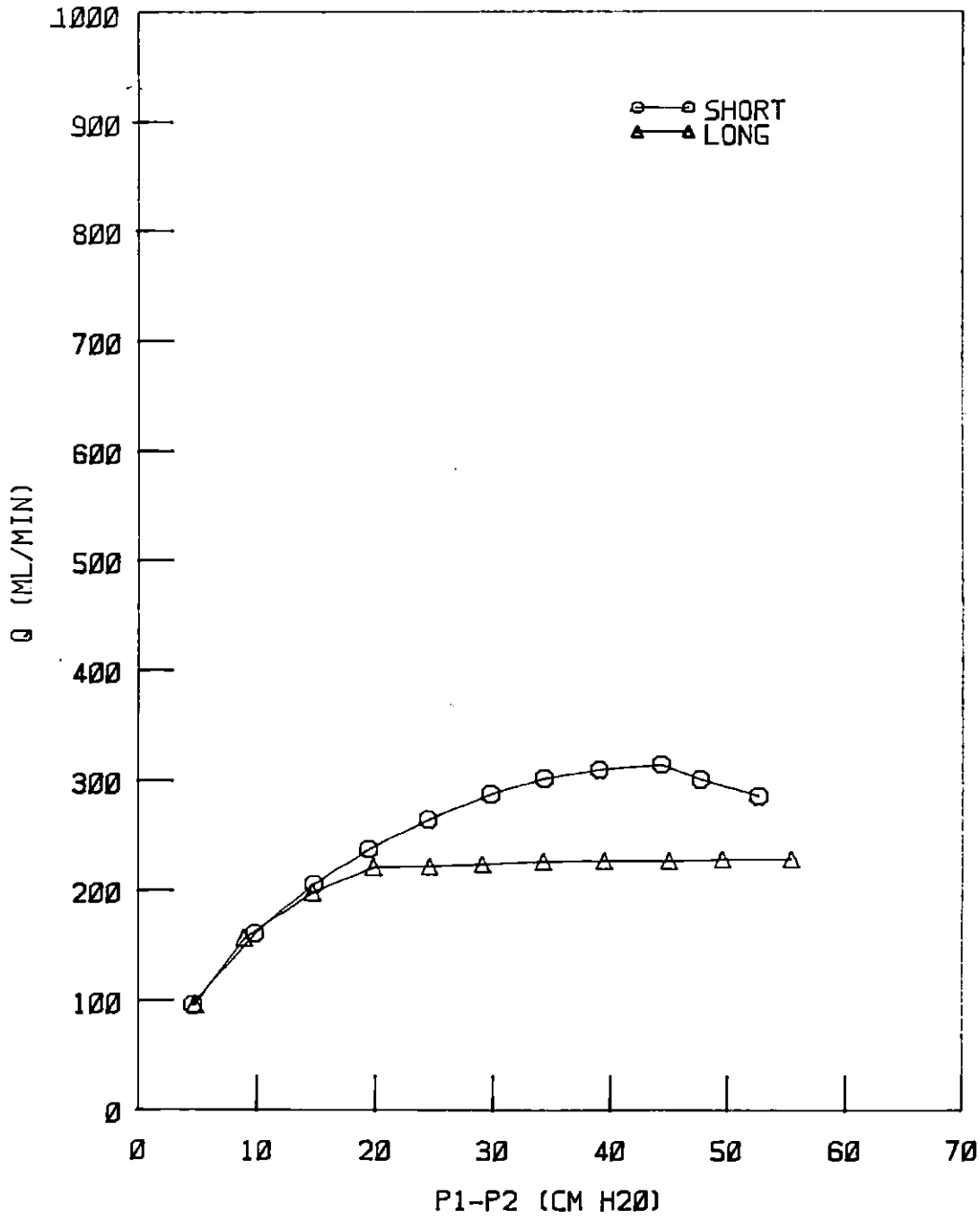

Figure 46. Comparison between short and long configurations: data for the 89.4% stenoses at an upstream pressure of 54.5 cm water and an external pressure of 40 cm water

in severity was great enough. As long as further decreases in downstream pressure caused significant increases in effective stenosis severity, flow continued to decrease. It seemed that as the short segment reached the region of (hypothesized) lesser compliance in the post-buckling mode, flow began to level off, as in the long segment.

Significance of upstream pressure minus external pressure

In addition to these differences in behavior between the two types of test section, differences were seen between the two values of proximal pressure that were studied for the short configuration. At equivalent values of external pressure, pressure-flow relations at the two values of P_1 were not the same, as shown in Figure 47. This is because the magnitude of the effect of collapse on flow depended on the pressure differential P_1-P_e, as illustrated in Figures 48-50. These figures include the data for both values of P_1 for a given percent stenosis on one graph, with the data for P_1 = 54.5 cm water indicated by solid lines, and the data for P_1 = 69.5 indicated by dashed lines. These plots reveal that for a given pressure drop across the stenosis, flow varied with P_1-P_e (most significantly after collapse). Higher flow rates were achieved at lower values of P_1-P_e. Thus, since the value of P_1-P_e at a given external pressure for a P_1 of 69.5 cm water is 15 cm water higher than the value of P_1-P_e for a P_1 of 54.5 cm water, the curves for the two values of P_1 were different at equal values of P_e.

Further proof of the significance of P_1-P_e for the short segments is given by examining the maximum flow rate as a function of P_1-P_e. An examination of these parameters revealed that the maximum flow rate for the short segments (at external pressures that caused collapse) was linearly

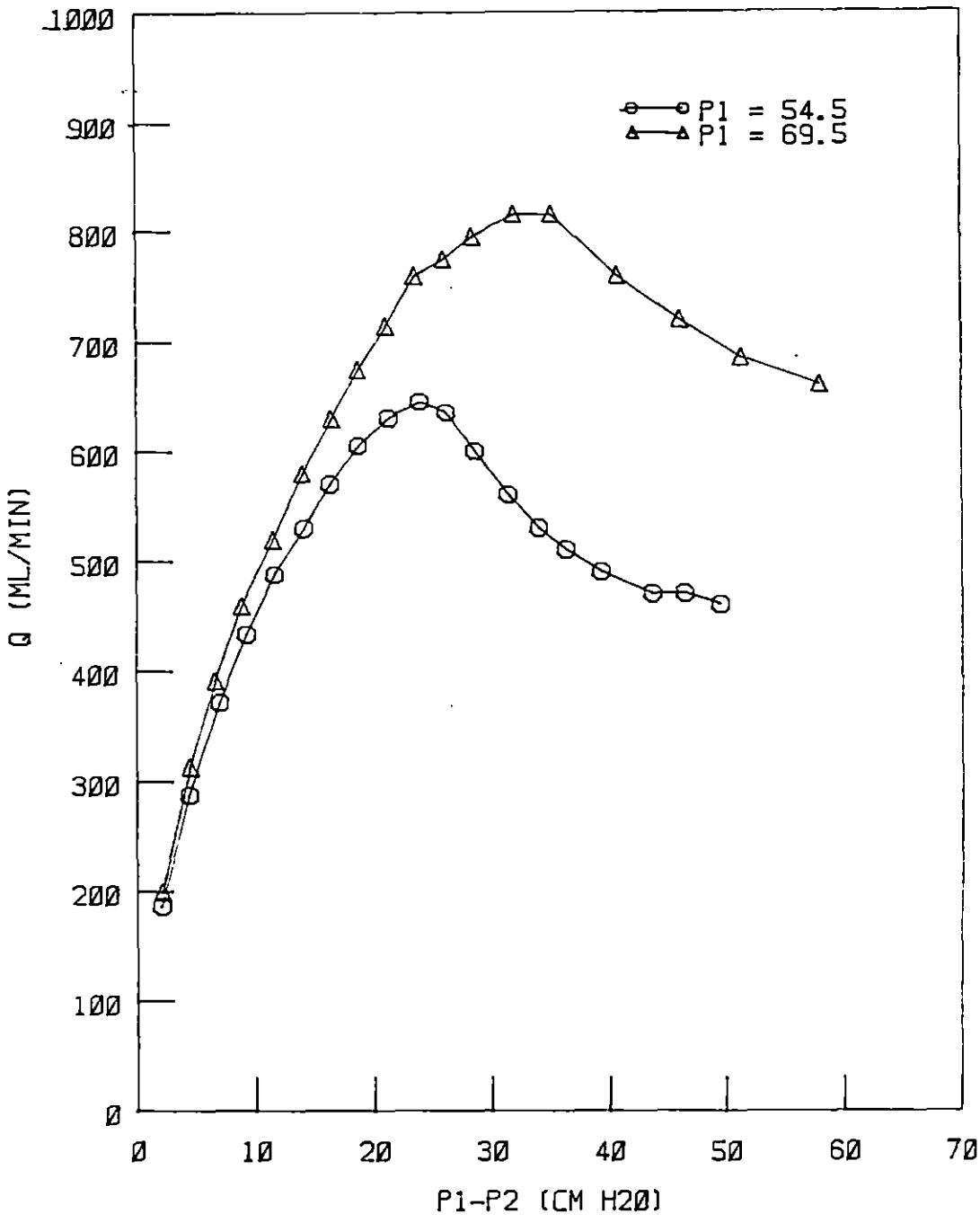

Figure 47. Comparison between different values of upstream pressure for the short configuration: data for the 75% stenosis at upstream pressures of 54.5 and 69.5 cm water and an external pressure of 50 cm water

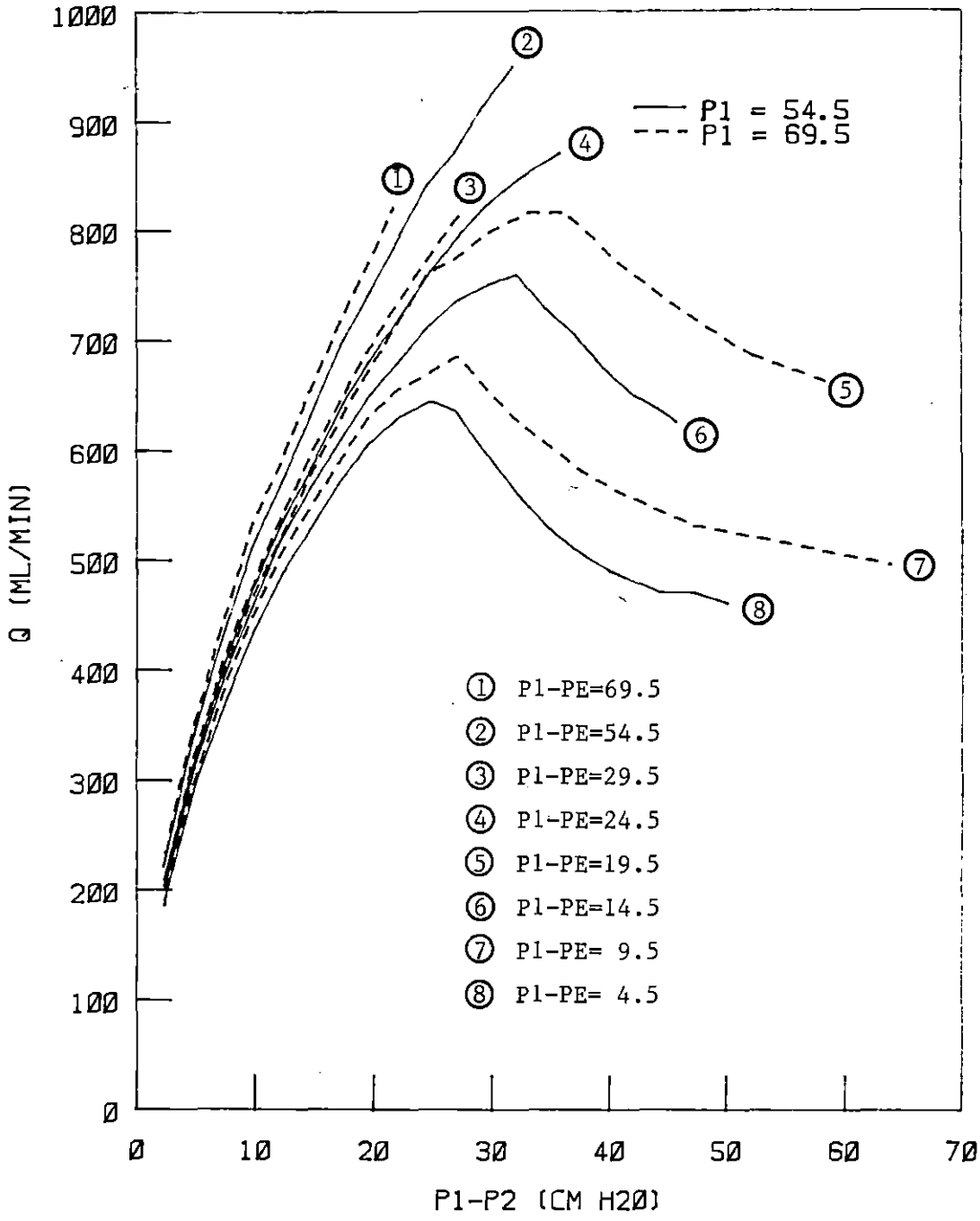

Figure 48. Significance of P1-PE for the short configuration: data for the 75% stenosis at upstream pressures of 54.5 and 69.5 cm water (symbols denoting the value of external pressure are deleted for clarity for each curve)

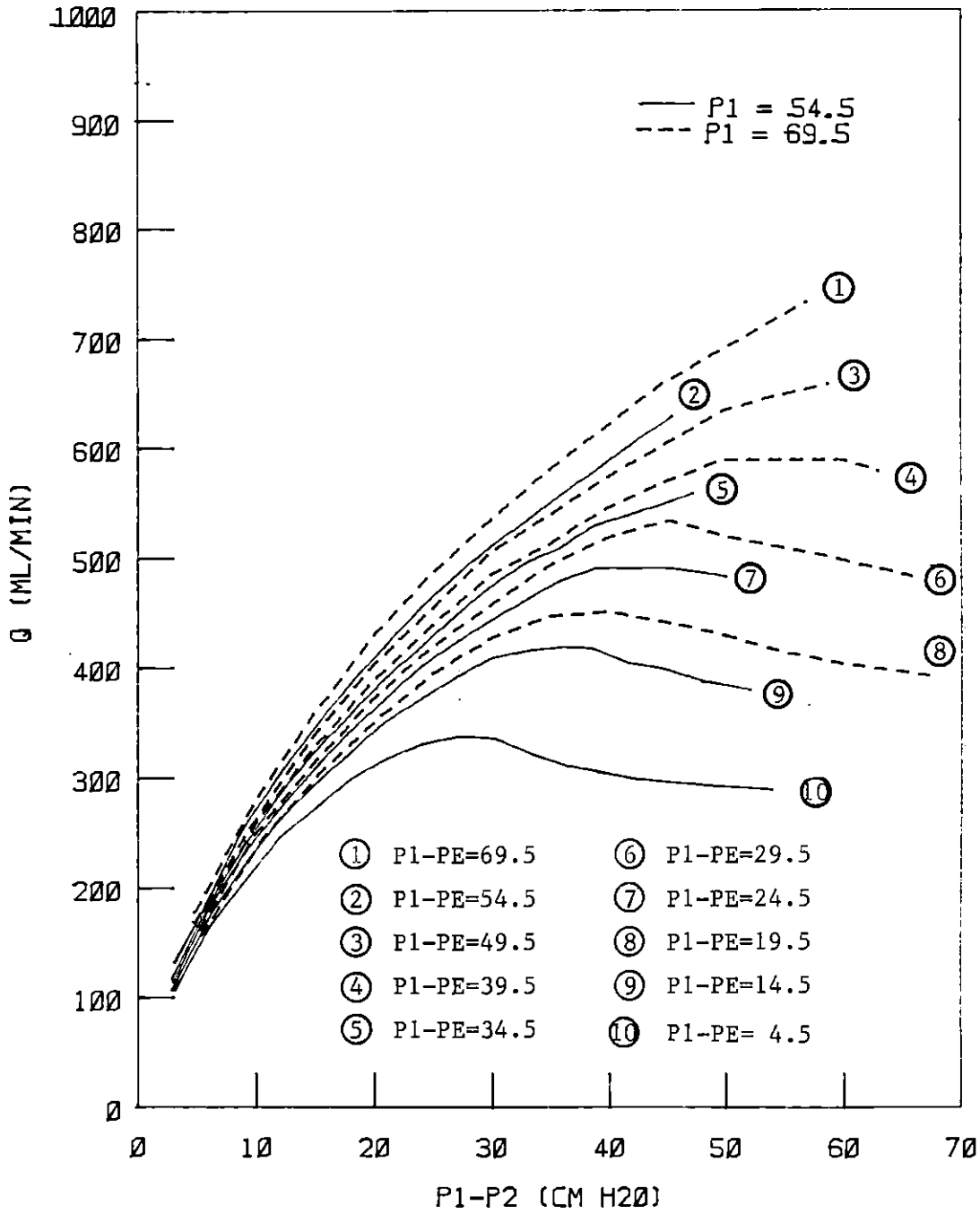

Figure 49. Significance of P1-PE for the short configuration: data for the 85% stenosis at upstream pressures of 54.5 and 69.5 cm water (symbols denoting the value of external pressure are deleted for clarity for each curve)

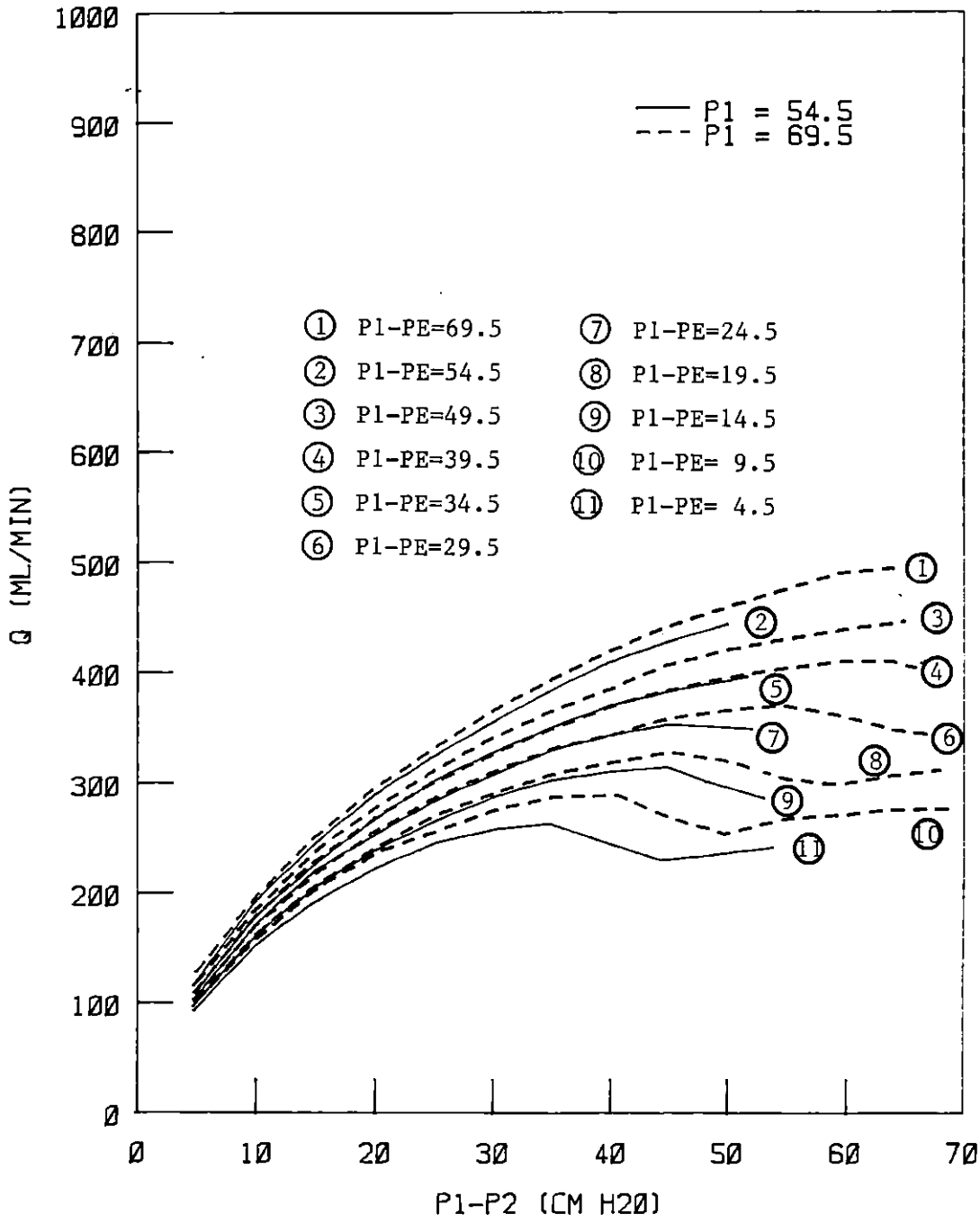

Figure 50. Significance of P1-PE for the short configuration: data for the 89.4% stenosis at upstream pressures of 54.5 and 69.5 cm water (symbols denoting the value of external pressure are removed for clarity for each curve)

related to P_1-P_e. Maximum flow rate (QMAX) vs. P_1-P_e for each percent stenosis is plotted in Figure 51, fitted with straight lines by the method of least squares. The slope decreased as percent stenosis increased, as did the intercept. All of the fitted values were within two percent of the actual values.

The curves of QMAX vs. P_1-P_e for the long configuration were also linear, as shown in Figure 52. The value of QMAX was taken to be the flow rate at which flow essentially leveled off. Slopes for the long configuration were higher than those for the short configuration, and decreased with decreasing percent stenosis. All of the fitted values were within two percent of the actual values.

For both collapsed configurations, plots of flow rate vs. P_1-P_e at roughly equivalent values of P_e-P_2 were also approximately linear. Thus, the flow rate in the collapsed segments was a function of P_1-P_e (consistent with the dimensional analysis).

Significance of external pressure minus downstream pressure

The value of P_1-P_e was found to be an important determinant of the flow rate in collapsed compliant stenoses, but to determine the point at which collapse and other important phenomena occur, the effects of transmural pressure had to be considered. Since the pressure in the collapsed regions of the two configurations was not measured, the pressure differential P_e-P_2 was used as an approximation of the negative transmural pressure to analyze the data.

The statically determined values of P_{cr} were analyzed for applicability to the fluid dynamic studies by partitioning the ΔP-Q

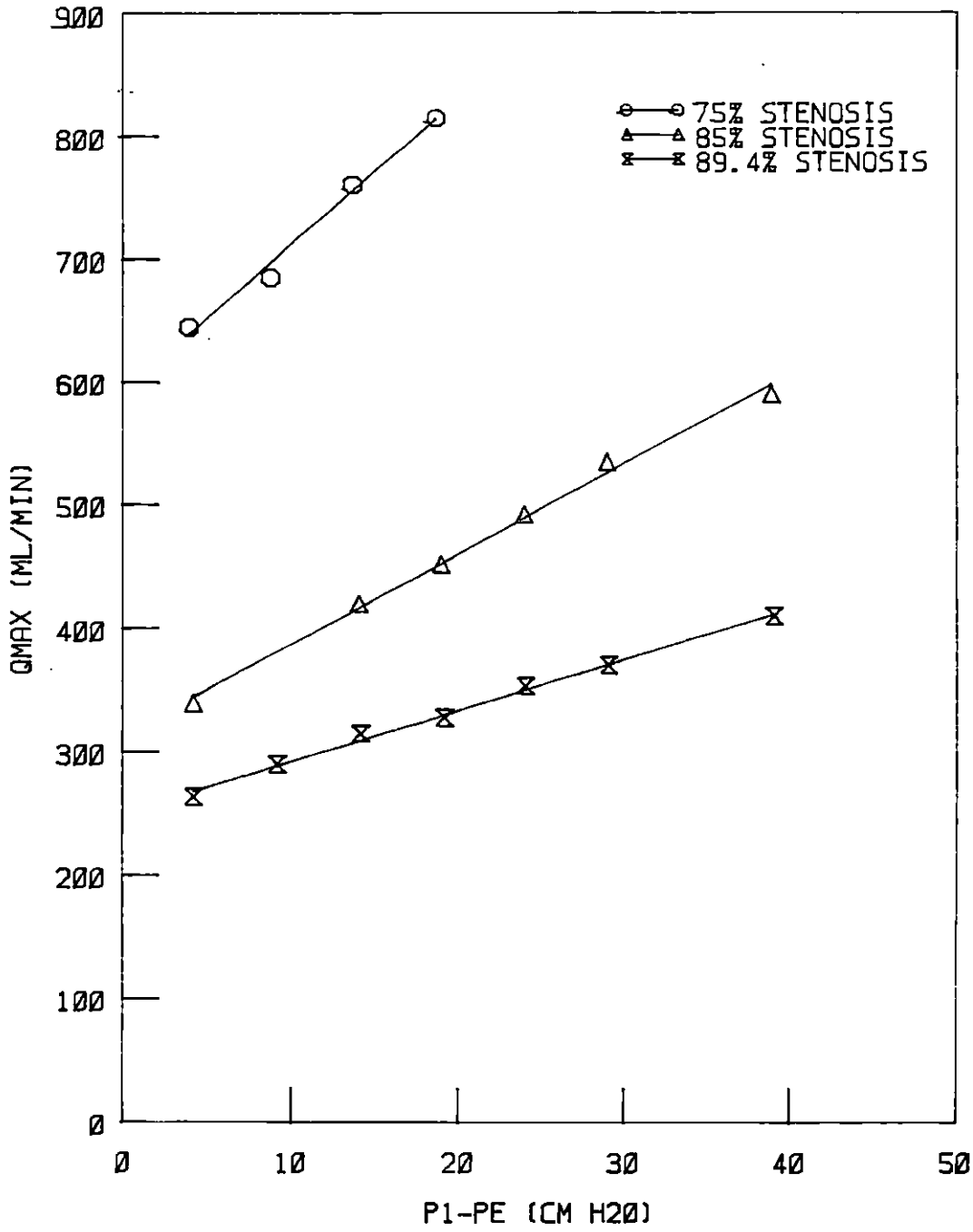

Figure 51. Maximum flow rate vs. P1-PE for the three values of percent stenosis for the short configuration (75%: slope = 11.9, intercept = 592; 85%: slope = 7.3, intercept = 314; 89.4%: slope = 4.1, intercept = 251--lines denote least squares curve fit)

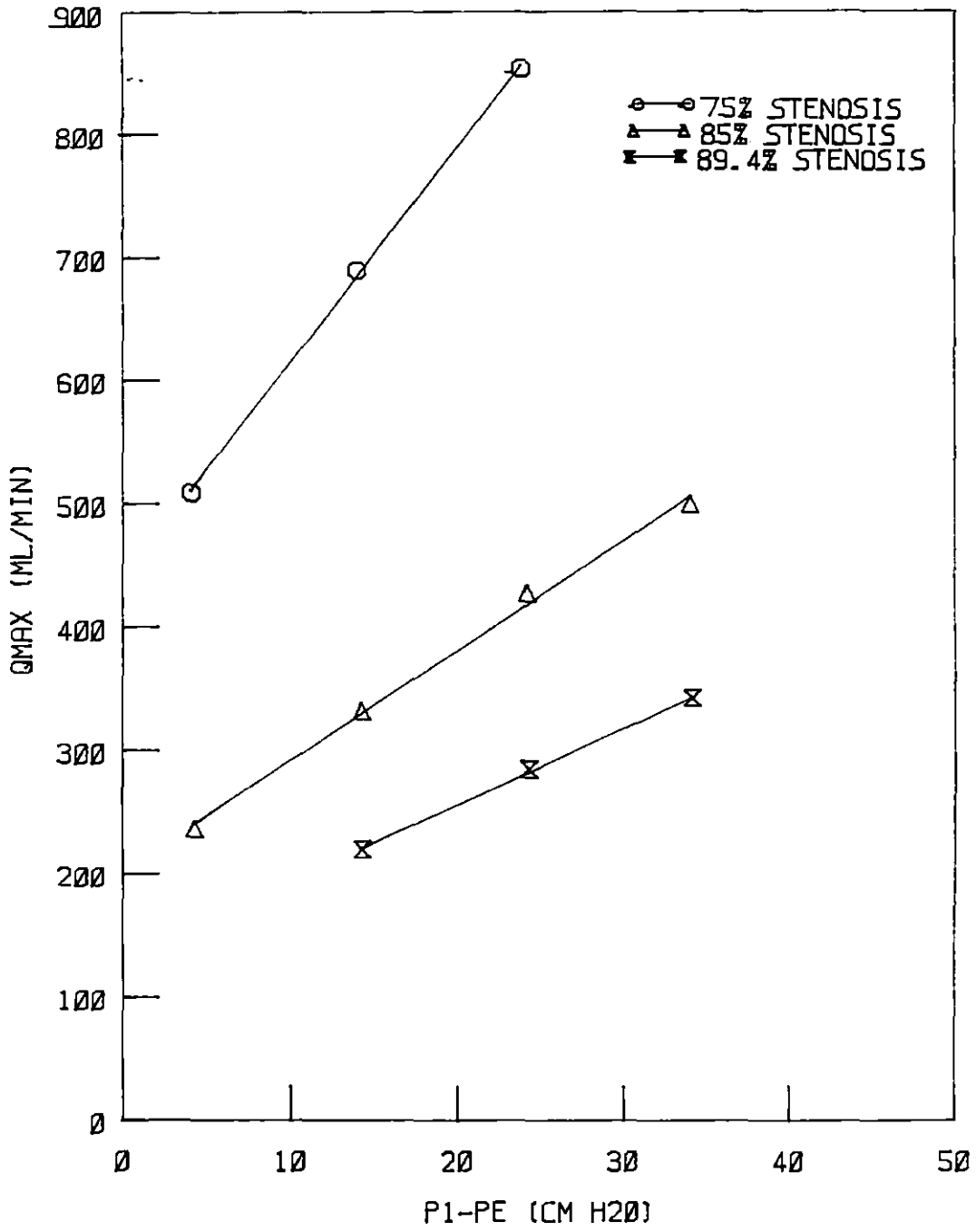

Figure 52. Maximum flow rate vs. P1-PE for the three values of percent stenosis for the long configuration (75%: slope = 17.4, intercept = 441; 85%: slope = 8.9, intercept = 204; 89.4%: slope = 6.1, intercept = 135)--lines denote least squares curve fit

curves into regions where P_e-P_2 was less than zero, greater than zero but less than P_{cr}, and greater than P_{cr}. These plots are shown in Figures 53-61 for the short and long configurations. For the short configuration, the values of P_{cr} were fairly applicable to the steady flow situation for the 75% stenosis, and to some extent for the 89.4% stenosis (for P_1 = 54.5 cm water). The value of P_{cr} for the 85% stenosis was too high for application to steady flow conditions, and the value for the 89.4% stenosis applied to the data for P_1 = 69.5 cm water was also too high. This may be because of the previously discussed increases in stenosis severity that occur prior to large collapse of those stenoses. That is, the statically determined values of P_{cr} represented significant collapse in the stenosed area, but only a small amount of contraction is needed to significantly decrease flow through a critical stenosis.

For the long configurations, P_{cr} seemed applicable for the 89.4% stenosis, but was too low for the 75% and 85% stenoses. This implies that for the two lower values of percent stenosis, the tube may have had to be into the post-buckling mode to limit the flow.

P_e-P_2 was also important in the study of the points of onset and cessation of oscillations. Table 5 lists the ranges of P_e-P_2 for which oscillations began and ended for both configurations at various external pressures for each percent stenosis. Ranges are specified because the specific value of P_e-P_2 at which oscillations initiated or ended may have been between data points in some cases. For a given percent stenosis and configuration, the ranges of values of P_e-P_2 at which oscillation initiated were approximately the same (overlapped) for different values of P_e-P_2, implying that for certain flow rates, oscillations occur at similar points

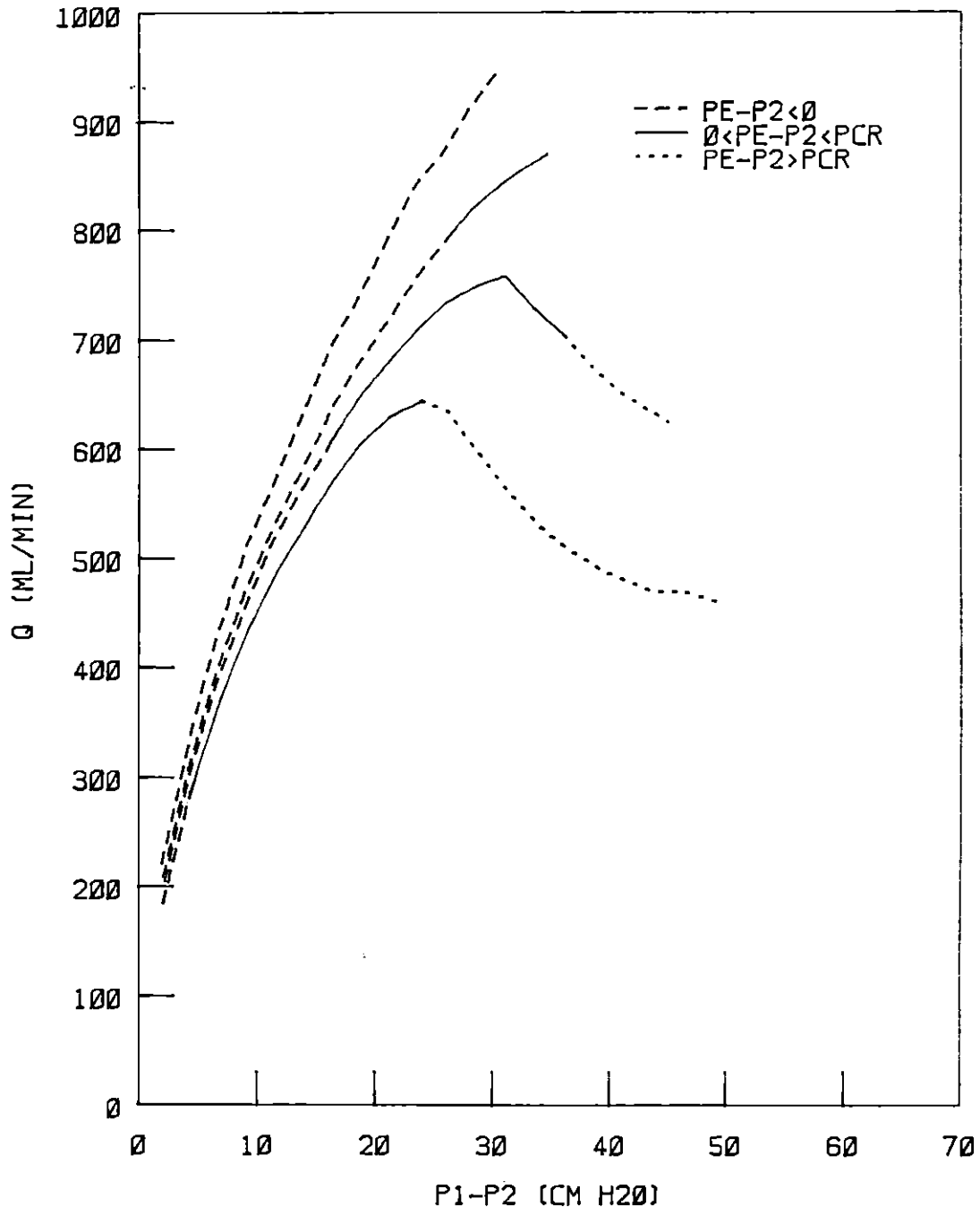

Figure 53. Significance of PE-P2: Pressure-flow data for the short 75% stenosis at an upstream pressure of 54.5 cm water partitioned into regions of PE-P2 relative to the measured static collapse pressure of 20.3 cm water

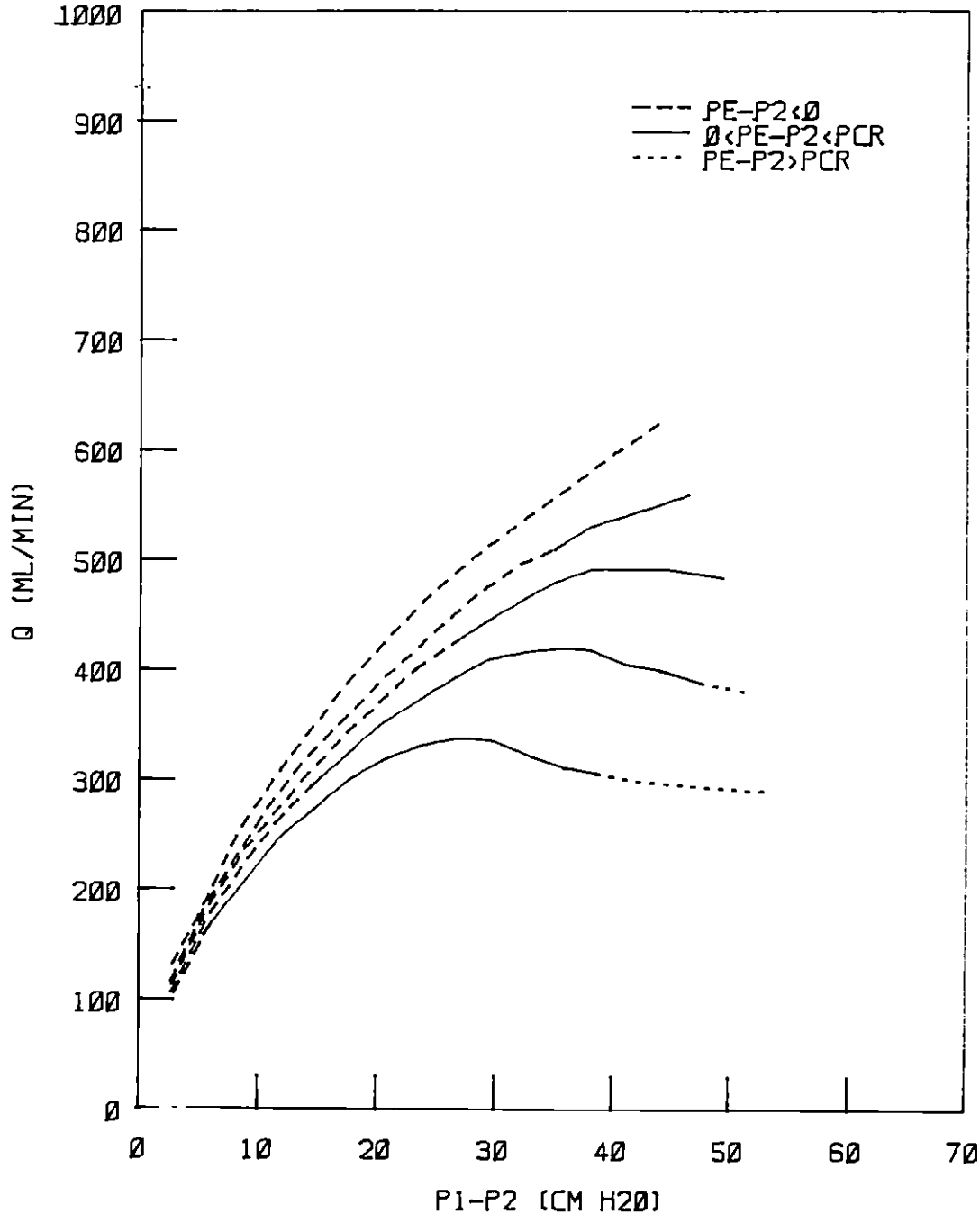

Figure 54. Significance of PE-P2: Pressure-flow data for the short 85% stenosis at an upstream pressure of 54.5 cm water partitioned into regions of PE-P2 relative to the measured static collapse pressure of 31.9 cm water

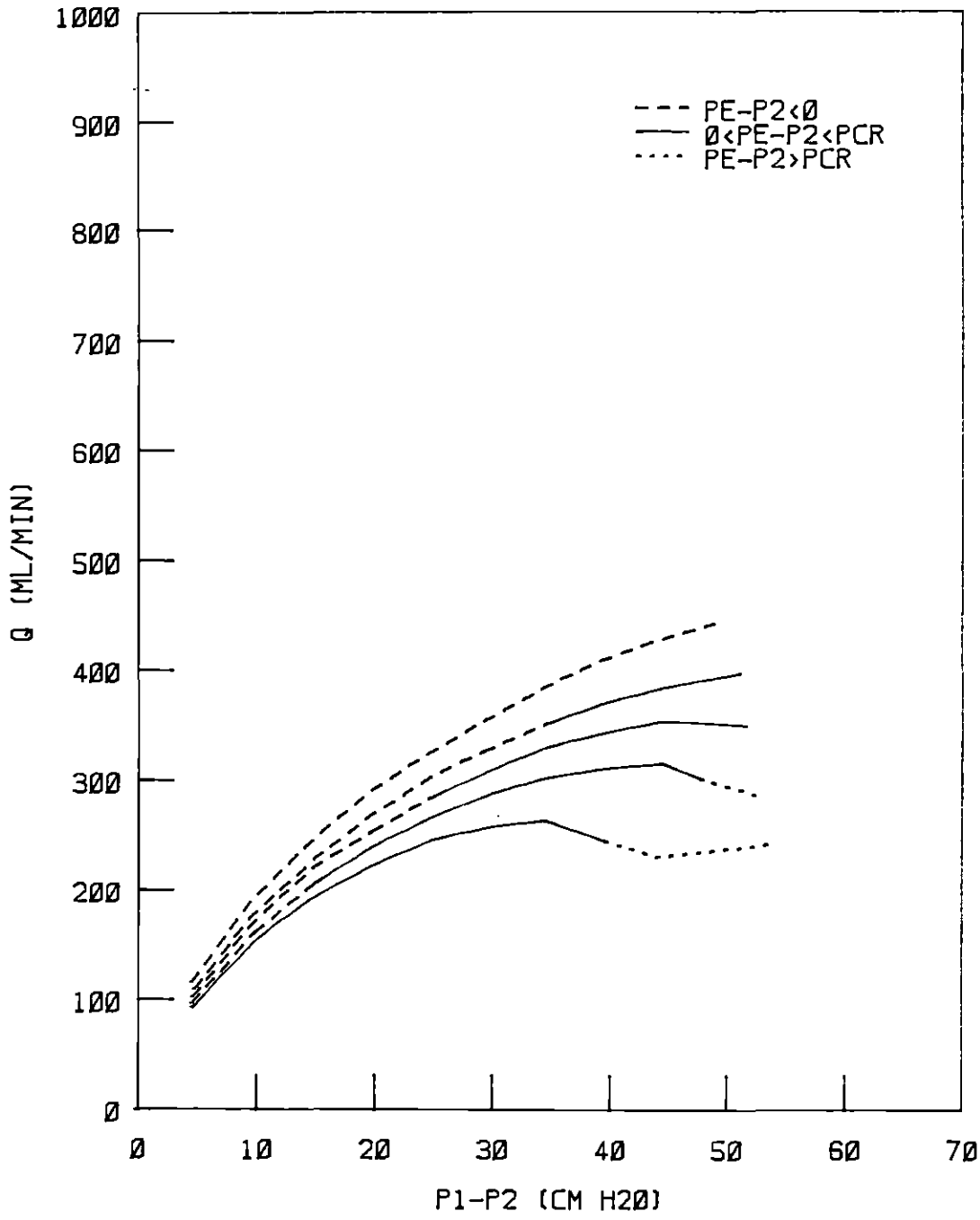

Figure 55. Significance of PE-P2: Pressure-flow data for the short 89.4% stenosis at an upstream pressure of 54.5 cm water partitioned into regions of PE-P2 relative to the measured static collapse pressure of 33.0 cm water

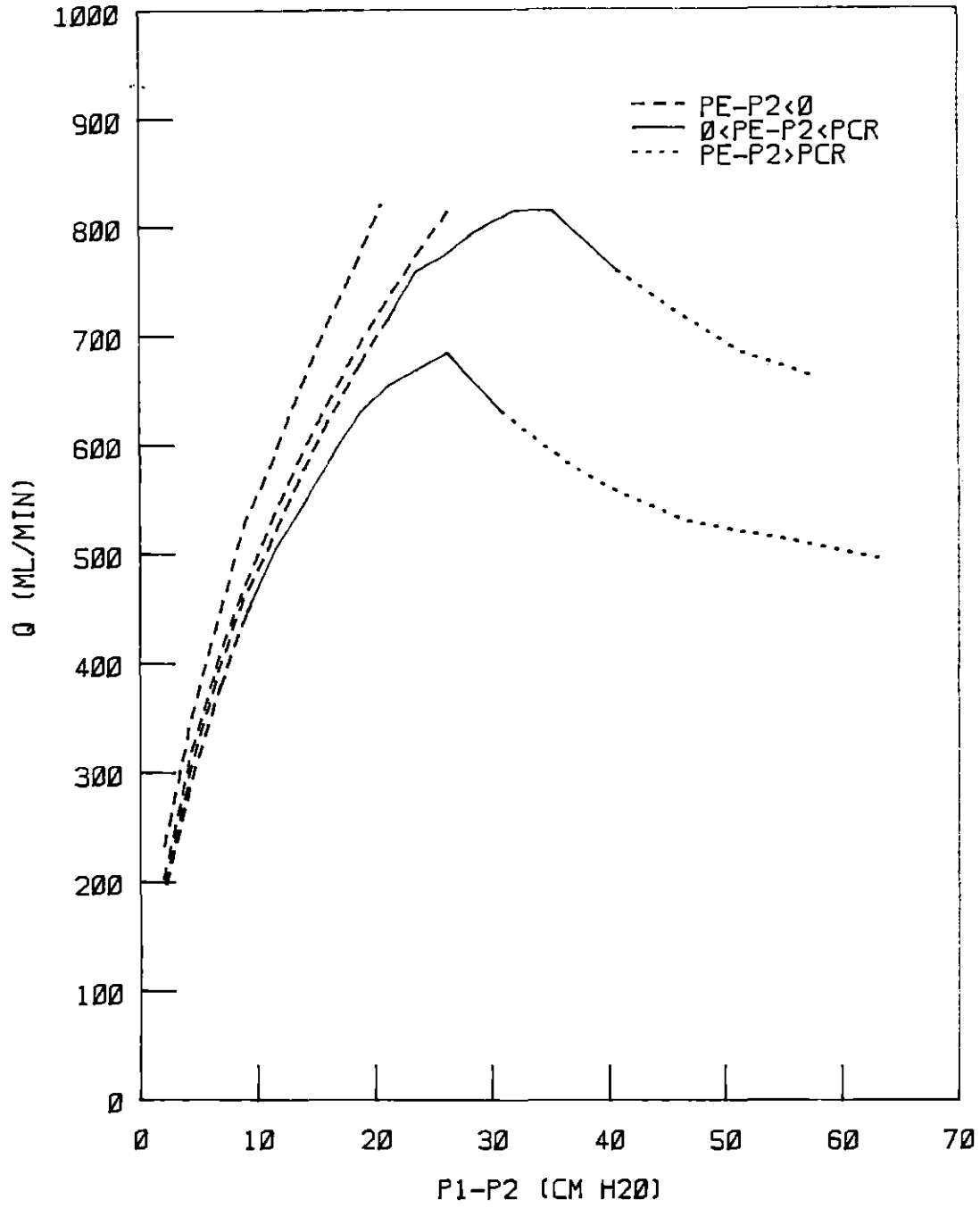

Figure 56. Significance of Pe-P2: Pressure-flow data for the short 75% stenosis at an upstream pressure of 69.5 cm water partitioned into regions of PE-P2 relative to the measured static collapse pressure of 20.3 cm water

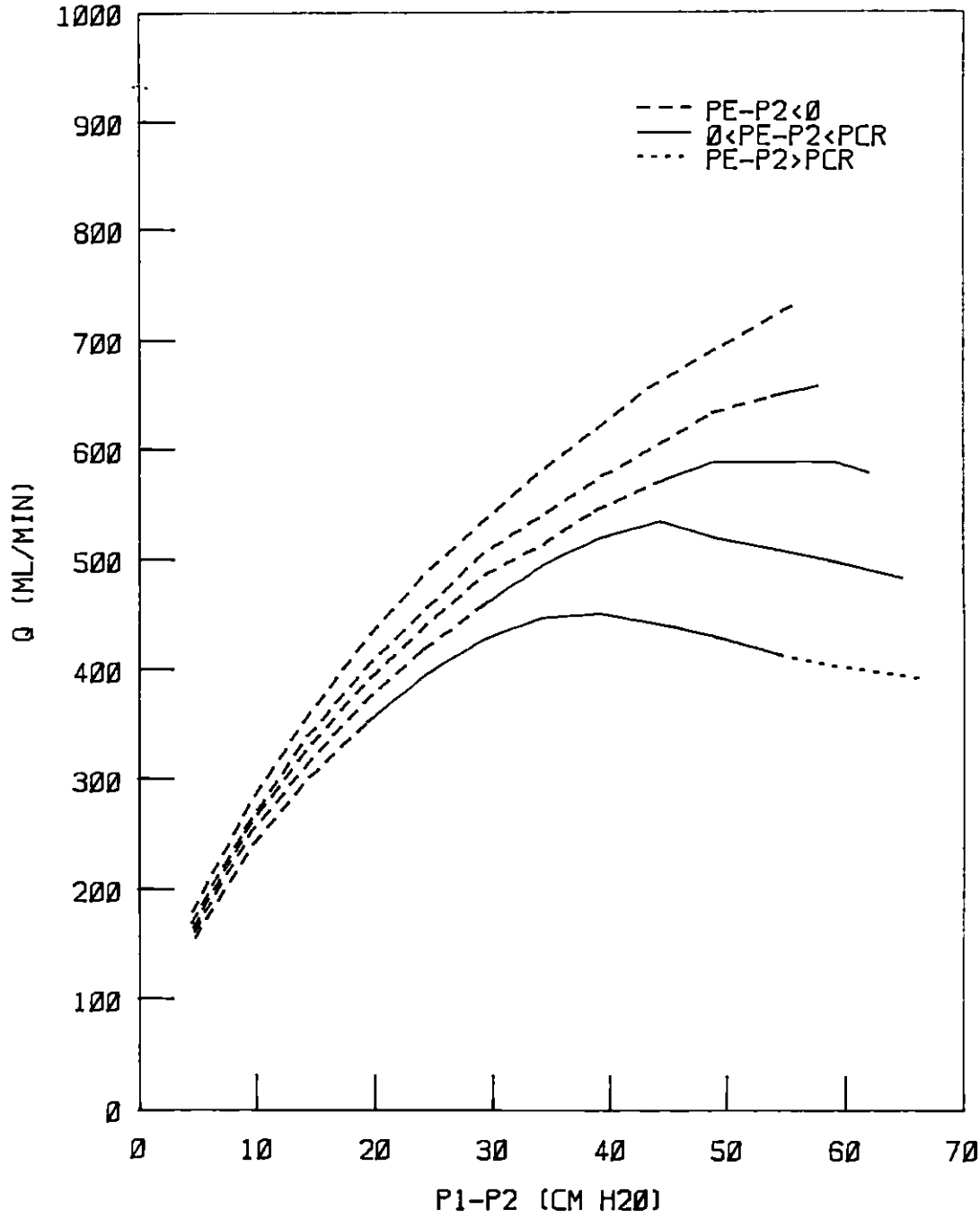

Figure 57. Significance of PE-P2: Pressure-flow data for the short 85% stenosis at an upstream pressure of 69.5 cm water partitioned into regions of PE-P2 relative to the measured static collapse pressure of 31.9 cm water

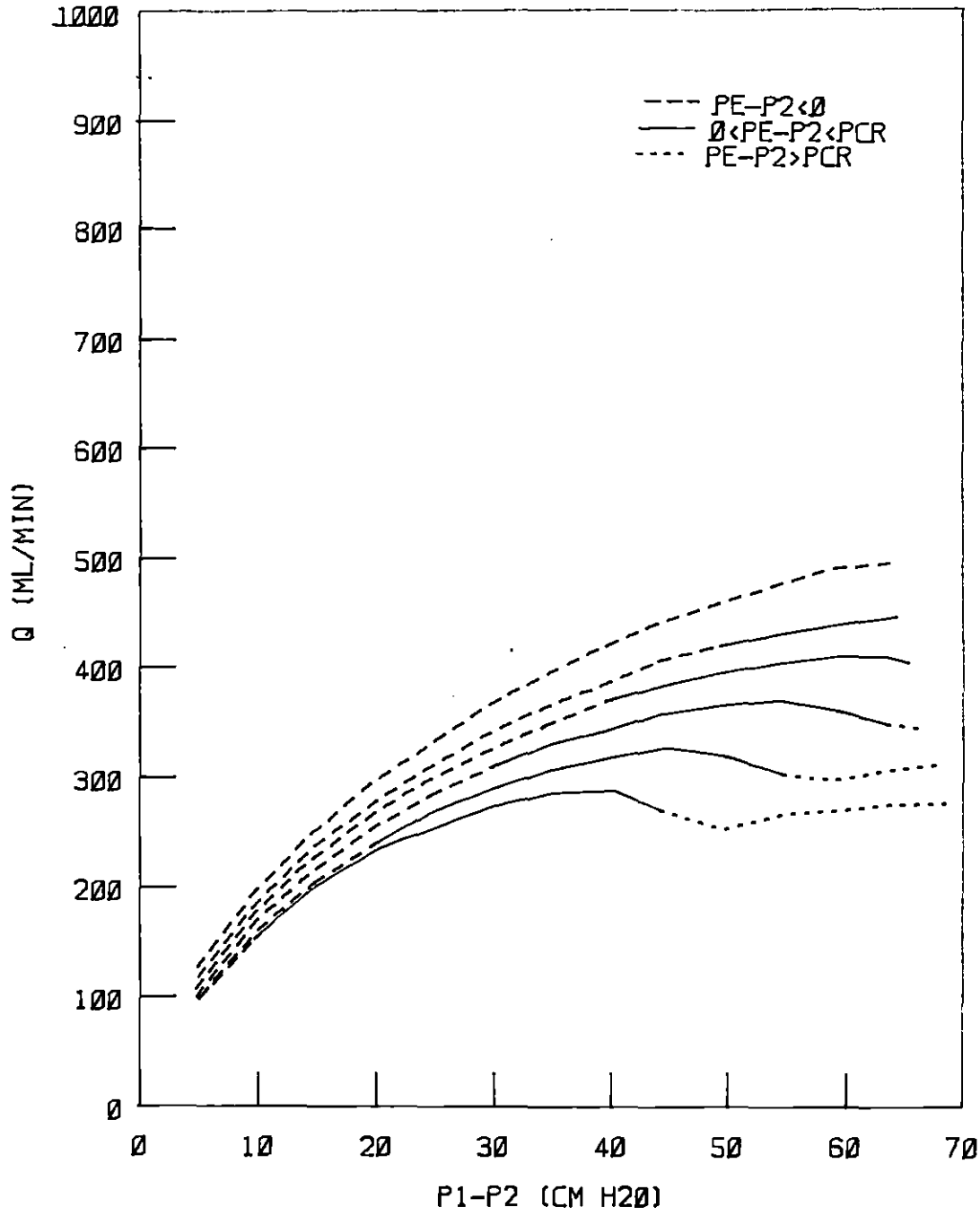

Figure 58. Significance of PE-P2: Pressure-flow data for the short 89.4% stenosis at an upstream pressure of 69.5 cm water partitioned into regions of PE-P2 relative to the measured static collapse pressure of 33.0 cm water

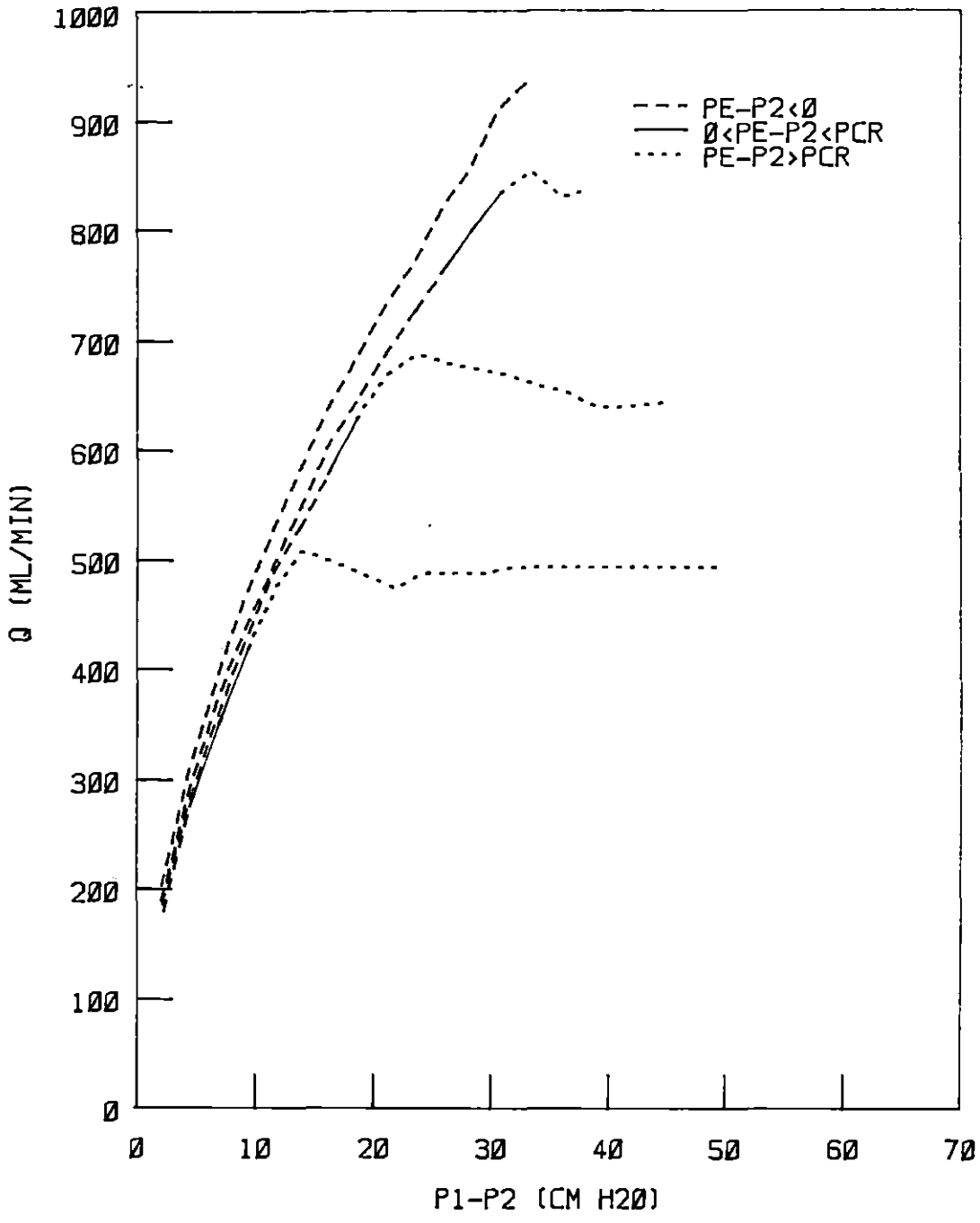

Figure 59. Significance of PE-P2: Pressure-flow data for the long 75% stenosis at an upstream pressure of 54.5 cm water partitioned into regions of PE-P2 relative to the measured static collapse pressure of 4.5 cm water

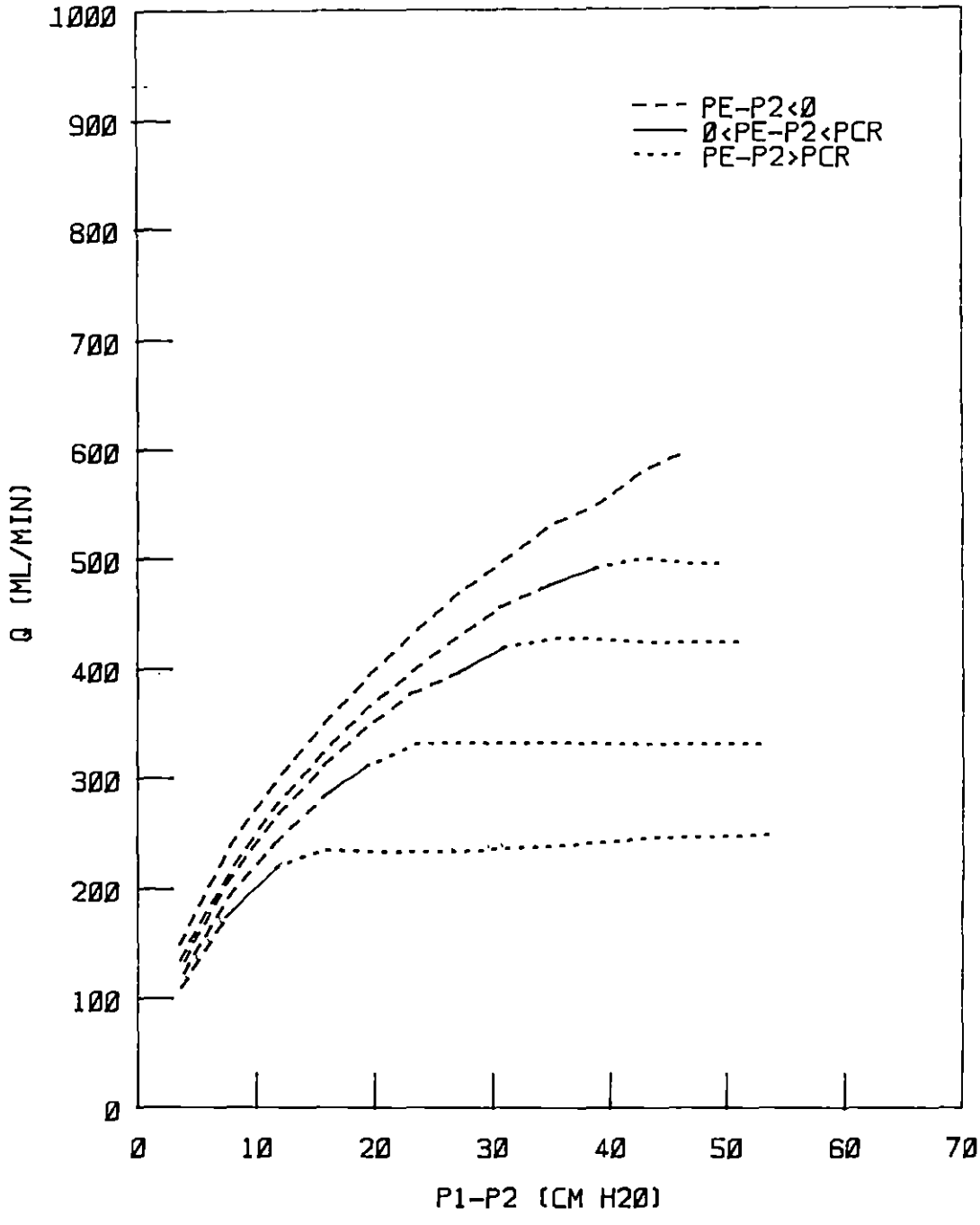

Figure 60. Significance of PE-P2: Pressure-flow data for the long 85% stenosis at an upstream pressure of 54.5 cm water partitioned into regions of PE-P2 relative to the measured static collapse pressure of 4.5 cm water

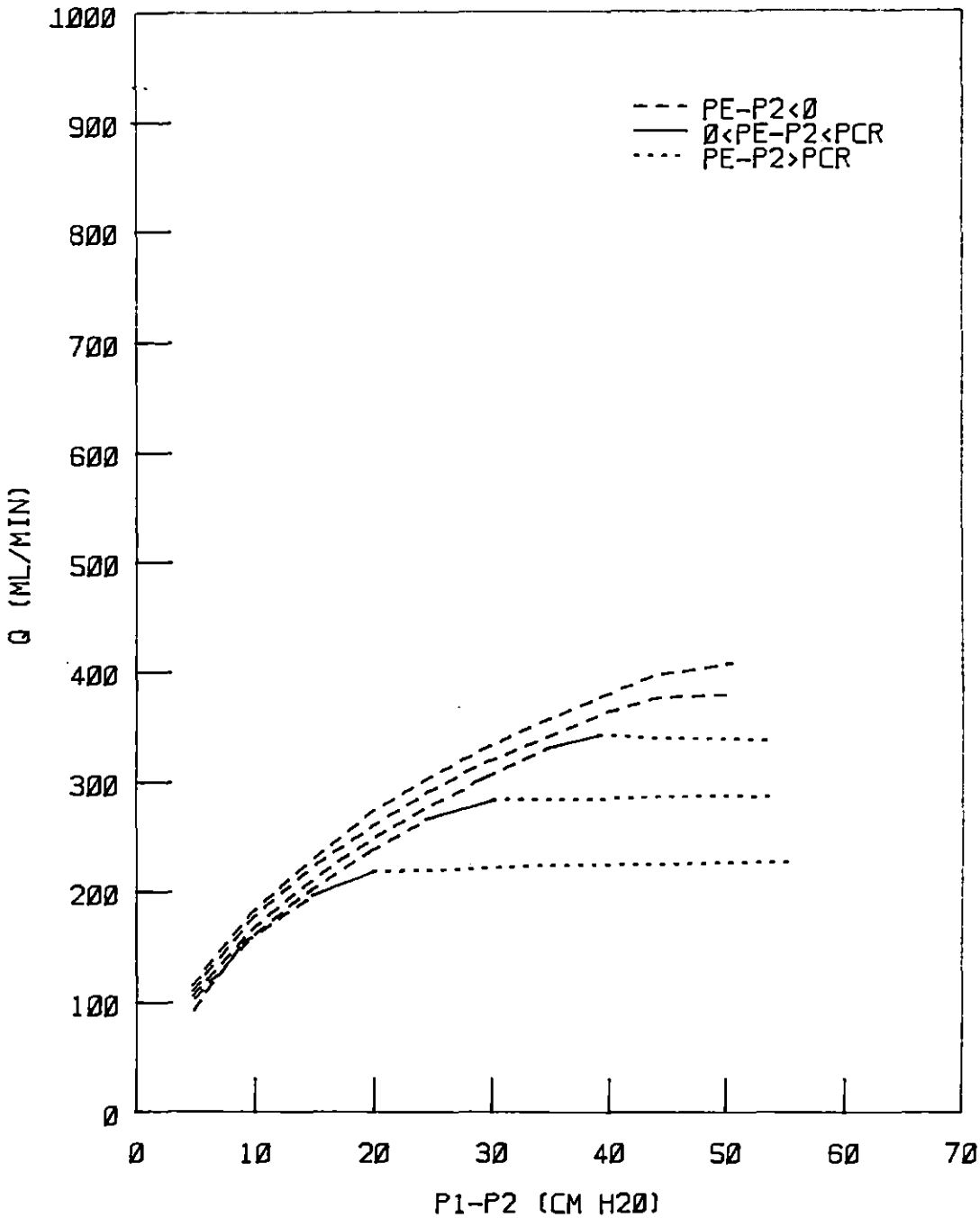

Figure 61. Significance of PE-P2: Pressure-flow data for the long 89.4% stenosis at an upstream pressure of 54.5 cm water partitioned into regions of PE-P2 relative to the measured static collapse pressure of 4.5 cm water

Table 5. Ranges of values of P_e-P_2 for the onset and cessation of tube oscillations (osc.)

Stenosis	P_1[a]	P_e[b]	Range of P_e-P_2[b] for begin osc.	Range of P_e-P_2[b] for end osc.
75% Short	L	50	35.3 - 39.6	(MAX 45.4)[c]
	H	50	32.5 - 39.1	(MAX 39.1)
	H	60	37.6 - 42.6	(MAX 54.2)
85% Short	L	40	33.3 - 37.4	(MAX 37.4)
	L	50	34.4 - 37.4	(MAX 49.3)
	H	40	25.0 - 29.6	(MAX 35.8)
	H	50	30.0 - 35.3	(MAX 47.6)
75% Long	L	30	9.5 - 12.2	(MAX 13.7)
	L	40	9.7 - 12.1	22.2 - 25.0
	L	50	9.8 - 12.4	14.8 - 17.6
85% Long	L	20	12.7 - 15.2	(MAX 15.2)
	L	30	11.5 - 15.3	18.9 - 22.6
89.4% Long	L	10	-5.0 - - 0.2	(MAX 6.5)
	L	20	-5.0 - 0.5	9.7 - 14.5
	L	30	0.1 - 5.7	9.6 - 15.3
	L	40	0.3 - 5.5	10.2 - 14.7

[a] L = low (54.5 cm water), H = high (69.5 cm water).

[b] All pressures are in cm water.

[c] The tube did not cease oscillating at the minimum value of P_2--MAX is the highest value of P_e-P_2 recorded.

on the pressure-area curves for the tubes. It is interesting to note that for the short configuration, for the values of external pressure that caused collapse, but not oscillation (75%, P_e = 40, 85%, P_e = 30, both at P_1 = 54.5 cm water), the maximum value of P_e-P_2 recorded was less than the values in the ranges of P_e-P_2 for which oscillations began at the higher external pressures. That is, since P_e-P_2 never reached the apparent critical value that initiates oscillations, oscillations did not occur for those curves. For the long configuration of the 89.4% stenosis, the ranges of values of P_e-P_2 for which oscillations ended also were the same (overlapped) for different values of P_1-P_e.

Results of the two-regime model

Since the values of P_{cr} determined statically were not applicable to the steady flow tests, segmentation of the model was performed by choosing values of P_{cr} that best fit the data. For simplification, the "best" values of P_{cr} were chosen so that one value could be used for all three values of percent stenosis for either the short configuration or the long configuration. A P_{cr} of 19.0 cm water was used for the short segments and a P_{cr} of 6.0 cm water was used for the long segments.

The model used to fit the data up to the critical pressure was of the form of Equation (5) for steady flow:

$$\frac{\Delta P}{\rho U^2} = \frac{K_v}{Re} + \frac{K_t}{2}\left[\frac{A_o}{A_1} - 1\right]^2 \qquad (11)$$

For values of P_e-P_2 greater than P_{cr}, flow rate was set equal to a constant (equal to the average of the measured flow rates in that region).

The data for P_e-P_2 less than P_{cr} for each value of external pressure were fit using an iterative least squares residuals method (Gauss-Newton). Goodness of fit of the model was determined by the R-squared statistic, which is the ratio of the sum of squares accounted for by fitting a model beyond the simplest representation to the total sum of squared deviations from the mean. Values close to unity represent good agreement between observed values and values predicted by the model. All values of R^2 were greater than 0.993, indicating a good fit between the measured and predicted values.

The values of K_v and K_t found for all of the configurations at all of the external pressures studied are given in Table 6. Both K_v and K_t increased with P_1-P_e , and K_v increased with percent stenosis. Values of K_t for the rigid 75% stenosis were 6% higher than the values for the 85% stenosis, and 15% higher than the values for the 89.4% stenosis. The values of K_t are higher than the average value of 1.5 found in past studies cited by Young (1979), even for the rigid configurations. The reason for this difference is unclear, although it may be due to the fact that the 1.5 value for K_t was obtained for stenoses with circular cross-section. Also, the value of 1.5 is an average--higher values were obtained for some stenoses. Since percent stenosis did not appear to be constant, even for zero external pressure, some variation in K_t between stenoses would be expected for the compliant stenoses (which did occur).

Plots of the predicted values against the observed values are shown in Figures 62-70. Very good fit was achieved for the rigid stenoses, but not for the short compliant stenoses at high values of P_e-P_2. Use of a constant flow equation was very inaccurate for the short 75% stenosis, but

Table 6. Summary of least-squares fit values of constants K_v and K_t

C[a]	P_1-P_e cm H_2O	75% Stenosis			85% Stenosis			89.4% Stenosis		
		n[b]	K_v	K_t	n	K_v	K_t	n	K_v	K_t
R	69.5	10	4629	2.43	11	16837	2.15	13	31273	2.04
S	69.5	9	2374	2.32	11	12973	1.87	13	13408	2.04
R	54.5	13	4437	2.54	15	13906	2.38	13	33335	2.15
S	54.5	13	2832	2.46	15	11598	2.15	10	23452	1.84
S	49.5				12	11427	2.29	13	13607	2.41
S	39.5				11	10595	2.54	11	18154	2.44
S	34.5				16	12207	2.53	10	23134	2.28
S	29.5	11	3452	2.78	9	11491	2.67	9	24114	2.48
S	24.5	14	2324	3.06	14	12456	2.79	8	25423	2.41
S	19.5	14	3111	3.12	7	10372	3.02	7	24338	2.71
S	14.5	13	1774	3.43	11	12426	3.12	6	29801	2.53
S	9.5	11	2332	3.54				5	23907	2.81
S	4.5	9	2812	3.64	7	12415	3.54	4	31365	2.77
L	54.5	14	4435	2.74	12	9388	2.45	10	16650	2.34
L	44.5							9	17803	2.48
L	34.5				10	10623	2.86	8	19087	2.66
L	24.5	12	4842	3.09	7	12567	2.96	6	21211	2.82
L	14.5	8	4443	3.33	5	13997	3.41	4	29430	2.64
L	4.5	4	4102	3.63	2	18782	3.40			

[a]Configuration (S = short, L = long, R = rigid short).

[b]Number of data points.

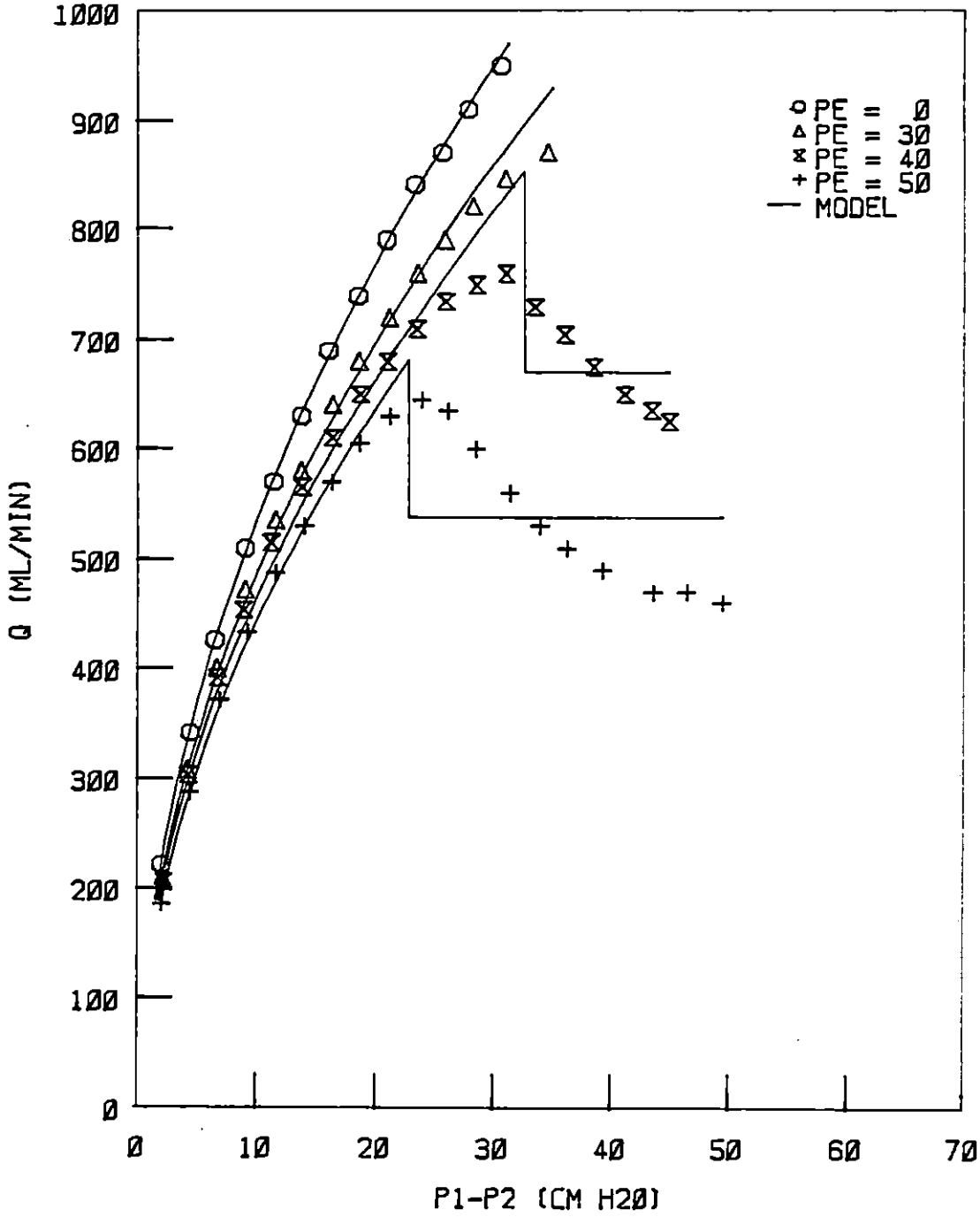

Figure 62. Results of the two-regime model for the short 75% stenosis at an upstream pressure of 54.5 cm water (all pressures in cm water, P_{cr} = 19.0 cm water)

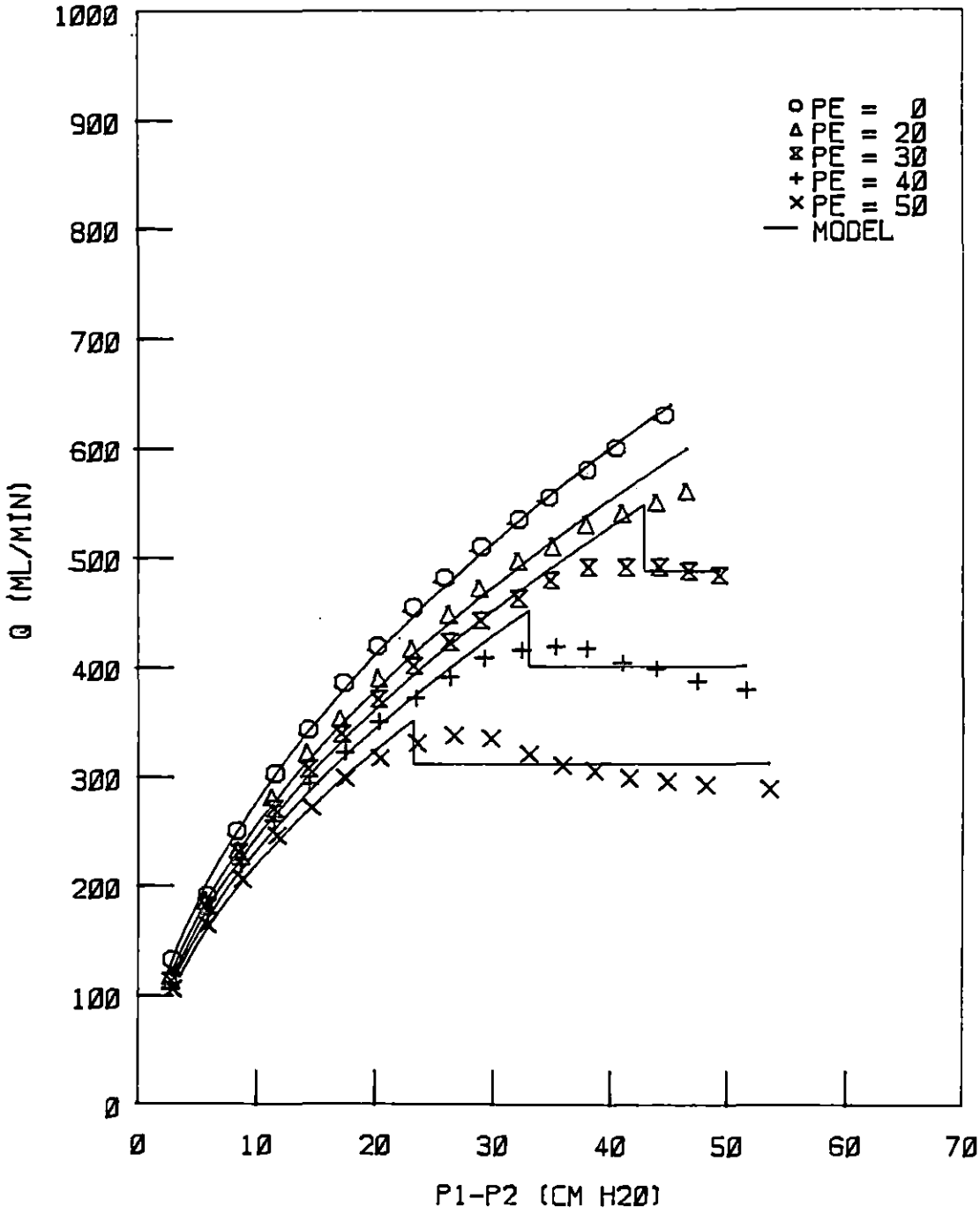

Figure 63. Results of the two-regime model for the short 85% stenosis at an upstream pressure of 54.5 cm water (all pressures in cm water, P_{cr} = 19.0 cm water

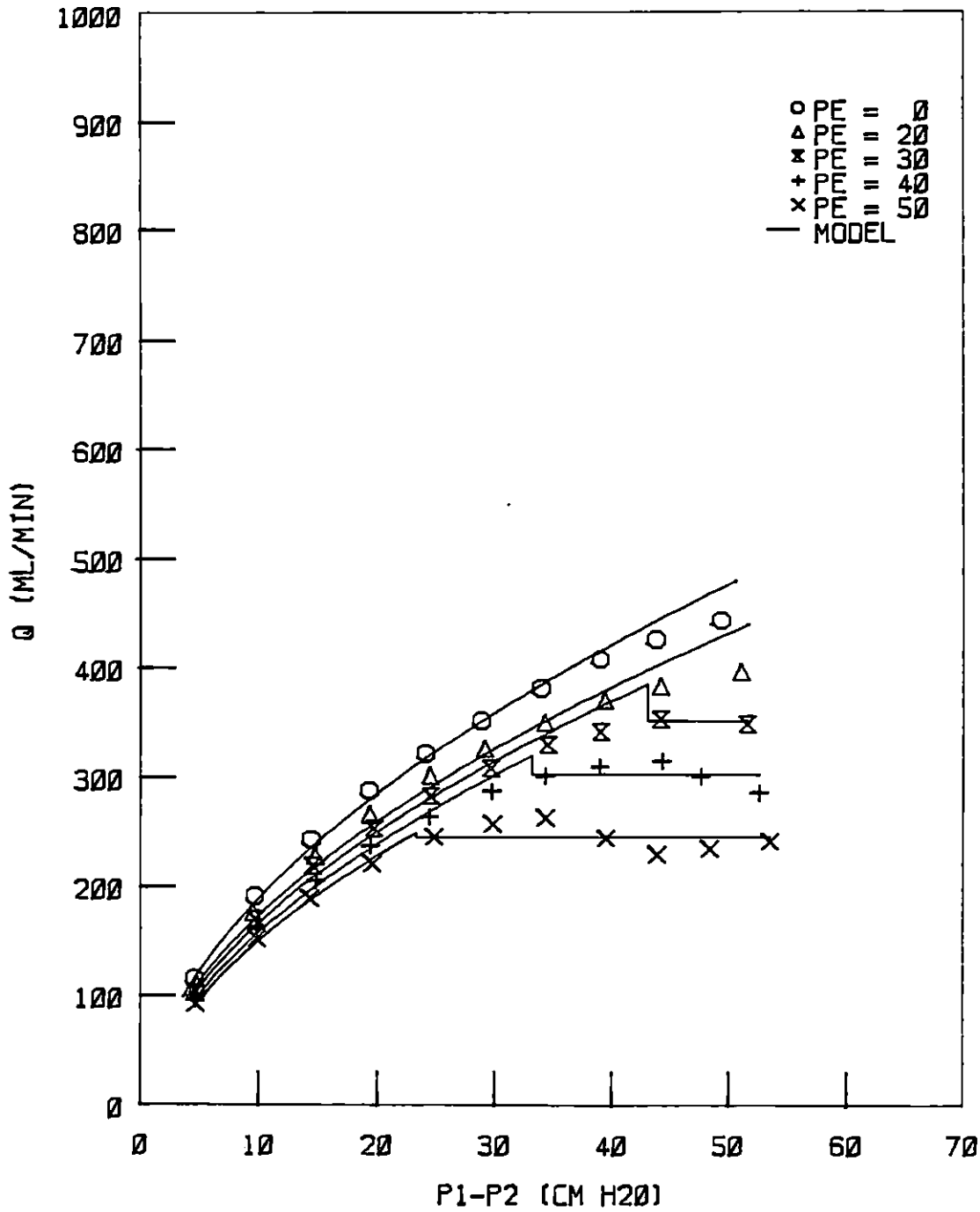

Figure 64. Results of the two-regime model for the short 89.4% stenosis at an upstream pressure of 54.5 cm water (all pressures in cm water, P_{cr} = 19.0 cm water)

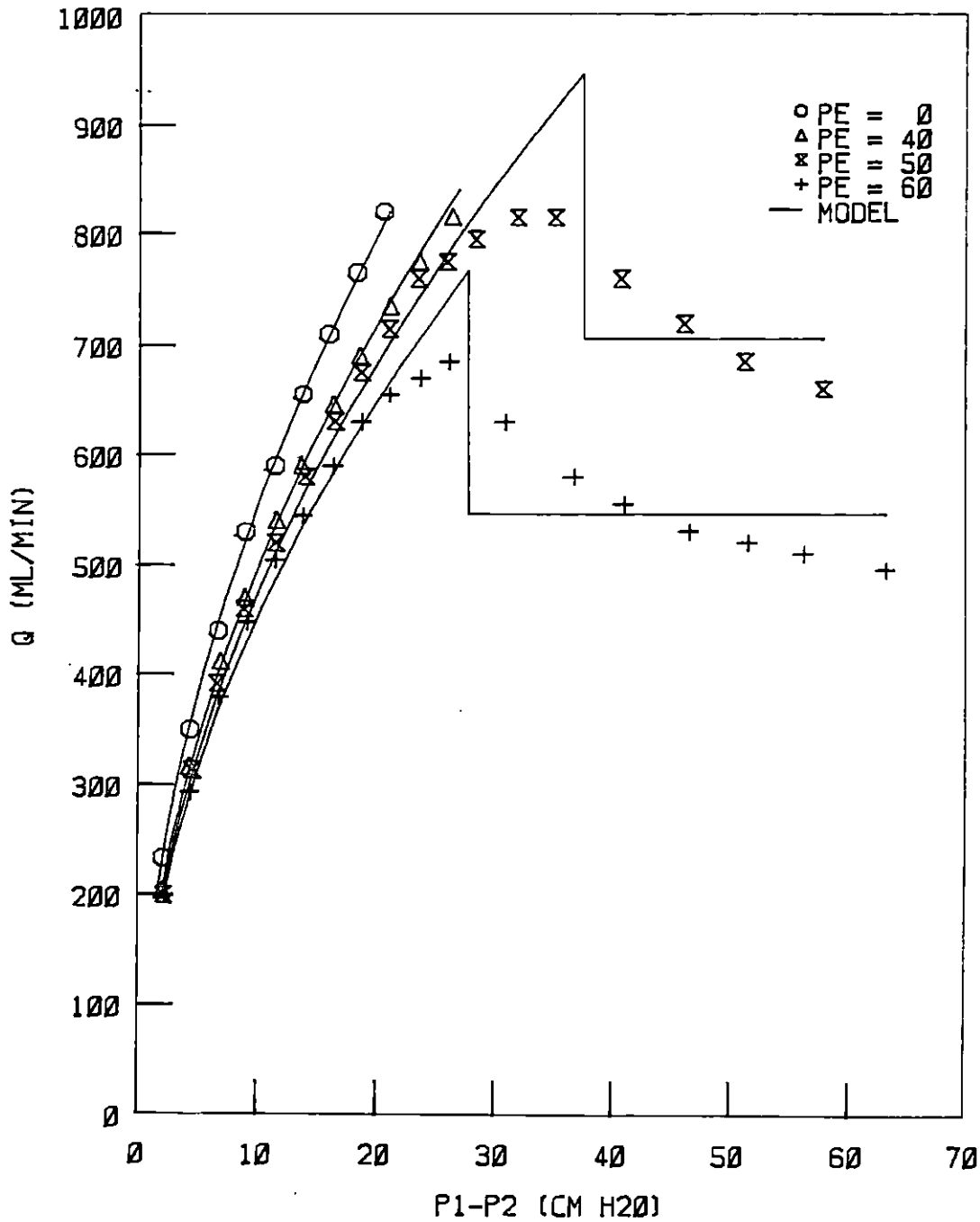

Figure 65. Results of the two-regime model for the short 75% stenosis at an upstream pressure of 69.5 cm water (all pressures in cm water, P_{cr} = 19.0 cm water)

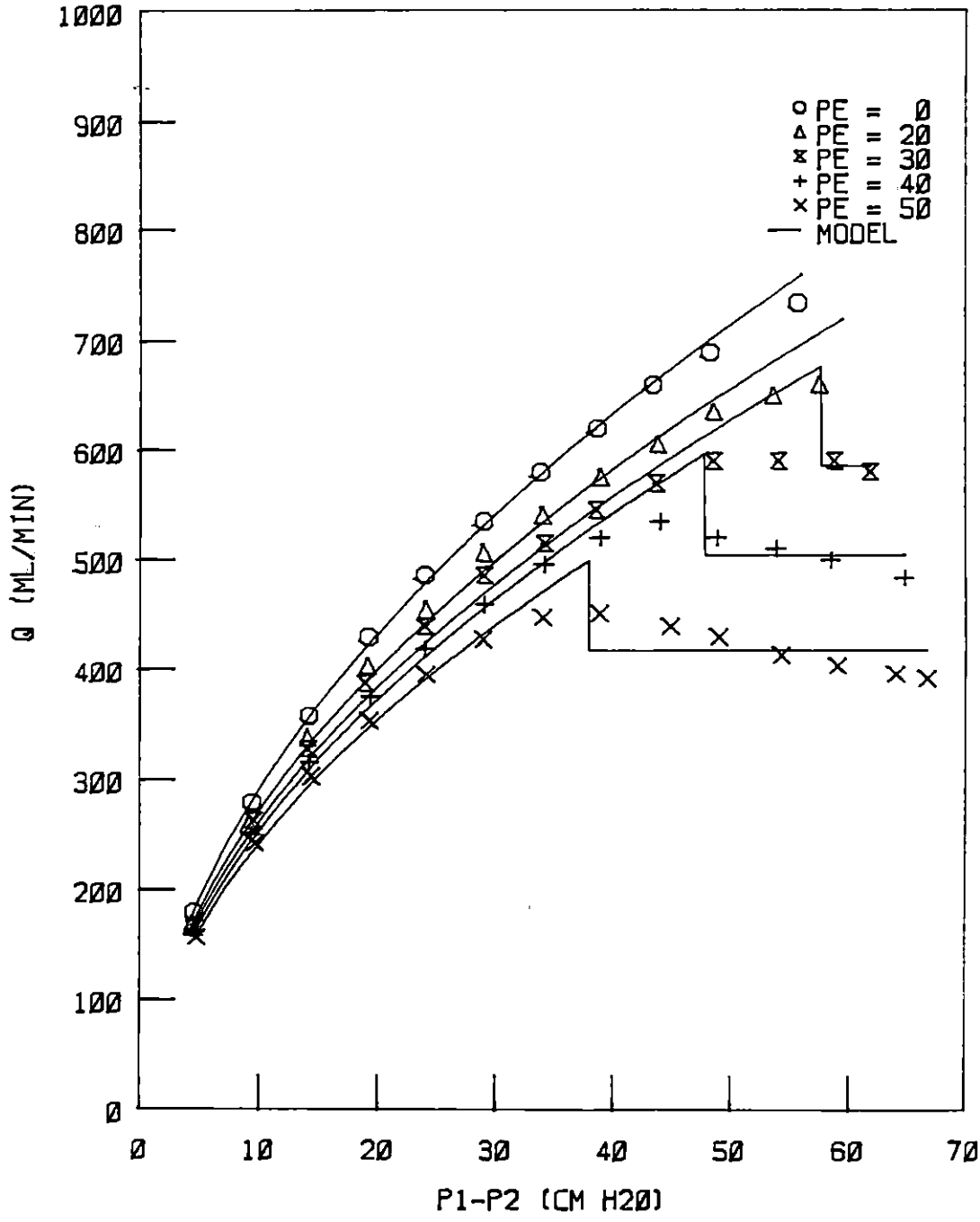

Figure 66. Results of the two-regime model for the short 85% stenosis at an upstream pressure of 69.5 cm water (all pressures in cm water, P_{cr} = 19.0 cm water)

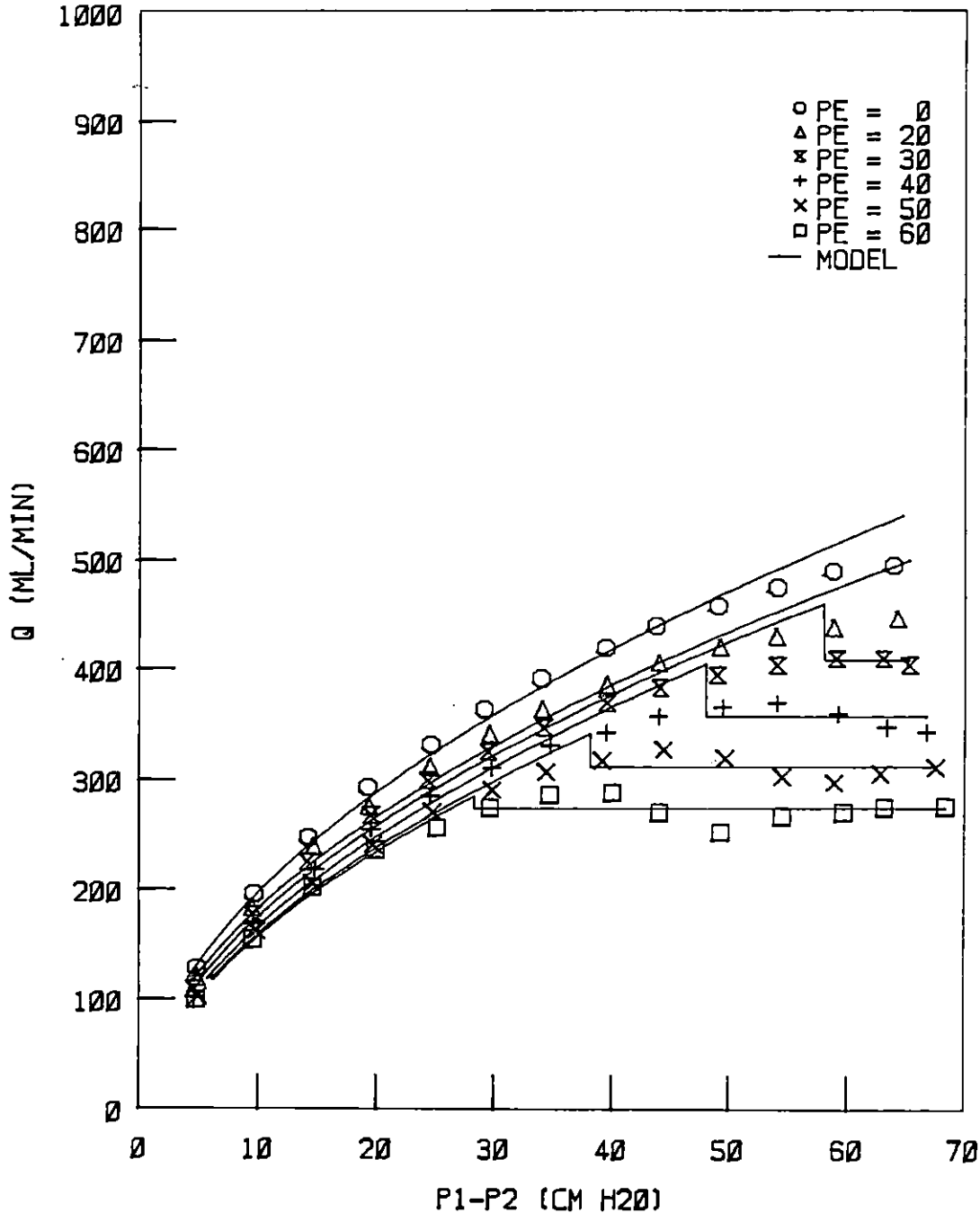

Figure 67. Results of the two-regime model for the short 89.4% stenosis at an upstream pressure of 69.5 cm water (all pressures in cm water, P_{cr} = 19.0 cm water)

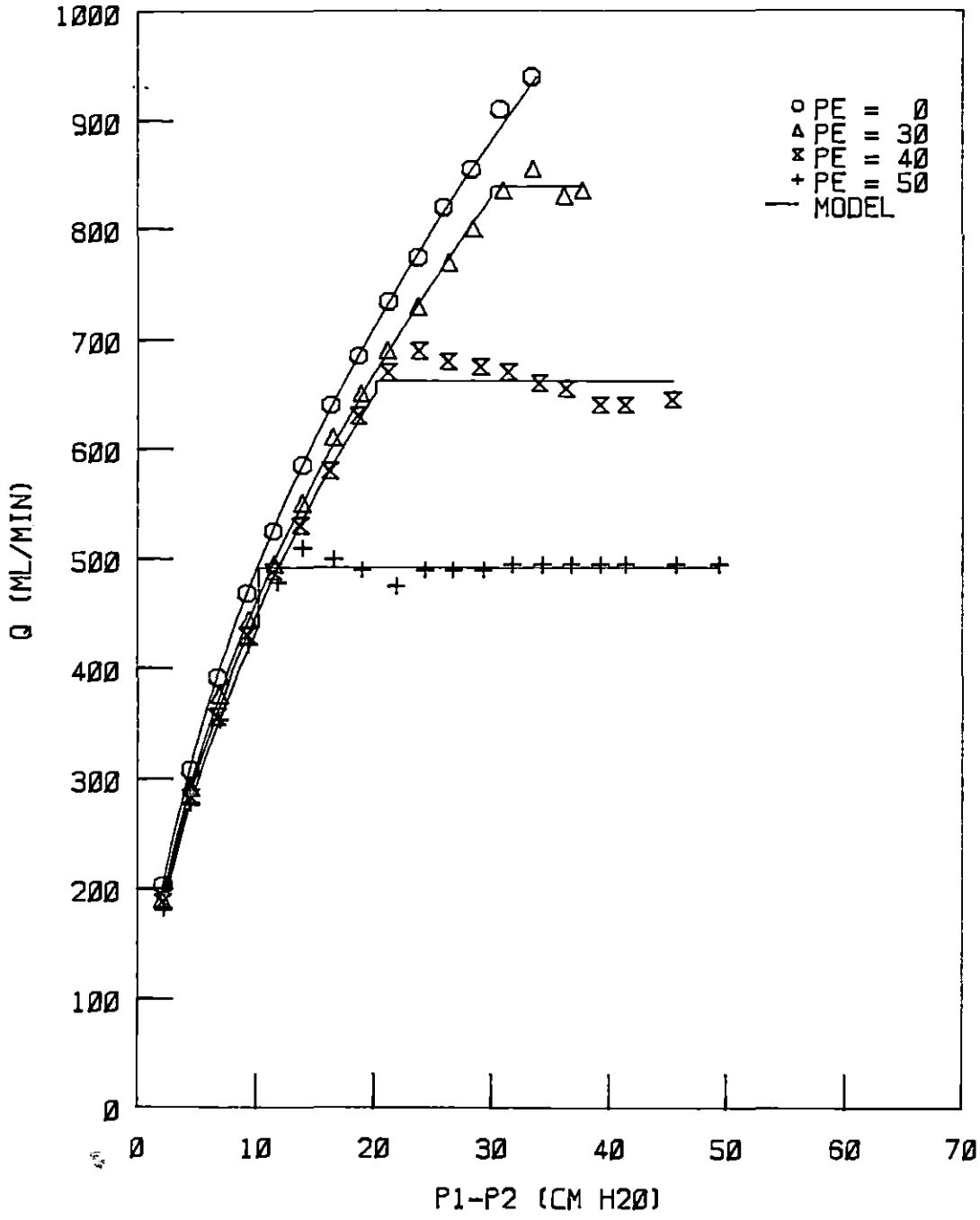

Figure 68. Results of the two-regime model for the long 75% stenosis at an upstream pressure of 54.5 cm water (all pressures in cm water, P_{cr} = 6.0 cm water

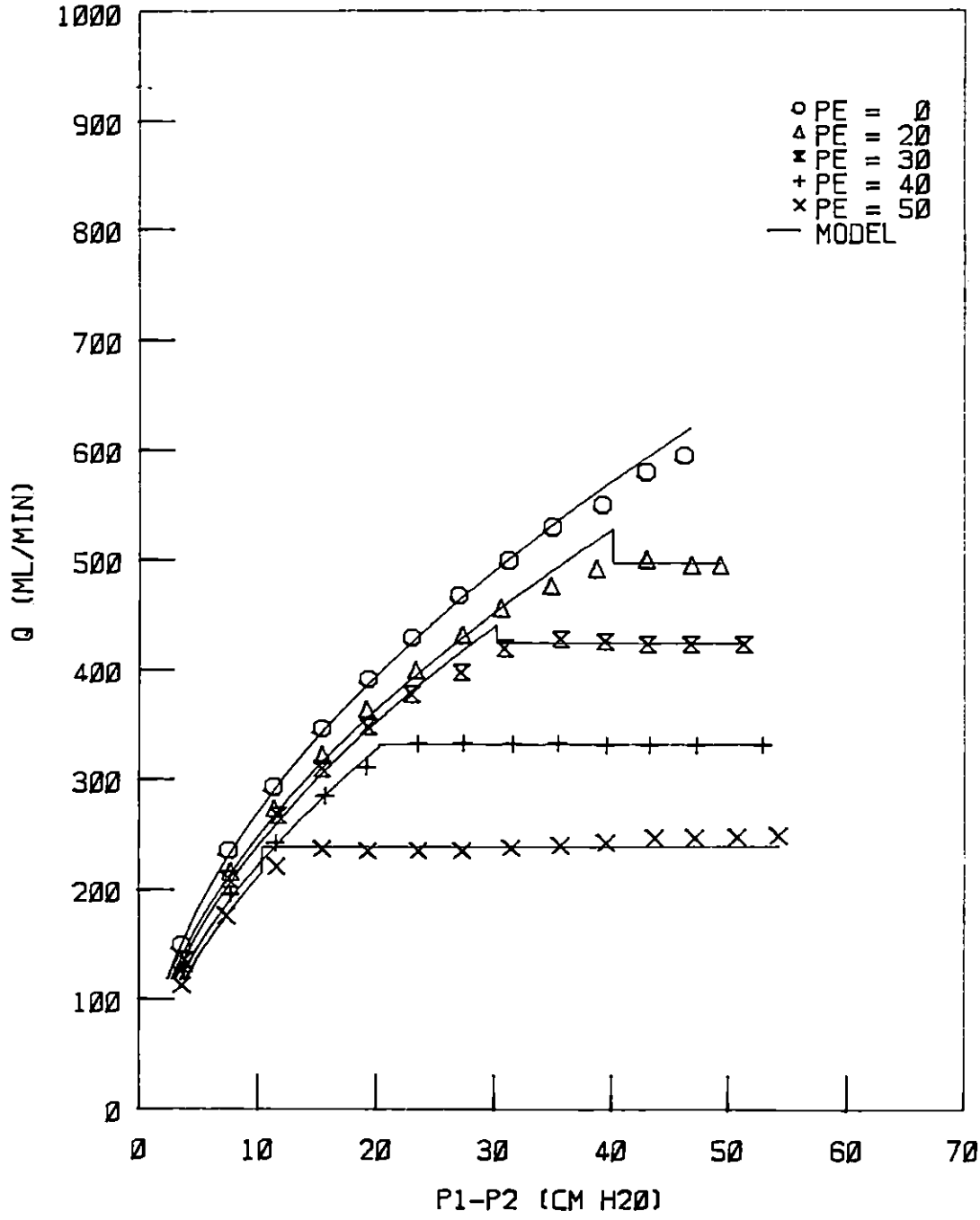

Figure 69. Results of the two-regime model for the long 85% stenosis at an upstream pressure of 54.5 cm water (all pressures in cm water, P_{cr} = 6.0 cm water)

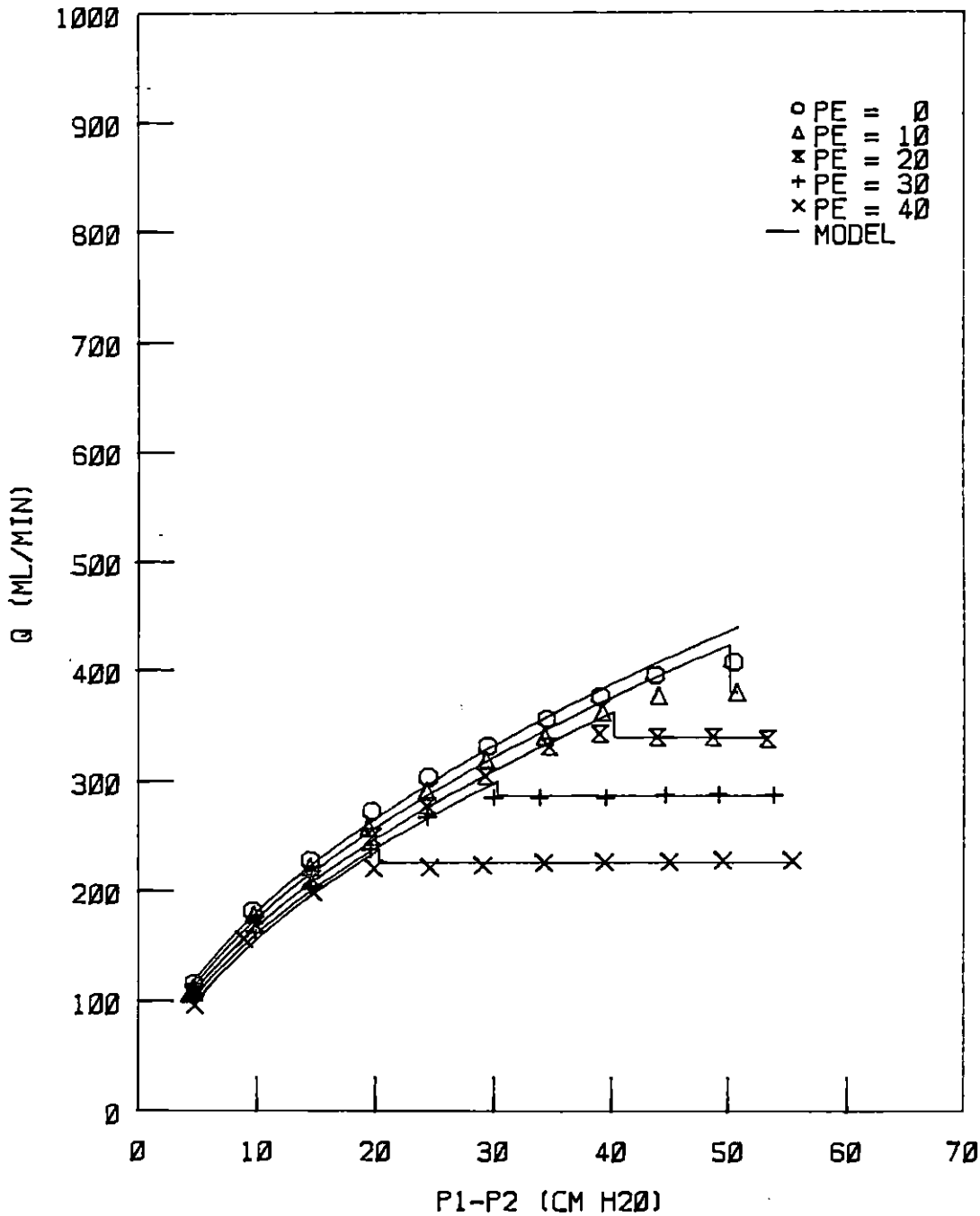

Figure 70. Results of the two-regime model for the long 89.4% stenosis at an upstream pressure of 54.5 cm water (all pressures in cm water, P_{cr} = 6.0 cm water)

fairly reasonable for the other stenoses, and especially for the long configurations. For the short segments, accuracy improved with increasing external pressure.

SUMMARY AND CONCLUSIONS

The results of this study indicate that flow limitation occurs for collapsible tubing with a stenosis, as it does for collapsible tubing without a stenosis. Large amplitude, self-excited oscillations of varying frequency occurred for collapse in the stenosed area or downstream of it, depending on the configuration. Effective severity of the collapsed segments increased as the downstream pressure was progressively reduced after collapse. The long configurations had greater effective severity than did the short configurations for a given pressure drop and external pressure, except for very high values of P_e-P_2 for the 75% stenosis. Qualitative differences were seen between the two configurations, with the short segment showing a decrease in flow after collapse, with subsequent leveling off, and the long segment tending to simply level off after collapse. The pressure differential P_1-P_e was found to be the determinant of the flow rate in the collapsed state for both configurations, and showed a linear relationship with the maximum flow rate reached. Statically determined values of critical collapse pressures were found to be relatively inaccurate measures of the critical values for steady flow conditions in some cases. P_e-P_2 was found to be an important determinant of whether the tube was open or collapsed, and whether it was oscillating or stable.

Use of a two-regime model with a quadratic relation between pressure drop and flow up to P_{cr}, and a constant flow beyond P_{cr} was found to be accurate for the long configuration for all values of percent stenosis, but not for the short configuration with a 75% stenosis. Values of K_v and

K_t increased with P_1-P_e and were higher for the longer configuration than for the shorter configuration. Values of K_t varied somewhat with percent stenosis, even for the rigid configurations. The reason for this is probably due primarily to a certain amount of lack of fit of the model.

The clinical significance of the study is somewhat limited by the fact that the model used steady flow and neglected to account for many of the physiologic considerations discussed previously; however, some clinically relevant conclusions may be drawn. One important conclusion is that if the pressure downstream of a stenosis is lowered by distal vasodilation, flow may be reduced, rather than augmented, as it has been found to be in studies with vasodilatory drugs. The only way to increase flow through a compliant stenosis in the flow limited region was to increase P_1, which verifies the (speculated) need for proximal arterial dilation to achieve an increase in flow to ischemic vascular beds.

Collapse of a stenosed artery might have different flow effects than collapse of latex tubing for equivalent geometric and mechanical properties because blood vessel muscle is known to shorten with collapse, whereas the perimeter of the latex tubing stays the same during collapse. Although collapse did not occur in the stenosis when it occurred in the downstream region, collapse in the stenosed area of an artery should not be completely ruled out as a possibility, considering the effects of passive narrowing and distention in in vivo segments of coronary arteries containing eccentric stenoses. That is, in vivo studies conducted at zero external pressure on naturally occurring stenoses revealed that eccentric stenoses showed greater resistance changes than did concentric stenoses. This could be because mechanical characteristics may not be constant along the entire

length of arteries, as they are in latex tubing. Had the in vivo studies been conducted at non-zero pressure, the effects of the compliant stenoses probably would have been even greater. In addition to reducing flow, collapse in the stenosed region might further the progression of the disease by damaging the atherosclerotic plaque (although this is a different type of problem).

Further studies should be done on the compliant stenosis problem, including pulsatile flow studies on models similar to the ones in the present study, and studies on similar values of percent stenosis with different values of $\ell_c/\pi D$. Also, studies on tubes of different thickness (and elasticity) might be useful, as well as detailed studies of pressures in the collapsed region of the stenosis and in the collapsed downstream section. Some theoretical analysis should be performed, and in vivo studies on either naturally occurring or artificially induced stenoses should be conducted. Even though current technology makes the identification of eccentric vs. concentric stenoses difficult, if not impossible to determine, more information on compliant stenoses and their implications for heart attacks, strokes and other circulatory problems is needed.

BIBLIOGRAPHY

Brower, Robert W., and Abraham Noordergraaf. 1973. Pressure-Flow Characteristics of Collapsible Tubes: A Reconciliation of Seemingly Contradictory Results. Annals of Biomedical Engineering 1:333-355.

Brower, R. W., and Ir. C. Scholten. 1972. 25th Annual Conference on Engineering in Medicine and Biology.

Brown, B. Greg, Bolson, Edward L., and Harold T. Dodge. 1984. Dynamic Mechanisms in Human Coronary Stenosis. Circulation 70(6):917-922.

Caro, C. G., Pedley, T. J., Schroter, R. C., and W. A. Seed. 1978. The Mechanics of the Circulation. Oxford University Press, Oxford, England.

Conrad, William A. 1969. Pressure-Flow Relationships in Collapsible Tubes. IEEE Transactions on Biomedical Engineering BME-16(4):284-295.

Conrad, W. A., McQueen, D. M., and E. L. Yellin. 1980. Steady Pressure Flow Relations in Compressed Arteries: Possible Origin of Korotkoff Sounds. Medical and Biological Engineering and Computing 18:419-426.

Doerner, Thomas C., Brown, B. Greg, Bolson, Edward, Frimer, Morris, and Harold T. Dodge. 1979. Vasodilatory Effects of Nitroglycerin and Nitroprusside--a Comparative Analysis. The American Journal of Cardiology 43:416. (abstr.)

Downey, James M., and Edward S. Kirk. 1975. Inhibition of Coronary Blood Flow by a Vascular Waterfall Mechanism. Circulation Research 36:753-760.

Elliott, E. A., and S. V. Dawson. 1978. Fluid Velocity Greater than Wavespeed and the Transition from Supercritical to Subcritical Flow in Elastic Tubes. Medical and Biological Engineering and Computing 17:192-198.

Eng, Calvin, and Edward S. Kirk. 1984. Flow into Ischemic Myocardium and across Coronary Collateral Vessels is Modulated by a Waterfall Mechanism. Circulation Research 55(1):10-17.

Freudenburg, H., and P. R. Lichtlen. 1981. The Normal Wall Segment in Coronary Stenosis--A Postmortem Study. Zeitschrift fur Kardiologie 70:863-869.

Fry, Donald L., Thomas, Lewis J., and Joseph C. Greenfield, Jr. 1980. Flow in Collapsible Tubes. Pages 407-424 in Dali J. Patel and Ramesh N. Vaishnav, eds. Basic Hemodynamics and its Role in Disease Processes. University Park Press, Baltimore, Maryland.

Fung, Y. C. 1984. Biodynamics Circulation. Springer Verlag, New York, New York.

Gould, K. Lance. 1978. Pressure-Flow Characteristics of Coronary Stenoses in Unsedated Dogs at Rest and during Coronary Vasodilation. Circulation Research 43(2):242-253.

Gould, K. Lance. 1980. Dynamic Coronary Stenosis. The American Journal of Cardiology 45:266-292.

Gould, K. Lance, Lipscomb, Kirk, and Cynthia Calvert. 1975. Compensatory Changes of the Distal Coronary Vascular Bed During Progressive Coronary Constriction. Circulation 51:1085-1094.

Griffiths, D. J. 1971a. Hydrodynamics of Male Micturition--I: Theory of Steady Flow Through Elastic-Walled Tubes. Medical and Biological Engineering and Computing 9:581-588.

Griffiths, D. J. 1971b. Steady Fluid Flow Through Veins and Collapsible Tubes. Medical and Biological Engineering and Computing 9:597-602.

Holmberg, J. L., and T. A. Wilson. 1970. Mechanics of the Flow in an Elastic Tube Extending from an Orifice into a Pressure Vessel. Journal of Applied Mechanics 70-APM-ZZ:1-5.

Holt, J. P. 1959. Flow of Liquids through "Collapsible" Tubes. Circulation Research 7:342-353.

Katz, Adolpho I., Chen, Yu, and Augusto H. Moreno. 1969. Flow Through a Collapsible Tube: Experimental Analysis and Mathematical Model. Biophysical Journal 9:1261-1279.

Lipscomb, Kirk, and Steven Hooten. 1978. Effect of Stenotic Dimensions and Blood Flow on the Hemodynamic Significance of Model Coronary Arterial Stenoses. The American Journal of Cardiology 42:781-792.

Logan, Samuel E. 1975. On the Fluid Mechanics of Human Coronary Artery Stenosis. IEEE Transactions on Biomedical Engineering BME-22(4):327-334.

Milnor, William R. 1982. Hemodynamics. Waverly Press, Inc., Baltimore, Maryland.

Moreno, Augusto H., Katz, Adolph I., Gold, Louis D., and R. V. Reddy. 1970. Mechanics of Distension of Dog Veins and Other Very Thin-Walled Tubular Structures. Circulation Research 27:1069-1080.

Permutt, S., and R. L. Riley. 1963. Hemodynamics of Collapsible Vessels with Tone: the Vascular Waterfall. Journal of Applied Physiology 18(5):924-932.

Rodbard, Simon. 1955. Flow Through Collapsible Tubes: Augmented Flow Produced by Resistance at the Outlet. Circulation 11:280-287.

Rodbard, Simon, and Hiroshi Saiki. 1953. Flow Through Collapsible Tubes. American Heart Journal 46:715-725.

Rubinow, S. I., and Joseph B. Keller. 1972. Flow of a Viscous Fluid Through an Elastic Tube with Applications to Blood Flow. Journal of Theoretical Biology 35:299-313.

Santamore, William P., and Paul Walinsky. 1980. Altered Coronary Flow Responses to Vasoactive Drugs in the Presence of Coronary Arterial Stenosis in the Dog. The American Journal of Cardiology 45:276-285.

Santamore, William P., Walinsky, Paul, Bove, Alfred A., Cox, Robert H., Carey, Rita A., and James F. Spann. 1980. The effects of Vasoconstriction on Experimental Coronary Artery Stenosis. American Heart Journal 100(6):852-858.

Santamore, William P., Bove, Alfred A., Carey, Rita, Walinsky, Paul, and James F. Spann. 1981. Synergistic Relation between Vasoconstriction and Fixed Epicardial Vessel Stenosis in Coronary Artery Disease. American Heart Journal 101(4):428-434.

Schwartz, Jeffrey S., Carlyle, Peter F., and Jay N. Cohn. 1979. Effect of Dilation of the Distal Coronary Bed on Flow and Resistance in Severely Stenotic Coronary Arteries in the Dog. The American Journal of Cardiology 43:219-224.

Schwartz, Jeffrey S., Carlyle, Peter F., and Jay N. Cohn. 1980. Effect of Coronary Arterial Pressure on Coronary Stenosis Resistance. Circulation 61(1):70-76.

Shapiro, Ascher H. 1977. Steady Flow in Collapsible Tubes. Journal of Biomechanical Engineering 99:126-147.

Uhlig, Paul N., Baer, Robert W., Vlahakes, Gus J., Hanley, Frank L., Messina, Louis M., and Julien I. E. Hoffman. 1984. Arterial and Venous Coronary Pressure-Flow Relations in anesthetized Dogs: Evidence for a Vascular Waterfall in Epicardial Coronary Veins. Circulation Research 55(2):238-248.

Walinsky, P., Santamore, W. P., Wiener, L., and A. N. Brest. 1979. Dynamic Changes in the Haemodynamic Severity of Coronary Artery Stenosis in a Canine Model. Cardiovascular Research 13:113-118.

Weast, Robert C. 1976. Handbook of Chemistry and Physics. 57th ed. CRC Press, Inc., Cleveland, Ohio.

Young, D. F. 1979. Fluid Mechanics of Arterial Stenoses. Journal of Biomechanical Engineering 101:157-175.

ACKNOWLEDGEMENTS

I would like to thank Dr. Donald F. Young for his guidance and patience and Mike Anderson and Dr. Pam McAllister for their help with designing the laboratory apparatus and taking experimental measurements and photographs. I would also like to thank the Iowa Chapter of the American Heart Association for supporting this research.

APPENDIX A

Apparatus Dimensions and Specifications

Dimensions of stenoses

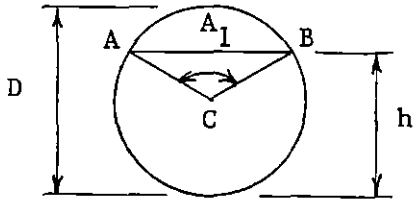

75%: h = 0.1526 in.
85%: h = 0.1764 in.
89.4%: h = 0.1880 in.

$r = D/2 \quad \angle ACB° = 180° - 2\sin^{-1}((h-r)/r)$

$$A_1 = \frac{r^2}{2}\left[\frac{\pi \angle ACB°}{180°} - \sin(\angle ACB)\right]$$

$$\text{Percent stenosis} = \left(1 - \frac{A_1}{A_o}\right) \times 100 \quad (A_o = \pi D^2/4)$$

Location of pressure taps

Short

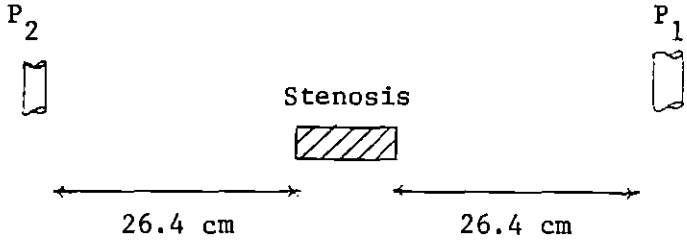

Long

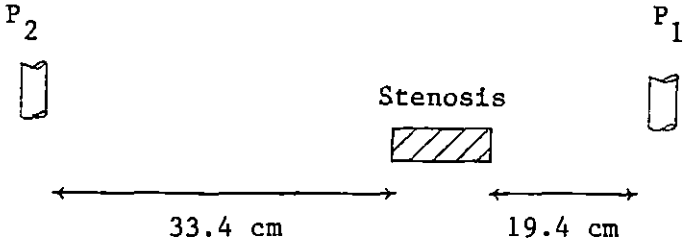

Specifications of recording equipment for oscillation measurements

Dynograph recorder	Beckman R-611
	Serial number: 603-26459
	Channel: 3
Pressure transducer	Statham P23Dc
	Serial number: 28162

APPENDIX B: PRESSURE-FLOW DATA FOR THE RIGID CONFIGURATION AT AN UPSTREAM PRESSURE OF 54.5 CM WATER

TABLE 7. DATA FOR A RIGID CONFIGURATION 75% STENOSIS

MEASURED P1-P2 (CM H20)	CORRECTED P1-P2 (CM H20)	Q (ML/MIN)	RE	P1 (CM H20)	P2 (CM H20)
2.4	2.0	204.	763	54.3	52.3
5.0	4.4	316.	1182	54.2	49.8
7.4	6.6	408.	1526	54.1	47.5
10.2	9.2	488.	1826	54.0	44.8
12.6	11.5	550.	2058	54.0	42.4
14.9	13.7	605.	2263	53.9	40.2
17.6	16.3	665.	2488	53.8	37.6
20.0	18.6	710.	2656	53.8	35.2
22.5	21.0	755.	2825	53.7	32.8
25.0	23.4	805.	3012	53.7	30.3
27.4	25.8	845.	3162	53.7	27.9
30.0	28.2	890.	3330	53.6	25.4
33.8	31.9	950.	3555	53.6	21.6

TABLE 8. DATA FOR A RIGID CONFIGURATION 85% STENOSIS

MEASURED P1-P2 (CM H2O)	CORRECTED P1-P2 (CM H2O)	Q (ML/MIN)	RE	P1 (CM H2O)	P2 (CM H2O)
3.0	2.8	120.	449	54.4	51.6
6.0	5.7	187.	699	54.3	48.6
9.1	8.7	240.	898	54.3	45.6
11.8	11.2	280.	1047	54.2	43.0
14.9	14.3	322.	1204	54.2	39.9
17.7	17.0	354.	1324	54.1	37.2
20.8	20.0	392.	1466	54.1	34.1
24.3	23.5	424.	1586	54.1	30.6
26.8	26.0	448.	1676	54.1	28.1
30.1	29.2	478.	1788	54.0	24.8
32.8	31.8	500.	1871	54.0	22.2
36.0	35.0	520.	1945	54.0	19.0
38.8	37.7	540.	2020	54.0	16.2
42.0	40.9	560.	2095	53.9	13.1
45.1	44.0	585.	2189	53.9	9.9

TABLE 9. DATA FOR A RIGID CONFIGURATION 89.4% STENOSIS

MEASURED P1-P2 (CM H20)	CORRECTED P1-P2 (CM H20)	Q (ML/MIN)	RE	P1 (CM H20)	P2 (CM H20)
3.9	3.7	85.	318	54.4	50.7
7.7	7.4	137.	512	54.4	46.9
11.9	11.5	184.	688	54.3	42.8
15.9	15.5	220.	823	54.3	38.8
20.3	19.8	254.	950	54.2	34.5
24.0	23.4	278.	1040	54.2	30.8
28.0	27.4	304.	1137	54.2	26.8
32.3	31.6	328.	1227	54.2	22.5
36.0	35.3	346.	1294	54.2	18.8
39.8	39.1	367.	1373	54.1	15.1
43.6	42.8	385.	1440	54.1	11.3
47.3	46.5	404.	1511	54.1	7.6
52.4	51.5	432.	1616	54.1	2.5

APPENDIX C: PRESSURE-FLOW DATA FOR THE RIGID CONFIGURATION AT AN UPSTREAM PRESSURE OF 69.5 CM WATER

TABLE 10. DATA FOR A RIGID CONFIGURATION 75% STENOSIS

MEASURED P1-P2 (CM H2O)	CORRECTED P1-P2 (CM H2O)	Q (ML/MIN)	RE	P1 (CM H2O)	P2 (CM H2O)
2.4	2.0	206.	770	69.3	67.3
5.1	4.5	324.	1212	69.2	64.7
7.6	6.8	416.	1556	69.1	62.3
10.0	9.0	496.	1856	69.0	60.0
12.4	11.3	560.	2095	68.9	57.6
15.2	14.0	625.	2338	68.9	54.9
17.6	16.3	670.	2507	68.8	52.6
19.8	18.4	720.	2694	68.8	50.4
22.6	21.1	770.	2881	68.7	47.6
25.0	23.4	820.	3068	68.7	45.3

TABLE 11. DATA FOR A RIGID CONFIGURATION 85% STENOSIS

MEASURED P1-P2 (CM H20)	CORRECTED P1-P2 (CM H20)	Q (ML/MIN)	RE	P1 (CM H20)	P2 (CM H20)
4.8	4.5	159.	594	69.3	64.9
10.1	9.6	260.	972	69.2	59.7
14.9	14.2	326.	1219	69.2	54.9
19.8	19.0	390.	1459	69.1	50.1
25.0	24.1	442.	1654	69.1	44.9
30.1	29.2	492.	1841	69.0	39.8
35.0	33.9	530.	1983	69.0	35.0
40.0	38.9	565.	2114	68.9	30.1
45.0	43.8	600.	2245	68.9	25.1
50.0	48.7	635.	2376	68.9	20.1
56.6	55.3	675.	2525	68.8	13.6

TABLE 12. DATA FOR A RIGID CONFIGURATION 89.4% STENOSIS

MEASURED P1-P2 (CM H20)	CORRECTED P1-P2 (CM H20)	Q (ML/MIN)	RE	P1 (CM H20)	P2 (CM H20)
4.8	4.6	103.	385	69.4	64.8
10.1	9.8	170.	636	69.3	59.5
14.8	14.4	218.	815	69.3	54.9
19.8	19.3	258.	965	69.2	49.9
25.0	24.4	292.	1092	69.2	44.8
29.9	29.3	324.	1212	69.2	39.9
34.7	34.0	350.	1309	69.2	35.1
40.0	39.2	380.	1422	69.1	29.9
44.8	43.9	404.	1511	69.1	25.2
49.7	48.8	434.	1624	69.1	20.2
55.1	54.2	464.	1736	69.0	14.9
59.5	58.5	485.	1814	69.0	10.5
65.7	64.7	510.	1908	69.0	4.3

APPENDIX D: PRESSURE-FLOW DATA FOR THE SHORT COMPLIANT CONFIGURATION AT AN UPSTREAM PRESSURE OF 54.5 CM WATER

TABLE 13. DATA FOR A SHORT CONFIGURATION 75% STENOSIS AT PE= 0 CM H20

MEASURED P1-P2 (CM H20)	CORRECTED P1-P2 (CM H20)	Q (ML/MIN)	RE	P1 (CM H20)	P2 (CM H20)	PE-P2 (CM H20)
2.4	2.0	222.	830	54.3	52.3	-52.3
5.1	4.4	342.	1279	54.2	49.7	-49.7
7.4	6.5	426.	1594	54.1	47.5	-47.5
10.0	9.0	510.	1908	54.0	45.0	-45.0
12.6	11.5	570.	2133	53.9	42.5	-42.5
15.0	13.7	630.	2357	53.9	40.1	-40.1
17.4	16.0	690.	2582	53.8	37.8	-37.8
20.0	18.5	740.	2769	53.8	35.2	-35.2
22.5	20.9	790.	2956	53.7	32.8	-32.8
25.0	23.3	840.	3143	53.7	30.3	-30.3
27.4	25.7	870.	3255	53.6	28.0	-28.0
29.7	27.9	910.	3405	53.6	25.7	-25.7
32.5	30.6	950.	3555	53.6	22.9	-22.9

TABLE 14. DATA FOR A SHORT CONFIGURATION 75% STENOSIS AT PE=30 CM H20

MEASURED P1-P2 (CM H20)	CORRECTED P1-P2 (CM H20)	Q (ML/MIN)	RE	P1 (CM H20)	P2 (CM H20)	PE-P2 (CM H20)
2.5	2.1	210.	785	54.3	52.2	-22.2
4.8	4.2	308.	1152	54.2	50.0	-20.0
7.5	6.7	400.	1496	54.1	47.4	-17.4
10.0	9.1	472.	1766	54.0	45.0	-15.0
12.6	11.6	535.	2002	54.0	42.4	-12.4
14.9	13.7	580.	2170	53.9	40.2	-10.2
17.6	16.4	640.	2394	53.9	37.5	-7.5
19.9	18.6	680.	2544	53.8	35.2	-5.2
22.6	21.2	720.	2694	53.8	32.6	-2.6
25.1	23.6	760.	2844	53.7	30.2	-0.2
27.4	25.9	790.	2956	53.7	27.8	2.2
29.9	28.3	820.	3068	53.7	25.4	4.6
32.7	31.0	845.	3162	53.7	22.6	7.4
36.4	34.7	870.	3255	53.6	19.0	11.0

TABLE 15. DATA FOR A SHORT CONFIGURATION 75% STENOSIS AT PE=40 CM H20

MEASURED P1-P2 (CM H20)	CORRECTED P1-P2 (CM H20)	Q (ML/MIN)	RE	P1 (CM H20)	P2 (CM H20)	PE-P2 (CM H20)
2.6	2.2	206.	770	54.3	52.1	-12.1
4.8	4.2	304.	1137	54.2	50.0	-10.0
7.5	6.8	392.	1466	54.1	47.3	-7.3
9.8	8.9	454.	1698	54.0	45.1	-5.1
12.3	11.3	515.	1927	54.0	42.7	-2.7
15.0	13.9	565.	2114	53.9	40.1	-0.1
17.6	16.4	610.	2282	53.9	37.5	2.5
20.0	18.8	650.	2432	53.9	35.1	4.9
22.4	21.0	680.	2544	53.8	32.8	7.2
24.9	23.5	710.	2656	53.8	30.3	9.7
27.4	25.9	735.	2750	53.8	27.8	12.2
30.1	28.6	750.	2806	53.8	25.1	14.9
32.6	31.1	760.	2844	53.7	22.7	17.3
35.0	33.5	730.	2731	53.8	20.2	19.8
37.5	36.1	705.	2638	53.8	17.7	22.3
39.9	38.6	675.	2525	53.8	15.3	24.7
42.5	41.2	650.	2432	53.9	12.6	27.4
44.8	43.5	635.	2376	53.9	10.3	29.7
46.2	45.0	625.	2338	53.9	8.9	31.1

TABLE 16. DATA FOR A SHORT CONFIGURATION 75% STENOSIS AT PE=50 CM H20

MEASURED P1-P2 (CM H20)	CORRECTED P1-P2 (CM H20)	Q (ML/MIN)	RE	P1 (CM H20)	P2 (CM H20)	PE-P2 (CM H20)
2.4	2.0	186.	696	54.3	52.3	-2.3
4.9	4.4	288.	1077	54.2	49.8	0.2
7.7	7.0	372.	1392	54.1	47.2	2.8
10.1	9.2	434.	1624	54.1	44.8	5.2
12.6	11.6	488.	1826	54.0	42.4	7.6
15.1	14.0	530.	1983	54.0	39.9	10.1
17.4	16.3	570.	2133	53.9	37.6	12.4
19.8	18.6	605.	2263	53.9	35.3	14.7
22.5	21.2	630.	2357	53.9	32.6	17.4
25.2	23.9	645.	2413	53.9	29.9	20.1
27.4	26.1	635.	2376	53.9	27.7	22.3
29.7	28.5	600.	2245	53.9	25.4	24.6
32.5	31.4	560.	2095	53.9	22.6	27.4
35.0	33.9	530.	1983	54.0	20.0	30.0
37.3	36.3	510.	1908	54.0	17.7	32.3
40.3	39.3	490.	1833	54.0	14.7	35.3
44.6	43.7	470.	1758	54.0	10.4	39.6
47.4	46.5	470.	1758	54.0	7.6	42.4
50.4	49.5	460.	1721	54.0	4.6	45.4

TABLE 17. DATA FOR A SHORT CONFIGURATION 85% STENOSIS AT PE= 0 CM H20

MEASURED P1-P2 (CM H20)	CORRECTED P1-P2 (CM H20)	Q (ML/MIN)	RE	P1 (CM H20)	P2 (CM H20)	PE-P2 (CM H20)
3.1	2.8	134.	501	54.4	51.5	-51.5
6.1	5.8	192.	718	54.3	48.5	-48.5
8.8	8.3	252.	943	54.2	46.0	-46.0
12.1	11.5	304.	1137	54.2	42.7	-42.7
14.9	14.3	344.	1287	54.2	39.9	-39.9
18.1	17.3	386.	1444	54.1	36.8	-36.8
21.0	20.2	420.	1571	54.1	33.9	-33.9
24.1	23.2	455.	1702	54.0	30.9	-30.9
26.8	25.8	482.	1803	54.0	28.2	-28.2
30.0	29.0	510.	1908	54.0	25.0	-25.0
33.3	32.2	535.	2002	54.0	21.8	-21.8
35.8	34.7	555.	2076	53.9	19.2	-19.2
39.2	38.0	580.	2170	53.9	15.9	-15.9
41.7	40.5	600.	2245	53.9	13.4	-13.4
45.9	44.6	630.	2357	53.9	9.2	-9.2

TABLE 18. DATA FOR A SHORT CONFIGURATION 85% STENOSIS AT PE=20 CM H20

MEASURED P1-P2 (CM H20)	CORRECTED P1-P2 (CM H20)	Q (ML/MIN)	RE	P1 (CM H20)	P2 (CM H20)	PE-P2 (CM H20)
2.9	2.7	118.	441	54.4	51.7	-31.7
6.0	5.7	187.	699	54.3	48.6	-28.6
8.8	8.3	234.	875	54.3	45.9	-25.9
11.8	11.2	282.	1055	54.2	43.0	-23.0
14.8	14.2	322.	1204	54.2	40.0	-20.0
17.7	17.0	353.	1320	54.1	37.2	-17.2
21.0	20.2	390.	1459	54.1	33.9	-13.9
23.8	23.0	417.	1560	54.1	31.1	-11.1
27.1	26.2	448.	1676	54.1	27.8	-7.8
29.8	28.8	472.	1766	54.0	25.2	-5.2
33.1	32.2	497.	1859	54.0	21.8	-1.8
36.1	35.1	510.	1908	54.0	18.9	1.1
39.0	37.9	530.	1983	54.0	16.0	4.0
42.1	41.0	540.	2020	54.0	12.9	7.1
45.0	43.9	550.	2058	54.0	10.0	10.0
47.6	46.5	560.	2095	53.9	7.5	12.5

TABLE 19. DATA FOR A SHORT CONFIGURATION 85% STENOSIS AT PE=30 CM H20

MEASURED P1-P2 (CM H20)	CORRECTED P1-P2 (CM H20)	Q (ML/MIN)	RE	P1 (CM H20)	P2 (CM H20)	PE-P2 (CM H20)
3.0	2.8	115.	430	54.4	51.6	-21.6
6.1	5.7	183.	684	54.3	48.6	-18.6
9.0	8.5	232.	868	54.3	45.7	-15.7
12.0	11.5	272.	1017	54.2	42.8	-12.8
14.9	14.3	308.	1152	54.2	39.9	-9.9
17.8	17.1	340.	1272	54.2	37.0	-7.0
21.0	20.3	372.	1392	54.1	33.9	-3.9
24.1	23.3	402.	1504	54.1	30.8	-0.8
27.1	26.3	424.	1586	54.1	27.8	2.2
29.9	29.0	443.	1657	54.1	25.0	5.0
33.1	32.2	463.	1732	54.0	21.8	8.2
35.9	34.9	480.	1796	54.0	19.1	10.9
39.1	38.2	492.	1841	54.0	15.8	14.2
42.3	41.4	492.	1841	54.0	12.6	17.4
45.2	44.2	492.	1841	54.0	9.8	20.2
47.7	46.7	488.	1826	54.0	7.3	22.7
50.3	49.3	484.	1811	54.0	4.7	25.3

TABLE 20. DATA FOR A SHORT CONFIGURATION 85% STENOSIS AT PE=40 CM H20

MEASURED P1-P2 (CM H20)	CORRECTED P1-P2 (CM H20)	Q (ML/MIN)	RE	P1 (CM H20)	P2 (CM H20)	PE-P2 (CM H20)
2.9	2.7	108.	404	54.4	51.7	-11.7
6.2	5.8	177.	662	54.3	48.5	-8.5
9.1	8.7	222.	830	54.3	45.6	-5.6
11.9	11.4	262.	980	54.2	42.8	-2.8
15.0	14.4	295.	1103	54.2	39.8	0.2
18.1	17.5	324.	1212	54.2	36.7	3.3
21.0	20.3	351.	1313	54.1	33.9	6.1
24.1	23.4	373.	1395	54.1	30.7	9.3
27.1	26.3	392.	1466	54.1	27.8	12.2
30.1	29.3	410.	1534	54.1	24.8	15.2
33.3	32.5	417.	1560	54.1	21.6	18.4
36.3	35.4	420.	1571	54.1	18.7	21.3
38.8	38.0	418.	1564	54.1	16.1	23.9
41.9	41.1	405.	1515	54.1	13.0	27.0
44.8	44.0	400.	1496	54.1	10.1	29.9
48.2	47.4	388.	1451	54.1	6.7	33.3
52.3	51.5	380.	1422	54.1	2.6	37.4

TABLE 21. DATA FOR A SHORT CONFIGURATION 85% STENOSIS AT PE=50 CM H20

MEASURED P1-P2 (CM H2O)	CORRECTED P1-P2 (CM H2O)	Q (ML/MIN)	RE	P1 (CM H2O)	P2 (CM H2O)	PE-P2 (CM H2O)
3.1	2.9	108.	404	54.4	51.5	-1.5
6.1	5.8	167.	624	54.3	48.6	1.4
9.1	8.7	208.	778	54.3	45.6	4.4
12.1	11.7	248.	928	54.3	42.6	7.4
15.1	14.6	274.	1025	54.2	39.6	10.4
18.0	17.5	300.	1122	54.2	36.7	13.3
21.0	20.4	318.	1189	54.2	33.8	16.2
24.1	23.5	332.	1242	54.2	30.7	19.3
27.3	26.6	339.	1268	54.2	27.5	22.5
30.4	29.7	336.	1257	54.2	24.4	25.6
33.6	33.0	322.	1204	54.2	21.2	28.8
36.5	35.9	311.	1163	54.2	18.3	31.7
39.3	38.6	306.	1145	54.2	15.6	34.4
42.2	41.6	300.	1122	54.2	12.6	37.4
45.4	44.8	297.	1111	54.2	9.4	40.6
48.7	48.1	294.	1100	54.2	6.1	43.9
54.1	53.5	290.	1085	54.2	0.7	49.3

TABLE 22. DATA FOR A SHORT CONFIGURATION 89.4% STENOSIS AT PE= 0 CM H20

MEASURED P1-P2 (CM H20)	CORRECTED P1-P2 (CM H20)	Q (ML/MIN)	RE	P1 (CM H20)	P2 (CM H20)	PE-P2 (CM H20)
4.8	4.6	116.	434	54.4	49.8	-49.8
10.0	9.6	192.	718	54.3	44.7	-44.7
14.9	14.4	244.	913	54.3	39.8	-39.8
19.9	19.3	288.	1077	54.2	34.9	-34.9
24.8	24.1	322.	1204	54.2	30.1	-30.1
29.6	28.9	352.	1317	54.1	25.3	-25.3
34.7	33.9	382.	1429	54.1	20.2	-20.2
39.8	39.0	408.	1526	54.1	15.1	-15.1
44.6	43.8	426.	1594	54.1	10.3	-10.3
50.3	49.4	444.	1661	54.1	4.7	-4.7

TABLE 23. DATA FOR A SHORT CONFIGURATION 89.4% STENOSIS AT PE=20 CM H20

MEASURED P1-P2 (CM H20)	CORRECTED P1-P2 (CM H20)	Q (ML/MIN)	RE	P1 (CM H20)	P2 (CM H20)	PE-P2 (CM H20)
5.0	4.8	110.	411	54.4	49.6	-29.6
9.8	9.5	176.	658	54.3	44.8	-24.8
15.2	14.7	228.	853	54.3	39.5	-19.5
19.9	19.4	266.	995	54.2	34.9	-14.9
25.1	24.5	302.	1130	54.2	29.7	-9.7
29.8	29.1	326.	1219	54.2	25.0	-5.0
35.0	34.3	350.	1309	54.2	19.8	0.2
40.1	39.4	370.	1384	54.1	14.7	5.3
45.0	44.2	383.	1433	54.1	9.9	10.1
51.9	51.1	396.	1481	54.1	3.0	17.0

TABLE 24. DATA FOR A SHORT CONFIGURATION 89.4% STENOSIS AT PE=30 CM H20

MEASURED P1-P2 (CM H20)	CORRECTED P1-P2 (CM H20)	Q (ML/MIN)	RE	P1 (CM H20)	P2 (CM H20)	PE-P2 (CM H20)
4.8	4.6	103.	385	54.4	49.8	-19.8
10.1	9.8	171.	639	54.3	44.6	-14.6
15.0	14.6	220.	823	54.3	39.7	-9.7
20.2	19.7	254.	950	54.2	34.6	-4.6
25.1	24.5	284.	1062	54.2	29.7	0.3
30.3	29.7	309.	1156	54.2	24.5	5.5
35.2	34.5	330.	1234	54.2	19.6	10.4
39.8	39.1	342.	1279	54.2	15.1	14.9
44.9	44.2	353.	1320	54.1	10.0	20.0
52.3	51.6	349.	1305	54.2	2.5	27.5

TABLE 25. DATA FOR A SHORT CONFIGURATION 89.4% STENOSIS AT PE=40 CM H20

MEASURED P1-P2 (CM H20)	CORRECTED P1-P2 (CM H20)	Q (ML/MIN)	RE	P1 (CM H20)	P2 (CM H20)	PE-P2 (CM H20)
4.8	4.6	97.	362	54.4	49.8	-9.8
10.1	9.8	162.	606	54.3	44.6	-4.6
15.2	14.8	206.	770	54.3	39.5	0.5
19.9	19.4	238.	890	54.3	34.8	5.2
24.9	24.4	265.	991	54.2	29.8	10.2
30.3	29.7	288.	1077	54.2	24.5	15.5
34.9	34.3	302.	1130	54.2	19.9	20.1
39.6	39.0	310.	1160	54.2	15.2	24.8
44.9	44.3	315.	1178	54.2	9.9	30.1
48.3	47.6	301.	1126	54.2	6.6	33.4
53.2	52.6	286.	1070	54.2	1.6	38.4

TABLE 26. DATA FOR A SHORT CONFIGURATION 89.4% STENOSIS AT PE=50 CM H20

MEASURED P1-P2 (CM H20)	CORRECTED P1-P2 (CM H20)	Q (ML/MIN)	RE	P1 (CM H20)	P2 (CM H20)	PE-P2 (CM H20)
4.8	4.6	93.	348	54.4	49.8	0.2
10.1	9.8	153.	572	54.3	44.6	5.4
14.7	14.3	190.	711	54.3	40.0	10.0
20.0	19.6	222.	830	54.3	34.7	15.3
25.3	24.8	246.	920	54.3	29.4	20.6
30.3	29.8	258.	965	54.2	24.5	25.5
34.8	34.3	264.	987	54.2	19.9	30.1
40.0	39.5	245.	916	54.3	14.7	35.3
44.3	43.9	230.	860	54.3	10.4	39.6
48.8	48.4	235.	879	54.3	5.9	44.1
54.0	53.5	242.	905	54.3	0.7	49.3

APPENDIX E: PRESSURE-FLOW DATA FOR THE SHORT COMPLIANT CONFIGURATION AT AN UPSTREAM PRESSURE OF 69.5 CM WATER

TABLE 27. DATA FOR A SHORT CONFIGURATION 75% STENOSIS AT PE= 0 CM H20

MEASURED P1-P2 (CM H20)	CORRECTED P1-P2 (CM H20)	Q (ML/MIN)	RE	P1 (CM H20)	P2 (CM H20)	PE-P2 (CM H20)
2.5	2.0	234.	875	69.3	67.2	-67.2
5.0	4.3	350.	1309	69.2	64.8	-64.8
7.5	6.6	440.	1646	69.1	62.4	-62.4
10.0	8.9	530.	1983	69.0	60.0	-60.0
12.6	11.4	590.	2207	68.9	57.5	-57.5
15.1	13.8	655.	2451	68.8	55.1	-55.1
17.3	15.9	710.	2656	68.8	52.9	-52.9
19.8	18.3	765.	2862	68.7	50.4	-50.4
22.3	20.6	820.	3068	68.7	48.1	-48.1

TABLE 28. DATA FOR A SHORT CONFIGURATION 75% STENOSIS AT PE=40 CM H20

MEASURED P1-P2 (CM H20)	CORRECTED P1-P2 (CM H20)	Q (ML/MIN)	RE	P1 (CM H20)	P2 (CM H20)	PE-P2 (CM H20)
2.4	2.0	204.	763	69.3	67.3	-27.3
4.9	4.3	316.	1182	69.2	64.9	-24.9
7.7	6.9	412.	1541	69.1	62.2	-22.2
9.8	8.9	470.	1758	69.0	60.2	-20.2
12.6	11.5	540.	2020	69.0	57.4	-17.4
14.8	13.6	590.	2207	68.9	55.3	-15.3
17.6	16.3	645.	2413	68.9	52.5	-12.5
19.9	18.5	690.	2582	68.8	50.3	-10.3
22.6	21.1	735.	2750	68.8	47.6	-7.6
25.1	23.6	775.	2900	68.7	45.2	-5.2
28.0	26.4	815.	3049	68.7	42.3	-2.3

TABLE 29. DATA FOR A SHORT CONFIGURATION 75% STENOSIS AT PE=50 CM H20

MEASURED P1-P2 (CM H20)	CORRECTED P1-P2 (CM H20)	Q (ML/MIN)	RE	P1 (CM H20)	P2 (CM H20)	PE-P2 (CM H20)
2.5	2.1	200.	748	69.3	67.2	-17.2
5.1	4.5	314.	1175	69.2	64.7	-14.7
7.4	6.6	392.	1466	69.1	62.5	-12.5
9.8	8.8	460.	1721	69.0	60.2	-10.2
12.5	11.5	520.	1945	69.0	57.5	-7.5
15.1	14.0	580.	2170	68.9	54.9	-4.9
17.7	16.4	630.	2357	68.9	52.4	-2.4
20.1	18.8	675.	2525	68.8	50.1	-0.1
22.5	21.1	715.	2675	68.8	47.7	2.3
25.0	23.5	760.	2844	68.7	45.3	4.7
27.5	26.0	775.	2900	68.7	42.8	7.2
30.0	28.4	795.	2974	68.7	40.3	9.7
33.6	32.0	815.	3049	68.7	36.7	13.3
36.8	35.2	815.	3049	68.7	33.5	16.5
42.3	40.8	760.	2844	68.7	28.0	22.0
47.6	46.2	720.	2694	68.8	22.6	27.4
52.7	51.3	685.	2563	68.8	17.5	32.5
59.3	58.0	660.	2469	68.8	10.9	39.1

TABLE 30. DATA FOR A SHORT CONFIGURATION 75% STENOSIS AT PE=60 CM H20

MEASURED P1-P2 (CM H20)	CORRECTED P1-P2 (CM H20)	Q (ML/MIN)	RE	P1 (CM H20)	P2 (CM H20)	PE-P2 (CM H20)
2.6	2.2	200.	748	69.3	67.1	-7.1
4.9	4.3	294.	1100	69.2	64.9	-4.9
7.5	6.7	380.	1422	69.1	62.4	-2.4
10.0	9.1	448.	1676	69.1	59.9	0.1
12.5	11.5	505.	1889	69.0	57.5	2.5
14.9	13.8	545.	2039	69.0	55.1	4.9
17.5	16.3	590.	2207	68.9	52.6	7.4
20.0	18.7	630.	2357	68.9	50.1	9.9
22.4	21.1	655.	2451	68.8	47.8	12.2
25.0	23.7	670.	2507	68.8	45.1	14.9
27.5	26.1	685.	2563	68.8	42.7	17.3
32.1	30.8	630.	2357	68.9	38.0	22.0
37.9	36.7	580.	2170	68.9	32.2	27.8
42.1	41.0	555.	2076	68.9	28.0	32.0
47.6	46.5	530.	1983	69.0	22.4	37.6
52.6	51.6	520.	1945	69.0	17.4	42.6
57.3	56.3	510.	1908	69.0	12.7	47.3
64.2	63.2	495.	1852	69.0	5.8	54.2

TABLE 31. DATA FOR A SHORT CONFIGURATION 85% STENOSIS AT PE= 0 CM H20

MEASURED P1-P2 (CM H20)	CORRECTED P1-P2 (CM H20)	Q (ML/MIN)	RE	P1 (CM H20)	P2 (CM H20)	PE-P2 (CM H20)
4.9	4.5	180.	673	69.3	64.8	-64.8
9.9	9.4	280.	1047	69.2	59.8	-59.8
14.9	14.2	358.	1339	69.1	54.9	-54.9
20.1	19.2	430.	1609	69.1	49.8	-49.8
24.9	24.0	486.	1818	69.0	45.0	-45.0
30.0	29.0	535.	2002	69.0	40.0	-40.0
35.0	33.8	580.	2170	68.9	35.1	-35.1
39.9	38.7	620.	2320	68.9	30.2	-30.2
44.8	43.5	660.	2469	68.8	25.4	-25.4
49.8	48.4	690.	2582	68.8	20.4	-20.4
57.3	55.8	735.	2750	68.8	12.9	-12.9

TABLE 32. DATA FOR A SHORT CONFIGURATION 85% STENOSIS AT PE=20 CM H20

MEASURED P1-P2 (CM H20)	CORRECTED P1-P2 (CM H20)	Q (ML/MIN)	RE	P1 (CM H20)	P2 (CM H20)	PE-P2 (CM H20)
4.8	4.5	170.	636	69.3	64.9	-44.9
9.7	9.2	260.	972	69.2	60.1	-40.1
14.8	14.1	338.	1264	69.2	55.0	-35.0
20.0	19.2	404.	1511	69.1	49.9	-29.9
25.0	24.1	455.	1702	69.0	45.0	-25.0
30.0	29.0	506.	1893	69.0	40.0	-20.0
35.1	34.0	540.	2020	69.0	34.9	-14.9
40.1	39.0	575.	2151	68.9	30.0	-10.0
45.0	43.8	605.	2263	68.9	25.1	-5.1
49.9	48.6	635.	2376	68.9	20.2	-0.2
55.0	53.7	650.	2432	68.9	15.1	4.9
58.9	57.6	660.	2469	68.8	11.2	8.8

TABLE 33. DATA FOR A SHORT CONFIGURATION 85% STENOSIS AT PE=30 CM H20

MEASURED P1-P2 (CM H20)	CORRECTED P1-P2 (CM H20)	Q (ML/MIN)	RE	P1 (CM H20)	P2 (CM H20)	PE-P2 (CM H20)
4.9	4.6	166.	621	69.3	64.8	-34.8
10.1	9.6	264.	987	69.2	59.7	-29.7
14.8	14.2	328.	1227	69.2	55.0	-25.0
19.8	19.0	388.	1451	69.1	50.1	-20.1
24.9	24.0	440.	1646	69.1	45.0	-15.0
30.0	29.0	486.	1818	69.0	40.0	-10.0
35.2	34.2	515.	1927	69.0	34.8	-4.8
39.7	38.6	545.	2039	69.0	30.3	-0.3
44.9	43.8	570.	2133	68.9	25.2	4.8
49.8	48.6	590.	2207	68.9	20.3	9.7
55.3	54.2	590.	2207	68.9	14.7	15.3
60.1	58.9	590.	2207	68.9	10.0	20.0
63.1	61.9	580.	2170	68.9	7.0	23.0

TABLE 34. DATA FOR A SHORT CONFIGURATION 85% STENOSIS AT PE=40 CM H20

MEASURED P1-P2 (CM H20)	CORRECTED P1-P2 (CM H20)	Q (ML/MIN)	RE	P1 (CM H20)	P2 (CM H20)	PE-P2 (CM H20)
5.0	4.7	163.	609	69.3	64.7	-24.7
9.8	9.3	252.	943	69.2	59.9	-19.9
14.9	14.3	316.	1182	69.2	54.9	-14.9
20.1	19.4	376.	1407	69.1	49.7	-9.7
24.8	24.0	420.	1571	69.1	45.1	-5.1
30.0	29.1	460.	1721	69.0	39.9	0.1
35.1	34.2	496.	1856	69.0	34.8	5.2
40.0	39.0	520.	1945	69.0	30.0	10.0
45.1	44.1	535.	2002	69.0	24.9	15.1
50.0	49.0	520.	1945	69.0	20.0	20.0
55.0	54.0	510.	1908	69.0	15.0	25.0
59.6	58.6	500.	1871	69.0	10.4	29.6
65.8	64.8	484.	1811	69.0	4.2	35.8

TABLE 35. DATA FOR A SHORT CONFIGURATION 85% STENOSIS AT PE=50 CM H20

MEASURED P1-P2 (CM H20)	CORRECTED P1-P2 (CM H20)	Q (ML/MIN)	RE	P1 (CM H20)	P2 (CM H20)	PE-P2 (CM H20)
5.0	4.7	158.	591	69.3	64.6	-14.6
10.1	9.7	244.	913	69.3	59.6	-9.6
15.0	14.4	304.	1137	69.2	54.8	-4.8
20.0	19.3	354.	1324	69.1	49.9	0.1
24.9	24.1	396.	1481	69.1	45.0	5.0
29.8	28.9	428.	1601	69.1	40.1	9.9
34.9	34.0	448.	1676	69.1	35.0	15.0
39.8	38.8	452.	1691	69.0	30.2	19.8
45.8	44.9	440.	1646	69.1	24.1	25.9
49.9	49.0	430.	1609	69.1	20.0	30.0
55.2	54.4	414.	1549	69.1	14.7	35.3
59.9	59.1	404.	1511	69.1	10.0	40.0
64.8	64.1	396.	1481	69.1	5.0	45.0
67.5	66.7	392.	1466	69.1	2.4	47.6

TABLE 36. DATA FOR A SHORT CONFIGURATION 89.4% STENOSIS AT PE= 0 CM H20

MEASURED P1-P2 (CM H20)	CORRECTED P1-P2 (CM H20)	Q (ML/MIN)	RE	P1 (CM H20)	P2 (CM H20)	PE-P2 (CM H20)
5.1	4.8	129.	482	69.4	64.5	-64.5
10.0	9.6	196.	733	69.3	59.7	-59.7
14.7	14.2	248.	928	69.3	55.0	-55.0
19.8	19.3	294.	1100	69.2	49.9	-49.9
25.2	24.5	332.	1242	69.2	44.6	-44.6
29.8	29.1	364.	1362	69.1	40.0	-40.0
34.8	34.0	392.	1466	69.1	35.1	-35.1
40.3	39.4	420.	1571	69.1	29.7	-29.7
44.6	43.7	440.	1646	69.1	25.3	-25.3
49.9	49.0	458.	1713	69.0	20.0	-20.0
55.0	54.1	475.	1777	69.0	15.0	-15.0
59.8	58.8	490.	1833	69.0	10.2	-10.2
64.9	63.9	495.	1852	69.0	5.1	-5.1

TABLE 37. DATA FOR A SHORT CONFIGURATION 89.4% STENOSIS AT PE=20 CM H20

MEASURED P1-P2 (CM H20)	CORRECTED P1-P2 (CM H20)	Q (ML/MIN)	RE	P1 (CM H20)	P2 (CM H20)	PE-P2 (CM H20)
5.1	4.9	120.	449	69.4	64.5	-44.5
9.9	9.5	184.	688	69.3	59.8	-39.8
15.2	14.7	240.	898	69.3	54.5	-34.5
19.9	19.3	276.	1032	69.2	49.9	-29.9
25.1	24.5	312.	1167	69.2	44.7	-24.7
30.3	29.6	342.	1279	69.2	39.6	-19.6
34.8	34.1	364.	1362	69.1	35.1	-15.1
40.3	39.5	386.	1444	69.1	29.6	-9.6
44.8	44.0	406.	1519	69.1	25.1	-5.1
50.1	49.3	420.	1571	69.1	19.8	0.2
54.9	54.0	430.	1609	69.1	15.0	5.0
59.8	58.9	438.	1639	69.1	10.2	9.8
65.2	64.3	446.	1668	69.1	4.7	15.3

TABLE 38. DATA FOR A SHORT CONFIGURATION 89.4% STENOSIS AT PE=30 CM H20

MEASURED P1-P2 (CM H20)	CORRECTED P1-P2 (CM H20)	Q (ML/MIN)	RE	P1 (CM H20)	P2 (CM H20)	PE-P2 (CM H20)
4.8	4.6	110.	411	69.4	64.8	-34.8
9.9	9.5	178.	666	69.3	59.8	-29.8
14.6	14.1	226.	845	69.3	55.1	-25.1
20.0	19.5	269.	1006	69.2	49.7	-19.7
24.9	24.3	300.	1122	69.2	44.9	-14.9
30.1	29.4	326.	1219	69.2	39.7	-9.7
34.8	34.2	348.	1302	69.2	35.0	-5.0
40.3	39.6	370.	1384	69.1	29.6	0.4
44.8	44.1	384.	1436	69.1	25.0	5.0
49.8	49.0	395.	1478	69.1	20.1	9.9
54.9	54.1	404.	1511	69.1	15.0	15.0
59.9	59.1	410.	1534	69.1	10.0	20.0
63.9	63.1	410.	1534	69.1	6.0	24.0
66.1	65.3	404.	1511	69.1	3.8	26.2

TABLE 39. DATA FOR A SHORT CONFIGURATION 89.4% STENOSIS AT PE=40 CM H20

MEASURED P1-P2 (CM H20)	CORRECTED P1-P2 (CM H20)	Q (ML/MIN)	RE	P1 (CM H20)	P2 (CM H20)	PE-P2 (CM H20)
4.8	4.6	103.	385	69.4	64.8	-24.8
9.9	9.6	170.	636	69.3	59.8	-19.8
15.3	14.8	220.	823	69.3	54.5	-14.5
20.0	19.5	256.	957	69.2	49.7	-9.7
25.0	24.5	286.	1070	69.2	44.7	-4.7
30.3	29.7	312.	1167	69.2	39.5	0.5
35.4	34.7	332.	1242	69.2	34.4	5.6
40.2	39.5	344.	1287	69.2	29.6	10.4
44.7	44.0	358.	1339	69.1	25.2	14.8
50.2	49.5	366.	1369	69.1	19.7	20.3
54.8	54.1	370.	1384	69.1	15.1	24.9
60.0	59.3	360.	1347	69.1	9.9	30.1
64.1	63.4	348.	1302	69.2	5.7	34.3
67.5	66.8	344.	1287	69.2	2.3	37.7

TABLE 40. DATA FOR A SHORT CONFIGURATION 89.4% STENOSIS AT PE=50 CM H2O

MEASURED P1-P2 (CM H2O)	CORRECTED P1-P2 (CM H2O)	Q (ML/MIN)	RE	P1 (CM H2O)	P2 (CM H2O)	PE-P2 (CM H2O)
5.1	4.9	104.	389	69.4	64.5	-14.5
10.1	9.8	163.	609	69.3	59.6	-9.6
15.0	14.6	207.	774	69.3	54.7	-4.7
20.1	19.7	242.	905	69.3	49.6	0.4
25.2	24.7	272.	1017	69.2	44.6	5.4
30.3	29.8	292.	1092	69.2	39.4	10.6
35.0	34.4	308.	1152	69.2	34.8	15.2
39.8	39.1	318.	1189	69.2	30.1	19.9
45.0	44.4	328.	1227	69.2	24.8	25.2
50.3	49.7	320.	1197	69.2	19.5	30.5
55.1	54.5	304.	1137	69.2	14.7	35.3
59.5	58.9	298.	1115	69.2	10.3	39.7
63.4	62.8	306.	1145	69.2	6.4	43.6
68.2	67.6	312.	1167	69.2	1.6	48.4

TABLE 41. DATA FOR A SHORT CONFIGURATION 89.4% STENOSIS AT PE=60 CM H2O

MEASURED P1-P2 (CM H2O)	CORRECTED P1-P2 (CM H2O)	Q (ML/MIN)	RE	P1 (CM H2O)	P2 (CM H2O)	PE-P2 (CM H2O)
4.9	4.7	101.	377	69.4	64.7	-4.7
9.8	9.5	156.	583	69.3	59.9	0.1
15.0	14.6	204.	763	69.3	54.7	5.3
20.3	19.9	238.	890	69.3	49.4	10.6
25.6	25.1	258.	965	69.2	44.2	15.8
30.1	29.6	276.	1032	69.2	39.6	20.4
35.2	34.6	288.	1077	69.2	34.6	25.4
40.6	40.0	290.	1085	69.2	29.2	30.8
44.6	44.1	272.	1017	69.2	25.2	34.8
49.8	49.3	254.	950	69.2	20.0	40.0
55.0	54.5	268.	1002	69.2	14.8	45.2
60.3	59.8	272.	1017	69.2	9.5	50.5
63.8	63.2	276.	1032	69.2	6.0	54.0
68.9	68.3	277.	1036	69.2	0.9	59.1

APPENDIX F: PRESSURE-FLOW DATA FOR THE LONG COMPLIANT CONFIGURATION AT AN UPSTREAM PRESSURE OF 54.5 CM WATER

TABLE 42. DATA FOR A LONG CONFIGURATION 75% STENOSIS AT PE= 0 CM H20

MEASURED P1-P2 (CM H20)	CORRECTED P1-P2 (CM H20)	Q (ML/MIN)	RE	P1 (CM H20)	P2 (CM H20)	PE-P2 (CM H20)
2.5	2.1	204.	763	54.4	52.3	-52.3
5.0	4.4	308.	1152	54.3	49.9	-49.9
7.5	6.7	392.	1466	54.2	47.5	-47.5
10.1	9.2	468.	1751	54.2	45.0	-45.0
12.4	11.4	525.	1964	54.1	42.8	-42.8
15.0	13.8	585.	2189	54.1	40.2	-40.2
17.5	16.2	640.	2394	54.0	37.8	-37.8
19.9	18.5	685.	2563	54.0	35.5	-35.5
22.5	21.1	735.	2750	54.0	32.9	-32.9
25.1	23.6	775.	2900	53.9	30.4	-30.4
27.4	25.8	820.	3068	53.9	28.1	-28.1
29.8	28.1	855.	3199	53.9	25.8	-25.8
32.4	30.6	910.	3405	53.8	23.2	-23.2
35.1	33.2	940.	3517	53.8	20.6	-20.6

TABLE 43. DATA FOR A LONG CONFIGURATION 75% STENOSIS AT PE=30 CM H20

MEASURED P1-P2 (CM H20)	CORRECTED P1-P2 (CM H20)	Q (ML/MIN)	RE	P1 (CM H20)	P2 (CM H20)	PE-P2 (CM H20)
2.4	2.1	190.	711	54.4	52.3	-22.3
5.0	4.4	292.	1092	54.3	49.9	-19.9
7.5	6.8	376.	1407	54.2	47.4	-17.4
10.2	9.3	444.	1661	54.2	44.9	-14.9
12.5	11.5	495.	1852	54.1	42.6	-12.6
14.9	13.8	550.	2058	54.1	40.3	-10.3
17.6	16.4	610.	2282	54.1	37.7	-7.7
20.1	18.8	650.	2432	54.0	35.2	-5.2
22.4	21.0	690.	2582	54.0	33.0	-3.0
25.0	23.5	730.	2731	54.0	30.4	-0.4
27.7	26.2	770.	2881	53.9	27.8	2.2
29.9	28.3	800.	2993	53.9	25.6	4.4
32.5	30.9	835.	3124	53.9	23.0	7.0
35.1	33.4	855.	3199	53.9	20.5	9.5
37.7	36.0	830.	3105	53.9	17.8	12.2
39.3	37.6	835.	3124	53.9	16.3	13.7

TABLE 44. DATA FOR A LONG CONFIGURATION 75% STENOSIS AT PE=40 CM H2O

MEASURED P1-P2 (CM H2O)	CORRECTED P1-P2 (CM H2O)	Q (ML/MIN)	RE	P1 (CM H2O)	P2 (CM H2O)	PE-P2 (CM H2O)
2.5	2.1	188.	703	54.4	52.2	-12.2
5.0	4.4	284.	1062	54.3	49.9	-9.9
7.3	6.6	356.	1332	54.2	47.6	-7.6
10.1	9.2	430.	1609	54.2	44.9	-4.9
12.3	11.4	488.	1826	54.1	42.8	-2.8
14.7	13.6	530.	1983	54.1	40.5	-0.5
17.3	16.1	580.	2170	54.1	37.9	2.1
19.8	18.5	630.	2357	54.0	35.5	4.5
22.4	21.1	670.	2507	54.0	32.9	7.1
25.0	23.7	690.	2582	54.0	30.3	9.7
27.5	26.1	680.	2544	54.0	27.9	12.1
30.2	28.9	675.	2525	54.0	25.2	14.8
32.6	31.3	670.	2507	54.0	22.7	17.3
35.2	33.9	660.	2469	54.0	20.1	19.9
37.5	36.2	655.	2451	54.0	17.8	22.2
40.3	39.1	640.	2394	54.0	15.0	25.0
42.5	41.2	640.	2394	54.0	12.8	27.2
46.6	45.3	645.	2413	54.0	8.7	31.3

TABLE 45. DATA FOR A LONG CONFIGURATION 75% STENOSIS AT PE=50 CM H20

MEASURED P1-P2 (CM H20)	CORRECTED P1-P2 (CM H20)	Q (ML/MIN)	RE	P1 (CM H20)	P2 (CM H20)	PE-P2 (CM H20)
2.5	2.1	183.	684	54.4	52.2	-2.2
5.0	4.4	278.	1040	54.3	49.9	0.1
7.6	6.9	354.	1324	54.2	47.3	2.7
10.2	9.4	422.	1579	54.2	44.8	5.2
12.8	11.8	478.	1788	54.1	42.4	7.6
14.9	13.9	510.	1908	54.1	40.2	9.8
17.5	16.5	500.	1871	54.1	37.6	12.4
19.9	18.9	490.	1833	54.1	35.2	14.8
22.7	21.8	475.	1777	54.2	32.4	17.6
25.2	24.2	490.	1833	54.1	29.9	20.1
27.5	26.6	490.	1833	54.1	27.6	22.4
30.1	29.2	490.	1833	54.1	25.0	25.0
32.6	31.6	495.	1852	54.1	22.5	27.5
35.2	34.2	495.	1852	54.1	19.9	30.1
37.6	36.6	495.	1852	54.1	17.5	32.5
40.1	39.2	495.	1852	54.1	15.0	35.0
42.3	41.3	495.	1852	54.1	12.8	37.2
46.6	45.6	495.	1852	54.1	8.5	41.5
50.3	49.3	495.	1852	54.1	4.8	45.2

TABLE 46. DATA FOR A LONG CONFIGURATION 85% STENOSIS AT PE= 0 CM H20

MEASURED P1-P2 (CM H20)	CORRECTED P1-P2 (CM H20)	Q (ML/MIN)	RE	P1 (CM H20)	P2 (CM H20)	PE-P2 (CM H20)
3.8	3.6	150.	561	54.4	50.8	-50.8
8.0	7.5	236.	883	54.3	46.8	-46.8
11.9	11.3	294.	1100	54.3	43.0	-43.0
16.1	15.4	346.	1294	54.2	38.8	-38.8
20.1	19.3	392.	1466	54.2	34.9	-34.9
23.8	23.0	430.	1609	54.2	31.2	-31.2
27.9	27.0	468.	1751	54.2	27.2	-27.2
32.2	31.2	500.	1871	54.1	22.9	-22.9
36.0	34.9	530.	1983	54.1	19.2	-19.2
40.3	39.2	550.	2058	54.1	14.9	-14.9
44.1	42.9	580.	2170	54.1	11.1	-11.1
47.4	46.2	595.	2226	54.1	7.9	-7.9

TABLE 47. DATA FOR A LONG CONFIGURATION 85% STENOSIS AT PE=20 CM H20

MEASURED P1-P2 (CM H20)	CORRECTED P1-P2 (CM H20)	Q (ML/MIN)	RE	P1 (CM H20)	P2 (CM H20)	PE-P2 (CM H20)
3.8	3.5	136.	508	54.4	50.9	-30.9
8.1	7.7	216.	808	54.3	46.6	-26.6
11.9	11.4	274.	1025	54.3	42.9	-22.9
16.1	15.5	322.	1204	54.3	38.8	-18.8
19.9	19.2	364.	1362	54.2	35.1	-15.1
24.1	23.4	400.	1496	54.2	30.9	-10.9
28.1	27.3	432.	1616	54.2	26.9	-6.9
31.5	30.6	456.	1706	54.2	23.6	-3.6
35.8	34.8	476.	1781	54.2	19.4	0.6
39.7	38.7	492.	1841	54.1	15.4	4.6
44.0	43.0	500.	1871	54.1	11.1	8.9
47.8	46.9	495.	1852	54.1	7.3	12.7
50.3	49.3	495.	1852	54.1	4.8	15.2

TABLE 48. DATA FOR A LONG CONFIGURATION 85% STENOSIS AT PE=30 CM H20

MEASURED P1-P2 (CM H20)	CORRECTED P1-P2 (CM H20)	Q (ML/MIN)	RE	P1 (CM H20)	P2 (CM H20)	PE-P2 (CM H20)
4.1	3.8	136.	508	54.4	50.6	-20.6
8.0	7.6	210.	785	54.3	46.8	-16.8
12.3	11.7	268.	1002	54.3	42.6	-12.6
16.0	15.4	310.	1160	54.3	38.9	-8.9
20.0	19.3	348.	1302	54.2	34.9	-4.9
23.8	23.0	378.	1414	54.2	31.2	-1.2
27.9	27.2	398.	1489	54.2	27.1	2.9
31.7	30.9	420.	1571	54.2	23.3	6.7
36.5	35.6	428.	1601	54.2	18.5	11.5
40.3	39.4	426.	1594	54.2	14.7	15.3
43.9	43.1	424.	1586	54.2	11.1	18.9
47.6	46.8	424.	1586	54.2	7.4	22.6
52.1	51.3	424.	1586	54.2	2.9	27.1

TABLE 49. DATA FOR A LONG CONFIGURATION 85% STENOSIS AT PE=40 CM H20

MEASURED P1-P2 (CM H20)	CORRECTED P1-P2 (CM H20)	Q (ML/MIN)	RE	P1 (CM H20)	P2 (CM H20)	PE-P2 (CM H20)
4.0	3.8	126.	471	54.4	50.6	-10.6
8.1	7.7	197.	737	54.4	46.6	-6.6
12.0	11.5	244.	913	54.3	42.8	-2.8
16.3	15.7	286.	1070	54.3	38.6	1.4
19.8	19.2	312.	1167	54.3	35.1	4.9
24.2	23.5	333.	1246	54.3	30.7	9.3
28.0	27.3	334.	1249	54.3	26.9	13.1
32.2	31.5	333.	1246	54.3	22.7	17.3
36.0	35.4	334.	1249	54.3	18.9	21.1
40.2	39.5	332.	1242	54.3	14.7	25.3
43.9	43.2	332.	1242	54.3	11.0	29.0
47.9	47.2	332.	1242	54.3	7.0	33.0
53.6	52.9	332.	1242	54.3	1.3	38.7

TABLE 50. DATA FOR A LONG CONFIGURATION 85% STENOSIS AT PE=50 CM H20

MEASURED P1-P2 (CM H20)	CORRECTED P1-P2 (CM H20)	Q (ML/MIN)	RE	P1 (CM H20)	P2 (CM H20)	PE-P2 (CM H20)
3.8	3.6	114.	426	54.4	50.8	-0.8
7.7	7.3	177.	662	54.4	47.0	3.0
12.0	11.6	222.	830	54.3	42.8	7.2
15.9	15.4	238.	890	54.3	38.9	11.1
19.7	19.2	236.	883	54.3	35.1	14.9
24.0	23.5	236.	883	54.3	30.8	19.2
27.7	27.2	236.	883	54.3	27.1	22.9
31.8	31.4	239.	894	54.3	23.0	27.0
36.0	35.6	241.	901	54.3	18.8	31.2
40.0	39.5	244.	913	54.3	14.8	35.2
44.1	43.7	248.	928	54.3	10.7	39.3
47.5	47.1	248.	928	54.3	7.3	42.7
51.2	50.7	249.	931	54.3	3.6	46.4
54.7	54.2	250.	935	54.3	0.1	49.9

TABLE 51. DATA FOR A LONG CONFIGURATION 89.4% STENOSIS AT PE= 0 CM H20

MEASURED P1-P2 (CM H20)	CORRECTED P1-P2 (CM H20)	Q (ML/MIN)	RE	P1 (CM H20)	P2 (CM H20)	PE-P2 (CM H20)
4.9	4.7	116.	434	54.4	49.7	-49.7
10.0	9.6	182.	681	54.4	44.7	-44.7
14.9	14.5	228.	853	54.3	39.8	-39.8
20.2	19.7	273.	1021	54.3	34.6	-34.6
25.0	24.4	304.	1137	54.3	29.8	-29.8
30.1	29.4	332.	1242	54.3	24.8	-24.8
35.2	34.5	356.	1332	54.2	19.7	-19.7
39.8	39.1	377.	1410	54.2	15.1	-15.1
44.5	43.8	396.	1481	54.2	10.5	-10.5
51.3	50.5	408.	1526	54.2	3.7	-3.7

TABLE 52. DATA FOR A LONG CONFIGURATION 89.4% STENOSIS AT PE=10 CM H20

MEASURED P1-P2 (CM H20)	CORRECTED P1-P2 (CM H20)	Q (ML/MIN)	RE	P1 (CM H20)	P2 (CM H20)	PE-P2 (CM H20)
4.9	4.7	112.	419	54.4	49.7	-39.7
10.1	9.7	178.	666	54.4	44.6	-34.6
14.9	14.5	222.	830	54.3	39.9	-29.9
19.9	19.4	258.	965	54.3	34.9	-24.9
24.9	24.3	291.	1088	54.3	30.0	-20.0
30.0	29.4	319.	1193	54.3	24.9	-14.9
34.9	34.3	340.	1272	54.3	20.0	-10.0
40.0	39.3	362.	1354	54.2	15.0	-5.0
44.8	44.0	377.	1410	54.2	10.2	-0.2
51.5	50.7	380.	1422	54.2	3.5	6.5

TABLE 53. DATA FOR A LONG CONFIGURATION 89.4% STENOSIS AT PE=20 CM H20

MEASURED P1-P2 (CM H20)	CORRECTED P1-P2 (CM H20)	Q (ML/MIN)	RE	P1 (CM H20)	P2 (CM H20)	PE-P2 (CM H20)
4.9	4.7	108.	404	54.4	49.7	-29.7
10.2	9.9	170.	636	54.4	44.5	-24.5
15.0	14.6	212.	793	54.3	39.8	-19.8
20.2	19.7	250.	935	54.3	34.6	-14.6
24.9	24.3	278.	1040	54.3	30.0	-10.0
29.9	29.3	305.	1141	54.3	25.0	-5.0
35.4	34.7	332.	1242	54.3	19.5	0.5
39.7	39.0	343.	1283	54.2	15.2	4.8
44.6	43.9	340.	1272	54.3	10.3	9.7
49.4	48.7	340.	1272	54.3	5.5	14.5
54.0	53.3	338.	1264	54.3	0.9	19.1

TABLE 54. DATA FOR A LONG CONFIGURATION 89.4% STENOSIS AT PE=30 CM H20

MEASURED P1-P2 (CM H20)	CORRECTED P1-P2 (CM H20)	Q (ML/MIN)	RE	P1 (CM H20)	P2 (CM H20)	PE-P2 (CM H20)
5.1	4.9	106.	396	54.4	49.5	-19.5
10.2	9.9	164.	613	54.4	44.5	-14.5
14.9	14.5	204.	763	54.4	39.8	-9.8
20.0	19.5	239.	894	54.3	34.8	-4.8
24.9	24.4	268.	1002	54.3	29.9	0.1
30.5	30.0	286.	1070	54.3	24.3	5.7
34.4	33.9	286.	1070	54.3	20.4	9.6
40.1	39.6	286.	1070	54.3	14.7	15.3
45.2	44.6	288.	1077	54.3	9.7	20.3
49.8	49.2	289.	1081	54.3	5.1	24.9
54.5	53.9	288.	1077	54.3	0.4	29.6

TABLE 55. DATA FOR A LONG CONFIGURATION 89.4% STENOSIS AT PE=40 CM H20

MEASURED P1-P2 (CM H20)	CORRECTED P1-P2 (CM H20)	Q (ML/MIN)	RE	P1 (CM H20)	P2 (CM H20)	PE-P2 (CM H20)
4.9	4.7	97.	362	54.4	49.7	-9.7
9.2	8.9	157.	587	54.4	45.5	-5.5
15.1	14.7	199.	744	54.4	39.7	0.3
20.3	19.9	221.	827	54.3	34.5	5.5
25.0	24.6	222.	830	54.3	29.8	10.2
29.5	29.1	224.	838	54.3	25.3	14.7
34.7	34.2	226.	845	54.3	20.1	19.9
39.9	39.4	227.	849	54.3	14.9	25.1
45.4	44.9	227.	849	54.3	9.4	30.6
50.0	49.5	228.	853	54.3	4.8	35.2
55.9	55.4	228.	853	54.3	-1.1	41.1